A STUDY OF THE DYNAMICS OF DELAY COUPLED NONLINEAR OSCILLATORS AND SOME MODEL APPLICATIONS

By

BHUMIKA THAKUR

PHYS06201204002

INSTITUTE FOR PLASMA RESEARCH, GANDHINAGAR

A thesis submitted to the
Board of Studies in Physical Sciences
In partial fulfillment of requirements
for the Degree of

DOCTOR OF PHILOSOPHY

of

HOMI BHABHA NATIONAL INSTITUTE

September 2017

Homi Bhabha National Institute

Recommendations of the Viva Voce Committee

As members of the Viva Voce Committee, we certify that we have read the dissertation prepared by **Bhumika Thakur** entitled **"A study of the dynamics of delay coupled nonlinear oscillators and some model applications"** and recommend that it may be accepted as fulfilling the thesis requirement for the award of Degree of Doctor of Philosophy.

_______________ **Date :** 21/11/2017
Chairman - Dr. R. Srinivasan

Devendra Sharma **Date :** 21/11/2017
Guide/Convener - Dr. Devendra Sharma

Abhijit **Date :** 21/11/2017
Co-guide - Prof. Abhijit Sen

Parmanand **Date :** 21/11/2017
Examiner - Prof. Punit Parmananda

_______________ **Date :** 21/11/2017
Member - Prof. P. K. Chattopadhyay

Mritunjay Kundu **Date :** 21/11/2017
Member - Dr. M. Kundu

Final approval and acceptance of this thesis is contingent upon the candidate's submission of the final copies of the thesis to HBNI.

We hereby certify that we have read this thesis prepared under our direction and recommend that it may be accepted as fulfilling the thesis requirement.

Date: 21/11/2017
Place: Gandhinagar

Abhijit
Prof. Abhijit Sen
Co-guide

Devendra Sharma
Dr. Devendra Sharma
Guide

A STUDY OF THE DYNAMICS OF DELAY COUPLED NONLINEAR OSCILLATORS AND SOME MODEL APPLICATIONS

By

BHUMIKA THAKUR

PHYS06201204002

INSTITUTE FOR PLASMA RESEARCH, GANDHINAGAR

A thesis submitted to the
Board of Studies in Physical Sciences
In partial fulfillment of requirements
for the Degree of

DOCTOR OF PHILOSOPHY

of

HOMI BHABHA NATIONAL INSTITUTE

September 2017

1

Introduction

1.1 Motivation and background

Collective oscillatory behavior is a common feature of many systems in nature [1], and plays a vital role in a wide variety of systems ranging from physical and biological to social. For instance, in biological cellular populations, collective behavior often arises from long-range coupling mediated by electrochemical mechanisms [2, 3], or by biomechanical interaction between the cells and their physical environment [4]. One such example is the "segmentation clock", which is an oscillating genetic network that sets the rhythm of sequential subdivision of the body axis of the vertebrate embryo into somites [5]. Another example is the cell-to-cell communication in microorganisms, termed quorum sensing [6–8]. Other biological examples include circadian rhythms [2, 9], cardiac pacemaker cells [10], insulin-secreting cells in the pancreas [11], and neural dynamics [12]. An important application of collective behavior in physical systems is in coupled laser arrays, where mutual coherence allows the generation of much greater power than would be available from a single laser [13]. In social systems, an example is the "opinion dynamics", where individuals have opinions that change under the influence of other individuals giving rise to a sort of collective behavior [14]. In finance also, business cycles synchronize, across regions and over time [15]. Hence, the collective oscillatory behavior is a universal phenomenon and even though the above-cited systems are seemingly very distinct from one another, the underlying principles of their collective dynamics are quite similar.

A powerful approach to model such real-world phenomena is using a network of coupled nonlinear oscillators [16], which has served as a useful paradigm to represent collective phenomena in a variety of applications in physical [17], chemical [18, 19], biological [20] as well as social sciences [21]. This is because the systems of coupled nonlinear oscillators are known to display a wide spectrum of collective behavior ranging from synchronization to spatiotemporal chaos [22, 23]. The existence and stability of these collective states in a given dynamical system is decided by the following factors: (*i*) the dynamics of the individual constituent oscillator, governed by its dynamical equation, (*ii*) the topology according to which the oscillators are connected to each other, (*iii*) the nature and the strength of interactions between the interacting oscillators, and (*iv*) the time delay in the interactions between the oscillators that results from the finite processing and transmission speed of information. It is the interplay between these factors that decides the collective behavior shown by the dynamical system. The work done in this thesis highlights the importance and consequences of the presence of time delay on the system dynamics for a variety of individual component dynamics, network topologies, and nature of interactions considered in different model systems.

In this introductory chapter, we first describe some of the interesting collective phenomena observed in real systems and the model systems comprised of coupled oscillators. Then we highlight the importance of inclusion of time delay in interactions in such model systems and the effect its presence has on the system dynamics. At the end, we give a brief overview of the work carried out by us in this direction.

1.1.1 Collective dynamics

Synchronization

Perhaps the most studied collective phenomenon is *synchronization* - “the adjustment of rhythms of oscillating objects due to their weak interaction” [24]. The first recorded observation of synchronization is by Christiaan Huygens (1629-1695), the famous Dutch mathematician, astronomer, and physicist who invented the pendulum clock in 1657. This is how the story of his discovery of synchronization goes. In February 1665, Huygens was confined to his room for few days because of some illness. During his confinement, he observed that two pendulum clocks hanging on the wall in his room showed a very interesting behavior. Their pendulums always moved such that when one was furthest left, the other was furthest right, and vice versa, so that they always moved opposite of one another. Huygens tested this phenomenon further by disturbing the oscillations but found that the pendulums always came back to the same relative orientation. He described this observation in the letter to his father dated 26 February 1665 [25] and called this the “sympathy of two clocks”. He came up with the explanation that each pendulum caused an imperceptible motion in the beam of the wall from which they were hanging, which tended to force the other pendulum towards moving in synchrony with it. Once the pendula were synchronized like this, their opposite forces would cancel and the beam would stay still. Huygens was right [26] and this is exactly the explanation we have today for the phenomenon of mutual synchronization [10, 24].

Examples of synchronization can be found all around us in nature. One such example is that of "circadian rhythms" of living beings. In 1729, Jean-Jacques d'Ortous de Mairan (1678-1771), a French astronomer, noted that the leaves of the *Mimosa* plant moved with a periodicity of 24 hours in conformity with the daily cycle of darkness and light. In addition, he found that the leaves still move at a nearly 24-hour cycle in a dark room without the influence of sunlight. Studies later found that these cycles, known as circadian rhythms, are governed by an internal biological clock, which in mammals is located in two brain areas called the suprachiasmatic nuclei [27]. Other examples of synchronization include cardiac pacemaker cells [28], synchronous flashing of fireflies [29], and vertebrate segmentation clock [5]. In all these examples, synchronization is essential for the proper functioning of the biological system. However, sometimes the synchronization of oscillations can also lead to a severe malfunction of a biological system, such as in epileptic seizures and Parkinson's disease [30].

Synchronization phenomena in large populations of interacting elements have been extensively studied in a wide variety of physical, biological, chemical, and social systems for the past several decades. The individual elements or oscillators in such systems have a common feature - they are capable of generating their own rhythm, which is maintained due to an internal source of energy that compensates the dissipation in the system [24]. Such systems or oscillators are said to be self-sustained and show limit-cycle behavior. Limit cycle is a trajectory for which the energy of the system is constant over a cycle, i.e., on an average, there is no loss or gain of energy. Therefore, a successful approach to understand synchronization consists of modeling each member of the population as a limit-cycle oscillator.

Early models of synchronization

One of the earliest attempts towards understanding the collective synchronization phenomena mathematically was by an American mathematician, Norbert Wiener (1894-1964), in late 1950's and early 1960's. Before that, scientists had restricted themselves to a single nonlinear oscillator being driven by an external periodic signal or to two coupled oscillators. Wiener's approach was based on Fourier integrals [31, 32], but he did not make sufficient mathematical progress with it. Then in 1960's, Arthur T. Winfree (1942-2002), a theoretical biologist, became interested in the spontaneous synchronization of populations of biological oscillators and addressed it in his first paper published in 1967 [33]. He considered a large population of interacting limit-cycle oscillators with the frequency of each oscillator chosen from a random distribution with a certain mean and standard deviation. This system is very complex and intractable but Winfree recognized that it can be rendered tractable in the limit of "weak coupling"- "weakly" meaning relative to the attractiveness of the limit cycles. Then amplitude variations could be neglected and the oscillators could be described solely by their phases along their limit cycles. Winfree made a further simplification by working within the framework of a mean-field model, where each oscillator is considered to be coupled to the collective rhythm generated by the entire population. His model is [34]

$$\dot{\theta}_i = \omega_i + \left(\sum_{j=1}^{N} P(\theta_j) \right) Q(\theta_i), \qquad i = 1, ..., N, \tag{1.1}$$

where θ_i denotes the phase of oscillator i and N is the number of oscillators. The natural frequencies ω_i are distributed according to a given probability density $g(\omega)$. Each oscillator j exerts a phase-dependent influence $P(\theta_j)$ on all the others; the corresponding response of oscillator i depends on its phase θ_i, through the sensitivity function $Q(\theta_i)$.

Winfree discovered that such oscillator populations can exhibit a remarkable cooperative phenomenon. When the coupling strength is small compared to the variance of natural frequencies, the system behaves incoherently, with each oscillator oscillating at its natural frequency. As the coupling strength increases past a certain threshold value (dependent on the variance of natural frequencies), the population of oscillators undergoes an abrupt transition to a synchronized state, where most individuals oscillate with the same "collective" frequency. Winfree pointed out that this phenomenon is a "temporal analog" of a thermodynamic phase transition; temporal because the oscillators align in time, not space.

Intrigued by Winfree's results, Yoshiki Kuramoto, a Japanese physicist, began working on collective synchronization. He simplified Winfree's approach further in the model he gave in 1975 [35], which is discussed in detail in the next section. But before that, it is worthwhile mentioning another remarkable contribution, by Charles S. Peskin, who modeled the synchronization of pacemaker cells with a simple physical setup consisting of parallely connected capacitors and resistors [28].

The Kuramoto Model

Preserving the fundamental assumptions that Winfree had proposed, Kuramoto used the perturbative method of averaging to show that the long-term dynamics of any system of nearly identical, weakly coupled limit-cycle oscillators can be described by the phase equations of following form [34, 36]:

$$\dot{\theta}_i = \omega_i + \sum_{j=1}^{N} \Gamma_{ij}\left(\theta_j - \theta_i\right), \tag{1.2}$$

where the interaction function Γ_{ij} determines the form of coupling between i^{th} and j^{th} oscillators. The Kuramoto model corresponds to equally weighted, all-to-all coupling, mediated by a sinusoidal interaction function:

$$\dot{\theta}_i = \omega_i + \frac{\kappa}{N}\sum_{j=1}^{N}\sin\left(\theta_j - \theta_i\right), \qquad i = 1, ..., N. \tag{1.3}$$

Kuramoto further introduced an order parameter to quantify the overall synchrony of the oscillator population. The complex order parameter

$$Re^{i\psi} = \frac{1}{N}\sum_{j=1}^{N} e^{i\theta_j}, \tag{1.4}$$

is a macroscopic quantity that can be interpreted as the collective rhythm produced by the whole population. Here $0 \leq R(t) \leq 1$ measures the phase coherence of the oscillator population and $\psi(t)$ is the average phase. The Kuramoto equation (1.3) can be rewritten in terms of the order parameter as

$$\dot{\theta}_i = \omega_i + \kappa R\sin(\psi - \theta_i). \tag{1.5}$$

In this form, the interactions between the oscillators are described solely through the mean-field quantities R and ψ. Each oscillator is coupled to the common average phase $\psi(t)$ with a coupling strength given by κR. For all κ less than a certain threshold κ_c, the oscillators act as if they were uncoupled: the phases become uniformly distributed around the circle. In this case, $R(t)$ decays to a small value of $O(N^{-1/2})$. This state is called the "incoherent state". When $\kappa > \kappa_c$, the incoherent state loses stability and $R(t)$ grows exponentially, thereby generating a collective oscillation. Eventually $R(t)$ saturates at some level $R_{t\to\infty} < 1$ with $O(N^{-1/2})$ fluctuations. In the limit of infinite number of oscillators $N \to \infty$, the threshold coupling strength for the onset of synchronization is given by $\kappa_c = \frac{2}{\pi g(0)}$ [34]. Detailed discussions on the Kuramoto model are provided in the review articles by Strogatz [34] and Acebr*ó*n et al. [37].

Despite its apparent simplicity and mathematical tractability, the Kuramoto model can exhibit quite complex non-trivial behavior displaying a large variety of synchronization patterns. Therefore, the Kuramoto model and its extensions have served as a paradigm for a variety of dynamical systems. For instance, it has been used to model neural networks [38], systems of coupled lasers [39], Josephson junction arrays [40], and power grid networks [41, 42]. A modified version of Kuramoto model called the *Opinion Changing Rate (OCR) model* has been proposed as a framework for opinion formation [14, 21]. An adapted Kuramoto model has also been used to study the synchronization dynamics in financial market networks [43].

Amplitude Death

Another well known collective phenomenon relevant to this thesis is the “Amplitude Death”. If the coupling between the oscillators is not weak or the attraction to the limit cycle is not large as compared to the coupling strength, the variations in amplitude cannot then be ignored. In that case many additional phenomena can occur, such as, oscillators can drive one another to a state of zero amplitude - often called the amplitude death (AD) state.

In 19^{th} century, Lord Rayleigh (1842-1919), an English physicist, made one of the first accounts of this phenomenon with his observation that two organ pipes standing close to one another can almost suppress each other to silence [44]. AD was first studied in mathematical oscillators by Yamaguchi and Shimizu [45] in 1984. They found that two ingredients are needed by AD to be stable: (i) a sufficiently strong coupling between the oscillators and (ii) a sufficiently wide distribution of natural frequencies. Subsequently in 1985, Bar-Eli [46] observed AD in a system of coupled chemical oscillators and this phenomenon was also known as the "Bar-Eli" effect at the time. Aronson et al. [47] verified Bar-Eli's results in 1990 and thoroughly investigated AD in two coupled non-identical limit-cycle oscillators having different intrinsic frequencies. They showed that there are parameter regimes in which the interactions cause the system to stop oscillating, and the rest state at zero, stabilized by the interaction, is the only stable solution. In the same year, Ermentrout [48] extended this study to globally coupled oscillators and Mirollo and Strogatz [49] studied AD in an array of instantaneously coupled limit-cycle oscillators with mean field coupling and randomly distributed natural frequencies. They showed that similar to the system of two coupled limit-cycle oscillators, when the coupling is sufficiently strong and the distribution of frequencies has sufficiently large variance, the system undergoes AD. Later, Reddy et al. [50] extended these studies to the systems with time-delayed interactions and found that the presence of time delay can lead to AD even if the oscillators have the same intrinsic frequency (i.e., they are identical). More recently, AD has also been reported, in the absence of time-delayed interactions, in systems of identical oscillators with dynamic coupling [51], conjugate coupling [52], nonlinear coupling [53], and environmental coupling [54].

An important instance where the attraction to the limit cycle is not "strong" is near a Hopf bifurcation point. In this case, the attraction to the limit cycle is proportional to the distance from criticality. The equation considered in most of the above-cited studies represents the normal form of a supercritical Hopf bifurcation, also known as the Stuart-Landau oscillator. It has the amplitude as well as the phase evolution information embedded in the time evolution of complex amplitude $Z(t)$:

$$\dot{Z}(t) = (\alpha + i\omega - |Z(t)|^2)Z(t), \tag{1.6}$$

where $\alpha, \omega \in \mathbb{R}$ and α is the bifurcation parameter. Writing $Z(t)$ in terms of its argument and modulus as $Z(t) = r(t)e^{i\theta(t)}$ with $r, \theta \in \mathbb{R}$ and $\theta \in [-\pi, \pi]$, the amplitude and phase evolution equations can be written as

$$\begin{aligned} \dot{r} &= \left(\alpha - r^2\right) r, \\ \dot{\theta} &= \omega. \end{aligned} \tag{1.7}$$

For $\alpha < 0$, Eq. (1.6) has a stable rest state at $Z(t) = 0$. When $\alpha > 0$, the rest state loses stability via supercritical Hopf bifurcation and the equation shows stable oscillations ($Z(t) = \sqrt{\alpha}e^{i\omega t}$) with amplitude equal to $\sqrt{\alpha}$. The phase variable θ rotates uniformly in time with an angular frequency equal to the parameter ω.

The governing set of equations for a population of N interacting Stuart-Landau oscillators, with natural frequencies distributed according to a given probability distribution $g(\omega)$, is

$$\dot{Z}_i(t) = (\alpha + i\omega_i - |Z_i(t)|^2)Z_i(t) + \sum_{j=1}^{N} \kappa_{ij}[Z_j(t) - Z_i(t)], \tag{1.8}$$

where $i = 1, ..., N$. In polar coordinates,

$$\begin{aligned} \dot{r}_i &= r_i\left(\alpha - r_i^2\right) + \sum_{j=1}^{N} \kappa_{ij}\left[r_j \cos\left(\theta_j - \theta_i\right) - r_i\right], \\ \dot{\theta}_i &= \omega_i + \sum_{j=1}^{N} \kappa_{ij}\frac{r_j}{r_i} \sin\left(\theta_j - \theta_i\right). \end{aligned} \tag{1.9}$$

The Kuramoto model can be obtained from the coupled set of equations Eq. (1.9) under the “weak coupling” approximation. As discussed before, in the weak coupling limit, the amplitude evolution can be ignored, that means $r_j = r_i$, and for the case of mean field coupling ($\kappa_{ij} = \kappa/N$), the phase evolution equations become

$$\dot{\theta}_i = \omega_i + \frac{\kappa}{N}\sum_{j=1}^{N} \sin\left(\theta_j - \theta_i\right), \tag{1.10}$$

which is the governing dynamical equation of the Kuramoto model (Eq. (1.3)). Therefore, the amplitude model (1.9) produces all the results of the phase-only models and captures additional phenomena such as amplitude death and chaos [55].

AD has been observed in systems of coupled synthetic genetic oscillators [56], chemical oscillators [57], electronic circuits [58], biological-electronic hybrid oscillators [59], thermo-optical oscillators [60], coupled lasers [61, 62], and very recently in thermoacoustic oscillators [63]. AD can have both desirable and undesirable effects. It has been proposed to utilize AD for stabilization of DC microgrids [64], which is desirable since constant-power loads on dc microgrids create a destabilizing effect on the circuit that can lead to severe voltage and frequency oscillations. However, AD can also be undesirable and detrimental if it suppresses oscillations that are important for the proper functioning of the system and therefore the revival of oscillations has also been a focus of recent studies [65].

1.1.2 Time-delayed interactions

Time delay is ubiquitous in most natural and physical systems due to the finiteness of the speed of propagation of electrical signals, reaction times in chemical interactions, and the finite conductance of neuronal connections. For example, in the dynamics of gene-regulatory networks, the time delay is caused by processes such as transcription, translation, and transport and can have an important influence on the system dynamics. The delays or lags can also represent incubation periods in the infectious disease dynamics. In the study of population dynamics within ecological models, delays result from processes such as growth, maturation, and regeneration.

If the delays are small in comparison to the relevant timescales of the system dynamics, they can be neglected and the dynamical equations reduce to the flow of ordinary differential equations (ODEs). However, when delays have the same order of magnitude as the system's typical timescales, then the system should be modeled with delay differential equations (DDEs). DDEs come under the category of functional differential equations which have been studied for at least last 200 years. In 1908, at the International Conference of Mathematics in Rome, Émile Picard (1856-1941), a French Mathematician, emphasized the importance of consideration of hereditary effects in the modeling of physical systems [66]. In 1931, Volterra wrote a fundamental book on the role of hereditary effects on models of the interaction of species. After the 1940s, the study of DDEs gained significant momentum due to delay considerations in various areas of applied science, particularly in control theory. An example is ground based satellite and rocket control, where the propagation time of the command signal is far from being negligible.

In DDEs, the derivatives not only depend on the current state of the system but also on the state of the system in the past. The form of delay differential equations relevant to this thesis is

$$\dot{\mathbf{x}}(t) = f\left(\mathbf{x}(t), \mathbf{x}(t-\tau)\right), \tag{1.11}$$

where τ is a constant delay. The most obvious difference between ODEs and DDEs is the initial data. The solution of an ODE is determined by the value of its variable at the initial point. For solving a DDE, we must provide not just the value of the solution at the initial point, but also the "history"- the solution at times prior to the initial point. To find the solution of a DDE, such as (1.11), we need to specify the initial conditions that provide the function values $\mathbf{x}(t)$ for all times between $-\tau$ and 0. Thus, the delay systems are infinite dimensional, because we have to provide an infinite set of numbers to specify the initial conditions. Therefore, DDEs show a wide variety of very complex behavior.

Delay models based on DDEs have been used to describe various aspects of a very large spectrum of problems ranging from ecology [67–69] to neurology [70]. In studies of infectious disease dynamics, examples include primary infection [71], drug therapy [72], and immune response [73]. Delays have also appeared in the study of circadian rhythms [74], epidemiology [75], respiratory system [76], tumor growth [77], white blood cells production [78], neural networks [79], and gene-regulatory networks [80]. Therefore, it is crucial to incorporate time delays while analyzing the dynamics of such systems.

Time delay in systems of coupled oscillators

The time-delayed dynamics in this thesis focuses on the communication delays or interaction delays appearing in the coupling term of the equations of a network of oscillators. Time delay introduces significant changes in the collective behavior of such systems by influencing the onset thresholds as well as the extent of the parametric domains of various collective regimes such as synchronization and AD.

Phase oscillators with coupling delays

Schuster and Wagner [81] were the first to introduce discrete time delays in the coupling between limit cycle oscillators. They considered a system of two coupled oscillators with time-delayed phase evolution of the following form:

$$\dot{\theta}_1(t) = \omega_1 + \kappa \sin(\theta_2(t-\tau) - \theta_1(t)),$$
$$\dot{\theta}_2(t) = \omega_2 + \kappa \sin(\theta_1(t-\tau) - \theta_2(t)). \tag{1.12}$$

They showed that the time-delayed system has multiple synchronized solutions with different collective frequencies, unlike the undelayed system that has at most one solution. This number increases either by increasing the coupling strength κ or the time delay τ. Subsequent works extended this study to larger systems of phase coupled oscillators and found that, similar to the system of two delay-coupled oscillators, these systems can have multiple synchronized solutions with different collective frequencies. These studies demonstrated metastability [82], clustering behavior [83], and multistability between synchronized and desynchronized states in such systems [84]. Yeung and Strogatz [85] have also extensively studied time delay effects in the Kuramoto model of coupled oscillators. The general form of time-delayed coupling in the Kuramoto model, considered in the above studies, is

$$\dot{\theta}_i(t) = \omega_i + \sum_{j=1}^{N} \kappa_{ij} \sin\left(\theta_j(t-\tau) - \theta_i(t)\right), \qquad i = 1, ..., N. \tag{1.13}$$

Further studies on collective behavior in phase models with delays have also considered heterogeneous coupling delays [86], and distance dependent delays [87, 88]. A delayed coupling theory based on phase oscillators has been successfully employed as a model of vertebrate segmentation [89].

Amplitude oscillators with coupling delays

Reddy et al. [50] were the first to report delay induced AD in the system of two coupled limit-cycle oscillators. They further analyzed the system of globally and diffusively delay-coupled Stuart-Landau oscillators [90], described by

$$\dot{Z}_j(t) = \left(1 + i\omega_j - |Z_j(t)|^2\right) Z_j(t) + \frac{\kappa}{N} \sum_{k=1}^{N} \left[Z_k(t-\tau) - Z_j(t)\right], \tag{1.14}$$

and showed that time-delays can induce AD even if the frequencies of the oscillators are identical. In these systems, AD occurs inside separate "death" islands in the parameter space of delay τ and coupling strength κ for any number of oscillators. Reddy et al. also gave an experimental evidence of time-delay-induced AD in two coupled nonlinear electronic circuits [58]. Later, Atay [91] demonstrated that the presence of distributed delays in a system of coupled oscillators can lead to the enlargement and merger of the "death islands". In such systems, if the variance of the distribution exceeds a threshold, the "death" region becomes unbounded and AD can occur for any average delay value. AD studies were further extended to the nearest neighbor coupling configuration by Reddy et al. [92] in a ring of delay coupled oscillators. They found that the size of "death islands" decreases with increasing number of oscillators N when N is odd but is independent of N when N is even. For a similar system with ring topology, Zou et al. [93] showed that delay-induced AD in the parameter space of the diffusive coupling and time delay can be eliminated by introducing gradient coupling between the oscillators. Recent studies include AD induced by a time-varying delay connection [94] and mixed time delays [95], among others.

1.2 Aim and scope of the thesis

The aim of this thesis is to examine the effect of time-delayed interactions on the collective dynamics of networks of coupled nonlinear oscillators. This theoretical study involves extensive analytical and numerical investigations. The thesis can be broadly divided into two parts. The first part investigates time-delay effects on the collective behavior of those systems whose dynamics can be represented by the phase evolution equations alone. In the second part, the complete description of the system dynamics requires both the amplitude as well as the phase evolution considerations. The thesis is organized as described below.

Thesis organization

Chapter 2 explores the effects of time-delayed interactions on the dynamics of those systems in which the combination of topology and repulsive interactions manifests itself in the form of geometric frustration. In the absence of time delay, such frustrated systems are known to possess a high degree of multistability among a large number of coexisting collective states, except for the fully synchronized state that is normally obtained for the attractively coupled systems. Time delay in the coupling is found to remove this constraint and lead to such a synchronized ground state over a range of parameter values. The study presented in this chapter examines three prototypical frustrated networks of phase-repulsive oscillators − a simple triangular unit, a triangular configuration with six nodes enclosing a triangle within a triangle, and a 4×4 triangular lattice. The expressions for the collective frequencies and the stability conditions for the in-phase and out-of-phase states of the simplest three oscillator network are discussed in detail. A systematic quantification of the network frustration is made by defining a suitable frustration parameter, which is a function of time-delayed phase differences between the oscillators. It is shown that time delay significantly alters the amount of frustration in such systems and thereby influences their collective dynamics. The most important result is the discovery of a universal scaling relation between frustration and time delay that is found to hold in a variety of such geometrically frustrated networks.

Chapter 3 provides a dynamical understanding of the multisensory information processing involved in perception through a simple phase-oscillators based model. A particular focus is on explaining the principal experimental features associated with the so-called McGurk effect and its temporal constraints that show how the audiovisual integration in speech perception starts to break down when the lag between the auditory and visual inputs becomes too long. Such a lag is modeled in our study by an appropriate time delay in the coupling between an oscillator representing one of the unisensory units (auditory or visual) and the multisensory oscillator (representing the audio-visual integrator such as posterior superior temporal sulcus (pSTS) or Superior Colliculus (SC)). Our model captures the functional connectivity between the unisensory and multisensory streams via the coupling parameters. The changes in the collective behavior of our model system, as seen through the variation of the order parameter as a function of time delay, show a remarkable qualitative agreement with the experimental observations of the McGurk effect. In particular, our model captures the temporal binding window of multisensory integration, and the inter-trial and inter-subject variability through the multistability seen in the dynamical states. We also investigate the situation where the information from either modality becomes less reliable by considering the coupling parameters between the two unisensory units (auditory/visual) and the multisensory unit to be unequal.

In **Chapter 4**, an extension of the model presented in the previous chapter is proposed in order to incorporate spatial aspects of multisensory processing into the model and to gain a better insight into the complexities involved in such processes at various cortical levels. The model again consists of two unimodal areas (auditory and visual), which communicate via feedforward and feedback synapses with a third multisensory area (pSTS or SC). However, instead of a single oscillator representing the dynamics of each cortical area (auditory, visual, and multisensory), here we consider a two-dimensional network/layer of coupled phase oscillators for each area. Each oscillator can be representative of a single neuron or a group of neurons. Inter-layer connections are only between the oscillators at the same spatial location. Our preliminary numerical investigation has been carried out for two types of intra-layer connections - (i) when there is only excitatory non-local coupling between the intra-layer oscillators, and (ii) when the intra-layer connections are arranged according to the Mexican-hat disposition. The results of the excitatory-only coupling are shown to match the results of the previous minimalistic model in terms of the order parameter variations with the time-delay parameter. The presence of Mexican-hat coupling with finite inhibitory strength is shown to facilitate the presence of spatiotemporal wave-patterns and related multistability that has been used to explain the perceptual variability in multisensory processes. We also study the effect of explicit inclusion of stimuli into the dynamical equations of the unisensory oscillators. The model provides a more realistic description of the cortical architecture and a wider range of multisensory processes that can be studied by bringing in the spatial aspects. Thus, it can act as a common framework for explaining spatial audiovisual illusions like the Ventriloquism effect along with temporal audiovisual illusions like the McGurk effect.

Chapter 5 investigates the influence of time-delayed interactions on the robustness of the collective dynamics of a network of coupled oscillators against the deterioration of some of its units, such as due to some elements turning non-self-oscillatory. The increase in proportion of the inactive or damaged elements which have lost their self-oscillatory behavior with time can be interpreted as the aging of the system. The transition of the system from a global-oscillatory state to a non-oscillatory steady state at a threshold proportion of such inactive elements is termed as the aging transition. Our results show that the presence of time-delayed interactions can lower the threshold of the aging transition of the system and thereby degrade its functional robustness. We start from a simple model of two time-delay coupled Stuart-Landau oscillators that have identical frequencies but are located at different distances from the Hopf bifurcation point. A systematic numerical and analytic study delineates the dependence of the critical coupling strength (at which the system experiences a total loss of synchrony) on time delay and the average distance of the system from the Hopf bifurcation point. We find that time delay can act to facilitate the aging transition by lowering the threshold coupling strength for amplitude death in the system. We then extend our study to larger systems of globally coupled active and inactive oscillators including an infinite system in the thermodynamic limit. Our model system and results can provide a useful paradigm for understanding the functional robustness of diverse physical and biological systems that are prone to aging transitions. For example, Alzheimer's disease and Huntington's disease are characterized by progressive neuron fall outs and time-delays are present in the brain due to finite neuronal conduction.

Finally in **Chapter 6**, an overall summary of the problems studied in this thesis is provided and the main results and conclusions are highlighted. Some possible future directions emerging from the work done in the thesis are identified at the end.

Our studies, taken together, highlight the important consequences of time-delayed coupling on the collective dynamics of oscillator networks which can have potential practical implications in a variety of real life applications.

Bibliography

[1] A. T. Winfree, *The Geometry of Biological Time* (Springer, 1980).

[2] E. D. Herzog, *Neurons and networks in daily rhythms*, Nat. Rev. Neurosci. **8**, 790–802 (2007).

[3] M. V. L. Bennett, and R. S. Zukin, *Electrical coupling and neuronal synchronization in the mammalian brain*, Neuron **41**, 495–511 (2004).

[4] S. Koride, et al., *Mechanochemical regulation of oscillatory follicle cell dynamics in the developing Drosophila egg chamber*, Mol. Biol. Cell **25**, 3709–3716 (2014).

[5] A. C. Oates, L. G. Morelli, and S. Ares, *Patterning embryos with oscillations: structure, function and dynamics of the vertebrate segmentation clock*, Development **139**, 625–639 (2012).

[6] C. M. Waters, and B. L. Bassler, *Quorum Sensing: cell-to-cell communication in bacteria*, Annu. Rev. Cell Dev. Biol. **21**, 319–346 (2005).

[7] D. J. Schwab, A. Baetica, and P. Mehta, *Dynamical quorum-sensing in oscillators coupled through an external medium*, Physica D **241**, 1782-1788 (2012).

[8] T. Gregor, K. Fujimoto, N. Masaki, and S. Sawai, *The onset of collective behavior in social amoebae*, Science **328**, 1021–1025 (2010).

[9] S. Yamaguchi, et al., *Synchronization of cellular clocks in the suprachiasmatic nucleus*, Science **302**, 1408–1412 (2003).

[10] S. H. Strogatz, *Sync: The Emerging Science of Spontaneous Order* (Hyperion, New York, 2003).

[11] A. Sherman, J. RiNZEL, and J. Keizer, *Emergence of organized bursting in clusters of pancreatic beta-cells by channel sharing*, Biophys. J. **54**, 411–425 (1988).

[12] D. R. Chialvo, *Emergent complex neural dynamics*, Nat. Phys. **6**, 744–750 (2010).

[13] H. G. Winful, and L. Rahman, *Synchronized chaos and spatiotemporal chaos in arrays of coupled lasers*, Phys. Rev. Lett. **65**, 1575–1578 (1990).

[14] A. Pluchino, V. Latora, and A. Rapisarda, *Compromise and synchronization in opinion dynamics*, Eur. Phys. J. B **50**, 169–176 (2006).

[15] S. Claessens, M. A. Kose, and M. E. Terrones, *Financial Cycles: What? How? When?*, IMF Working Paper **WP/11/76**, (2011).

[16] P. C. Matthews, R. E. Mirollo, and S. H. Strogatz, *Dynamics of a large system of coupled nonlinear oscillators*, Physica D **52**, 293–331 (1991).

[17] H. -J. Wünsche, et al., *Synchronization of delay-coupled oscillators: A study of Semiconductor lasers*, Phys. Rev. Lett. **94**, 163901 (2005).

[18] I. R. Epstein, *Coupled chemical oscillators and emergent system properties*, Chem. Commun. **50**, 10758–10767 (2014).

[19] T. Singla, F. Montoya, M. Rivera, S. Tajima, S. Nakabayashi, and P. Parmananda, *Synchronization using environmental coupling in mercury beating heart oscillators*, Chaos **26**, 063103 (2016).

[20] L. Glass, *Synchronization and rhythmic processes in physiology*, Nature **410**, 277–284 (2001).

[21] A. Pluchino, V. Latora, and A. Rapisarda, *Changing opinions in a changing world: A new perspective in sociophysics*, Int. J. Mod. Phys. C **16**, 515–531 (2005).

[22] G. Hu, Y. Zhang, H. A. Cerdeira, and S. Chen, *From low-dimensional synchronous chaos to high-dimensional desynchronous spatiotemporal chaos in coupled systems*, Phys. Rev. Lett. **85**, 3377 (2000).

[23] Y. Elskens, and D. F. Escande, *Microscopic Dynamics of Plasmas and Chaos* (CRC Press, 2002).

[24] A. Pikovsky, M. Rosenblum, and J. Kurths, *Synchronization : A Universal Concept in Nonlinear Sciences* (Cambridge University Press, Cambridge, 2001).

[25] Ch. Huygens, *Œvres Complètes, vol. 15* (Swets & Zeitlinger B. V., Amsterdam, 1967).

[26] M. Bennett, M. F. Schatz, H. Rockwood, and K. Wiesenfeld, *Huygens's clocks*, Proc. R. Soc. Lond. A **458**, 563–579 (2002).

[27] S. Panda, J. B. Hogenesch, and S. A. Kay, *Circadian rhythms from flies to human*, Nature **417**, 329–335 (2002).

[28] C. S. Peskin, *Mathematical Aspects of Heart Physiology* (Courant Institute of Mathematical Sciences, New York University, 1975).

[29] J. B. Buck, *Synchronous rhythmic flashing of fireflies*, Quart. Rev. Biol. **13**, 301–314 (1938).

[30] C. Hammond, H. Bergman, and P. Brown, *Pathological synchronization in Parkinson's disease: networks, models and treatments*, Trends Neurosci. **30**, 357–364 (2007).

[31] N. Wiener, *Nonlinear Problems in Random Theory* (MIT press, Cambridge, MA 1958).

[32] N. Wiener, *Cybernetics* (MIT press, Cambridge, MA 1961).

[33] A. T. Winfree, *Biological rhythms and the behavior of populations of coupled oscillators*, J. Theor. Biol. **16**, 15–42 (1967).

[34] S. H. Strogatz, *From Kuramoto to Crawford: exploring the onset of synchronization in populations of coupled oscillators*, Physica D **143**, 1–20 (2000).

[35] Y. Kuramoto, H. Arakai, ed., *Self-entrainment of a population of coupled nonlinear oscillators*, International Symposium on Mathematical Problems in Theoretical Physics, Lecture Notes in Physics **39**, (Springer, New York 1975).

[36] Y. Kuramoto, *Chemical Oscillations, Waves, and Turbulence*, (Springer-Verlag, New York 1984).

[37] J. A. Acebrón, L. L. Bonilla, C. J. P. Vicente, F. Ritort, and R. Spigler, *The Kuramoto model: A simple paradigm for synchronization phenomena*, Rev. Mod. Phys. **77**, 137–185 (2005).

[38] M. Breakspear, S. Heitmann, and A. Daffertshofer, *Generative models of cortical oscillations: neurobiological implications of the Kuramoto model*, Front. Hum. Neurosci. **4**, 190 (2010).

[39] M. Nixon, E. Ronen, A. A. Friesem, and N. Davidson, *Observing geometric frustration with thousands of coupled lasers*, Phys. Rev. Lett. **110**, 184102 (2013).

[40] K. Wiesenfeld, P. Colet, and S. H. Strogatz, *Synchronization transitions in a disordered Josephson series array*, Phys. Rev. Lett. **76**, 404–407 (1996); *Frequency locking in Josephson arrays: Connection with the Kuramoto model*, Phys. Rev. E **57**, 1563–1569 (1998).

[41] G. Filatrella, A. H. Nielsen, and N. F. Pedersen, *Analysis of a power grid using a Kuramoto-like model*, Eur. Phys. J. B **61**, 485–491 (2008).

[42] F. A. Rodrigues, T. K. Dal'Maso Peron, P. Ji, and J. Kurths, *The Kuramoto model in complex networks*, Phys. Rep. **610**, 1–98 (2016).

[43] T. K. Dal'Maso Peron, and F. A. Rodrigues, *Collective behavior in financial markets*, Europhys. Lett. **96**, 48004 (2011).

[44] J. W. S. Rayleigh, *The Theory of Sound* (Macmillan and Co., London 1877).

[45] Y. Yamaguchi, and H. Shimizu, *Theory of self-synchronization in the presence of native frequency distribution and external noises*, Physica D **11**, 212–226 (1984).

[46] K. Bar-Eli, *On the stability of coupled chemical oscillators*, Physica D **14**, 242–252 (1985).

[47] D. G. Aronson, G. B. Ermentrout, and N. Kopell, *Amplitude response of coupled oscillators*, Physica D **41**, 403–449 (1990).

[48] G. B. Ermentrout, *Oscillator death in populations of "all to all" coupled nonlinear oscillators*, Physica D **41**, 219–231 (1990).

[49] R. E. Mirollo, and S. H. Strogatz, *Amplitude death in an array of limit-cycle oscillators*, J. Stat. Phys. **60**, 245–262 (1990).

[50] D. V. R. Reddy, A. Sen, and G. L. Johnston, *Time delay induced death in coupled limit cycle oscillators*, Phys. Rev. Lett. **80**, 5109–5112 (1998).

[51] K. Konishi, *Amplitude death induced by dynamic coupling*, Phys. Rev. E **68**, 067202 (2003).

[52] R. Karnatak, R. Ramaswamy, and A. Prasad, *Amplitude death in the absence of time delays in identical coupled oscillators*, Phys. Rev. E **76**, 035201 (2007).

[53] A. Prasad, M. Dhamala, B. M. Adhikari, and R. Ramaswamy, *Amplitude death in nonlinear oscillators with nonlinear coupling*, Phys. Rev. E **81**, 027201 (2010).

[54] V. Resmi, G. Ambika, and R. E. Amritkar, *General mechanism for amplitude death in coupled systems*, Phys. Rev. E **84**, 046212 (2011).

[55] P. C. Matthews, and S. H. Strogatz, *Phase diagram for the collective behavior of limit-cycle oscillators*, Phys. Rev. Lett. **65**, 1701–1704 (1990).

[56] E. Ullner, A. Zaikin, E. I. Volkov, and J. García-Ojalvo, *Multistability and clustering in a population of synthetic genetic oscillators via phase-repulsive cell-to-cell communication*, Phys. Rev. Lett. **99**, 148103 (2007).

[57] M. F. Crowley and I. R. Epstein, *Experimental and theoretical studies of a coupled chemical oscillator: phase death, multistability and in-phase and out-of-phase entrainment*, J. Phys. Chem. **93**, 2496–2502 (1989).

[58] D. V. R. Reddy, A. Sen, and G. L. Johnston, *Experimental evidence of time-delay-induced death in coupled limit-cycle oscillators*, Phys. Rev. Lett. **85**, 3381–3384 (2000).

[59] I. Ozden, S. Venkataramani, M. A. Long, B. W. Connors, and A. V. Nurmikko, *Strong coupling of nonlinear electronic and biological oscillators: reaching the "amplitude death" regime*, Phys. Rev. Lett. **93**, 158102 (2004).

[60] R. Herrero, M. Figueras, J. Rius, F. Pi, and G. Orriols, *Experimental observation of the amplitude death effect in two coupled nonlinear oscillators*, Phys. Rev. Lett. **84**, 5312–5315 (2000).

[61] M.-D. Wei, and J.-C. Lun, *Amplitude death in coupled chaotic solid-state lasers with cavity-configuration-dependent instabilities*, Appl. Phys. Lett. **91**, 061121 (2007).

[62] R. Vicente, S. Tang, J. Mulet, C. R. Mirasso, and J. M. Liu, *Synchronization properties of two self-oscillating semiconductor lasers subject to delayed optoelectronic mutual coupling*, Phys. Rev. E **73**, 047201 (2006).

[63] T. Biwa, S. Tozuka, and T. Yazaki, *Amplitude death in coupled thermoacoustic oscillators*, Phys. Rev. Applied **3**, 034006 (2015).

[64] S. R. Huddy, and J. D. Skufca, *Amplitude death solutions for stabilization of dc microgrids with instantaneous constant-power loads*, IEEE Transactions on Power Electronics **28**, 247–253 (2013).

[65] W. Zou, et al., *Restoration of rhythmicity in diffusively coupled dynamical networks*, Nat. Commun. **6**, 7709 (2015).

[66] J. K. Hale, *History of Delay Equations*, O. Arino, M. L. Hbid, E. A. Dads (eds), Delay Differential Equations and Applications, NATO Science Series (II. Mathematics, Physics and Chemistry) **205**, (Springer, Dordrecht 2006).

[67] P. Turchin, *Rarity of density dependence or population regulation with lags?*, Nature **344**, 660–663 (1990).

[68] P. Turchin, and A. D. Taylor, *Complex dynamics in ecological time series*, Ecology **73**, 289–305 (1992).

[69] C. W. Eurich, A. Thiel, and L. Fahse, *Distributed delays stabilize ecological feedback systems*, Phys. Rev. Lett. **94**, 158104 (2005).

[70] B. Doiron, M. J. Chacron, L. Maler, A. Longtin, and J. Bastian, *Inhibitory feedback required for network oscillatory responses to communication but not prey stimuli*, Nature **421**, 539–543 (2003).

[71] M. S. Ciupe, B. L. Bivort, D. M. Bortz, and P. W. Nelson, *Estimating kinetic parameters from HIV primary infection data through the eyes of three different mathematical models*, Math. Biosci. **200**, 1–27 (2006).

[72] P. W. Nelson, J. D. Murray, and A. S. Perelson, *A model of HIV-1 pathogenesis that includes an intracellular delay*, Math. Biosci. **163**, 201–215 (2000).

[73] K. Cooke, Y. Kuang, and B. Li, *Analysis of an antiviral immune response model with time delays*, Canad. Appl. Math. Quart. **6**, 321–354 (1998).

[74] P. Smolen, D. A. Baxter, and J. H. Byrne, *A reduced model clarifies the role of feedback loops and time delays in the Drosophila circadian oscillator*, Biophys. J. **83**, 2349–2359 (2002).

[75] K. Cooke, P. van den Driessche, and X. Zou, *Interaction of maturation delay and nonlinear birth in population and epidemic models*, J. Math. Biol. **39**, 332–352 (1999).

[76] B. Vielle, and X. Chauvet, *Delay equation analysis of human respiratory stability*, Math. Biosci. **152**, 105–122 (1998).

[77] M. Villasana, and A. Radunskaya, *A delay differential equation model for tumor growth*, J. Math. Biol. **47**, 270–294 (2003).

[78] M. C. Mackey, and L. Glass, *Oscillation and chaos in physiological control systems*, Science **197**, 287–289 (1977).

[79] S. A. Campbell, R. Edwards, and P. van den Driessche, *Delayed coupling between two neural network loops*, SIAM J. Appl. Math. **65**, 316–335 (2004).

[80] H. De Jong, *Modeling and simulation of genetic regulatory systems: a literature review*, J. Comput. Biol. **9**, 67–103 (2002).

[81] H. G. Schuster, and P. Wagner, *Mutual entrainment of two limit cycle oscillators with time delayed coupling*, Prog. Theor. Phys. **81**, 939–945 (1989).

[82] E. Niebur, H. G. Schuster, and D. M. Kammen, *Collective frequencies and metastability in networks of limit-cycle oscillators with time delay*, Phys. Rev. Lett. **67**, 2753–2757 (1991).

[83] Y. Nakamura, F. Tominaga, and T. Munakata, *Clustering behavior of time-delayed nearest-neighbor coupled oscillators*, Phys. Rev. E **49**, 4849 (1994).

[84] S. Kim, S. H. Park, and C. S. Ryu, *Multistability in coupled oscillator systems with time delay*, Phys. Rev. Lett. **79**, 2911–2914 (1997).

[85] M. K. S. Yeung, and S. H. Strogatz, *Time delay in the Kuramoto model of coupled oscillators*, Phys. Rev. Lett. **82**, 648–651 (1999).

[86] W. S. Lee, E. Ott, and T. M. Antonsen, *Large coupled oscillator systems with heterogeneous interaction delays*, Phys. Rev. Lett. **103**, 044101 (2009).

[87] D. H. Zanette, *Propagating structures in globally coupled systems with time delays*, Phys. Rev. E **62**, 3167–3172 (2000).

[88] G. C. Sethia, A. Sen, and F. M. Atay, *Synchronous solutions and their stability in nonlocally coupled phase oscillators with propagation delays*, Phys. Rev. E **81**, 056213 (2010).

[89] L. G. Morelli, et al., *Delayed coupling theory of vertebrate segmentation*, HFSP J. **3**, 55–66 (2009).

[90] D. V. R. Reddy, A. Sen, and G. L. Johnston, *Time delay effects on coupled limit cycle oscillators at Hopf bifurcation*, Physica D **129**, 15–34 (1999).

[91] F. M. Atay, *Distributed delays facilitate amplitude death of coupled oscillators*, Phys. Rev. Lett. **91**, 094101 (2003).

[92] D. V. R. Reddy, A. Sen, and G. L. Johnston, *Phase-locked patterns and amplitude death in a ring of delay-coupled limit cycle oscillators*, Phys. Rev. E **69**, 056217 (2004).

[93] W. Zou, C. Yao, and M. Zhan, *Eliminating delay-induced oscillation death by gradient coupling*, Phys. Rev. E **82**, 056203 (2010).

[94] K. Konishi, H. Kokame, and N. Hara, *Stability analysis and design of amplitude death induced by a time-varying delay connection*, Phys. Lett. A **374**, 733–738 (2010).

[95] W. Zou, D. V. Senthilkumar, Y. Tang, Y. Wu, J. Lu, and J. Kurths, *Amplitude death in nonlinear oscillators with mixed time-delayed coupling*, Phys. Rev. E **88**, 032916 (2013).

2

Collective dynamics of delay-coupled phase oscillators in a frustrated geometry

Frustration is generated by the competition of different kinds of interaction and/or by the topological constraints. The concept of frustration was first introduced in spin systems by G. Toulouse [1] and J. Villain [2] in 1977 to describe a situation where a spin (or a number of spins) in the system cannot find an orientation to fully satisfy all the interactions with its neighboring spins [3].

Frustration arising when the topological constraints prevent the simultaneous minimization of the energy of all the interacting pairs of sub-units of a system, is known as “Geometric frustration”. A well known example is that of three Ising spins that are anti-ferromagnetically coupled to each other and placed on the corners of an equilateral triangle (Fig. 2.1). It is impossible to arrive at a configuration where each pair of

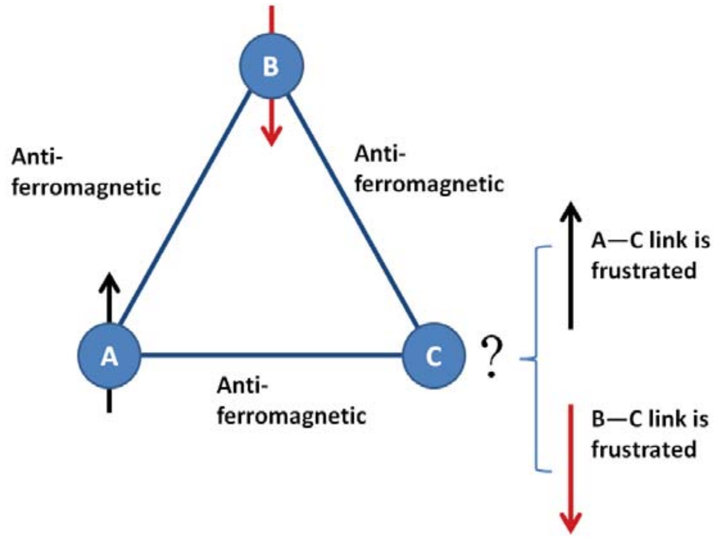

Figure 2.1: Example of a frustrated system: anti-ferromagnetically coupled Ising spins on the corners of an equilateral triangle.

spins is anti-parallel, and as a consequence the system continually flips between different states in trying to find a minimum energy state and thereby displays a multi-stable behavior. A large lattice model consisting of such triangular units can therefore lead to high ground state degeneracy and multiple phase transitions with increasing temperature [3]. In complex systems, frustration can arise from a combination of geometry and the nature of interaction among the subsystems, and it can give rise to a rich variety of collective behavior. Frustration plays an important role in the dynamics of many complex magnetic systems such as spin liquids, spin glasses, and a host of magnetic alloys [3–5]. Real magnetic materials are often frustrated due to several kinds of interactions. More recently, geometrical frustration arising in neuronal networks has also been recognized as a pivotal factor influencing the cortical dynamics of the brain, and it is believed to be responsible for introducing metastability and variability in the brain's collective states [6, 7]. The existence of metastability (or multiple operating regimes) is an essential and crucial feature for biological systems since it provides them with functional flexibility.

Frustration and its dynamical consequences are therefore receiving a great deal of theoretical and experimental attention in a wide variety of physical [8–10] and biological systems [11, 12]. Some such natural and synthetic systems, where geometric frustration plays an important role, are colloids [8], proteins [13], and liquid crystals [14]. A very recent application of geometric frustration is in acoustic channel lattices [15], where it can be harnessed to form band gaps.

The intimate relation between frustration, nature of interaction, and network topology has been well established through many past studies. When repulsive coupling is implemented in certain geometrical configurations, it can result in frustration. Some of the common topologies that lead to frustrated networks are triangular lattices [16], hexagonal lattices, and more exotic configurations such as the Kagome lattice [17]. Repulsive coupling is present in many real life systems, particularly in biological networks. An example is that of gene circuits consisting of a few genes which mutually repress each other so as to stabilize the oscillations of their protein concentrations [18]. The introduction of repulsive coupling in an oscillator network can have a significant influence on its collective dynamics such as in the manner and the rate of synchronization [19, 20] as well as in the stability properties of its synchronized states [21]. It has been shown, for example, that synchronization in neuronal oscillators can be improved by a combination of excitatory and inhibitory synaptic interactions [19, 22, 23]. The physical consequence of a repulsive coupling between two oscillators is to push them towards an out-of-phase behavior with respect to each other. Such an anti-phase synchronization has been experimentally observed in electrically coupled biological neurons that are repulsively coupled [24].

Our model investigation is carried out on a system of repulsively coupled phase oscillators that are configured in a frustrated geometry. The concept of frustration in oscillatory systems was first introduced by Daido [25]. Later, Zanette investigated frustration in systems of phase oscillators with undirected attractive and repulsive interactions [21]. He quantitatively characterized frustration in such systems in the absence of time-delayed interactions. Recently, Kaluza et al. [26] studied frustration in directed networks and excitable and oscillatory systems. It was shown that frustration in these systems can lead to a considerable increase in the number of stationary states and to multistability. Subsequent studies include the investigation of order-by-disorder in such frustrated oscillator systems in the presence of additive and multiplicative noise [16].

One of the important factors that can influence the collective dynamics of a complex network is the presence of time delay in the coupling between the network nodes or between individual functional elements of the network. As discussed in Chapter 1, time delay can significantly impact synchronization and other collective behavior in non-frustrated systems, and therefore it is of interest to investigate its influence on the dynamics of frustrated systems. The present chapter is devoted to such a study and is motivated by its potential utility in diverse practical applications.

The chapter examines in a quantitative manner the variations induced in the amount of frustration in a given system as a function of time delay in the coupling. For our study, we have considered three geometrical configurations that are representative of frustrated networks, namely a simple triangle, a triangular lattice with six nodes, and a hexagonal 4×4 lattice. Each node in these configurations is populated by a Kuramoto phase oscillator and the links representing the interaction between the oscillators are repulsive in nature with an intrinsic time delay τ. Our principal findings are that time delay can significantly influence the amount of frustration in a system and thereby control the number and nature of the equilibrium states of the system. For an amount of delay beyond a critical value, the system can transit to an in-phase collective state − an equilibrium condition that is normally not possible for frustrated configurations. The transition to such a synchronous state is found to occur with a characteristic behavior akin to first-order phase transitions. We also find that the variation of frustration as a function of the product of time delay and the collective frequency of the system follows a similar pattern for all three systems studied, which is suggestive of a universal scaling behavior.

The chapter is organized as follows. In Sec. 2.1, we present our model equations. Then we quantify frustration by introducing a frustration parameter that is a function of the time-delayed phase differences between the oscillators. In Sec. 2.2, we study the variation of this frustration parameter as a function of coupling delay in a system of three coupled oscillators repulsively linked to each other in a triangular configuration. We next study, in Sec. 2.3, a system of six oscillators repulsively linked in a configuration that encloses a triangle within a triangle. The study is further extended to a triangular 4×4 lattice of oscillators in Sec 2.4. We discuss our findings and conclude in Sec. 2.5.

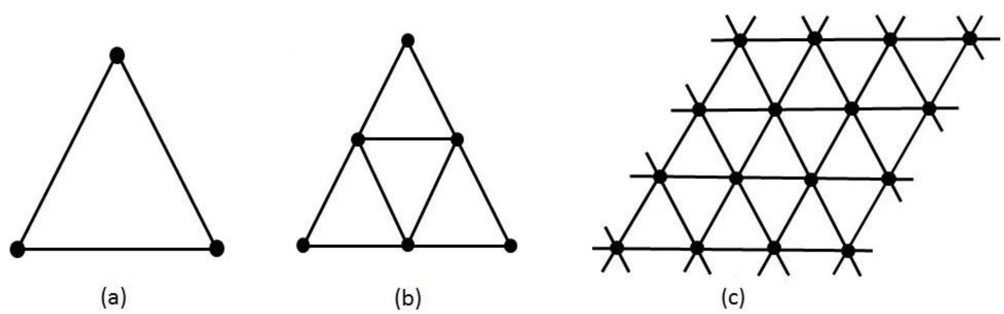

Figure 2.2: Frustrated systems of oscillators. Circles on the vertices represent phase oscillators and the edges represent repulsive coupling links between the oscillators.

2.1 The Model

We consider a network of N delay coupled phase oscillators with the dynamics of their phases ϕ_i governed by the equations:

$$\frac{d\phi_i(t)}{dt} = \omega_i + \frac{\kappa}{\nu_i} \sum_j A_{ij} \sin\left[\phi_j(t-\tau) - \phi_i(t)\right]. \tag{2.1}$$

Here ω_i is the natural frequency of the i-th oscillator, κ is the coupling strength, τ is the time delay in the interactions between the oscillators, and ν_i denotes the number of neighbors to which the i-th unit is connected. A_{ij} is the adjacency matrix with $A_{ii} = 0$, $A_{ij} = 1$ if $i \neq j$ and units i and j are connected, otherwise $A_{ij} = 0$. The initial phases, $\phi_i(0)$, of the oscillators are selected randomly from the interval $[0, 2\pi]$. We consider the oscillators to be identical, therefore we set $\omega_i = \omega$ and the coupling between the oscillators is nearest neighbor only. Since we are primarily interested in the dynamics of repulsively coupled oscillators, we take $\kappa = -|\kappa|$ unless otherwise stated.

In the case of phase-repulsive coupling, each pair of oscillators tries to attain the maximum phase difference of π. However, the topology of certain networks does not allow it, resulting in frustration. Previously, Zoran Levnajić investigated the collective dynamics of phase-repulsive oscillators for various network sizes and topologies in absence of time-delayed interactions [27]. He defined the global frustration F of the network as the average of the frustration of individual link between each pair of oscillators:

$$F = \frac{1}{L} \sum_{i>j} A_{ij} f_{ij}, \tag{2.2}$$

where L is the number of links or connections between the nodes of the network and f_{ij}

is the link frustration between i^{th} and j^{th} nodes/oscillators, defined as

$$f_{ij} = 1 + \cos(\phi_j - \phi_i). \tag{2.3}$$

If two oscillators synchronize anti-phase, then the repulsive link between them is not frustrated and $f_{ij} = 0$. Whereas, if the oscillators are forced to synchronize in-phase, the link between them becomes maximally frustrated with $f_{ij} = 2$.

Since we are interested in the dynamics of networks with time-delayed interactions, we define the frustration in such systems as

$$F = 1 - \frac{1}{\sum_i \nu_i} \frac{\kappa}{|\kappa|} \sum_{i,j=1}^{N} A_{ij} \cos\left[\phi_j(t-\tau) - \phi_i(t)\right], \tag{2.4}$$

where we have added the quantity 1 on the right hand side so that $F = 0$ defines the no frustration state. From (2.4) it is evident that $0 \leq F \leq 2$, where $F = 0$ corresponds to non-frustrated systems and $F = 2$ corresponds to maximally frustrated systems. In the absence of delay ($\tau = 0$), the definition of our frustration parameter reduces to the global frustration defined in Eq. (2.2) [21, 27]. Next, we explore the dynamics of some frustrated networks and investigate the role of time delay in influencing that dynamics.

2.2 Three oscillators

We first consider a system of three repulsively coupled oscillators linked in a triangular configuration (Fig. 2.2(a)). The dynamical equations (2.1) then reduce to:

$$\dot{\phi}_{i=1,2,3} = \omega + \frac{\kappa}{2} \sum_{j=1, j\neq i}^{3} \sin\left[\phi_j(t-\tau) - \phi_i(t)\right]. \tag{2.5}$$

2.2.1 Equilibrium states and their stability

In the absence of time delay, when the coupling between the oscillators is attractive, i.e., $\kappa > 0$, the oscillators can synchronize in-phase, whereas repulsively coupled ($\kappa < 0$) oscillators try to maximize the phase difference between them and synchronize to a state where there is a finite phase difference between them. In the simplest case of two repulsively coupled oscillators, they always synchronize in an anti-phase state with a phase difference of π between them. For three repulsively coupled oscillators (Fig. 2.2(a)), all the pairs of oscillators cannot simultaneously attain a phase difference of π. The equilibrium state of this system is one in which all the oscillators are frequency-synchronized with a phase difference of $\Delta\Phi = 2\pi/3$ along each link. The presence of time delay in the coupling can significantly change this simple picture. It can make the in-phase synchronous state as well as the out-of-phase synchronous state stable for both attractively coupled as well as repulsively coupled oscillators, depending upon the choice of time delay and other parameters.

A generalized stability criterion for the in-phase synchronous state in networks of identical phase oscillators with delayed sinusoidal coupling has been derived by Earl and Strogatz [28] to be

$$\kappa \cos(\Omega_{in}\tau) > 0, \tag{2.6}$$

where the collective frequency Ω_{in} of the in-phase synchronous state is given by

$$\Omega_{in} = \omega - \kappa \sin(\Omega_{in}\tau). \tag{2.7}$$

This stability condition holds for any network in which all the oscillators have the same number of connections (i.e., $\nu_i = \nu$), independent of all other details of its topology.

Using this criterion, we can deduce that when the coupling between the oscillators is repulsive (i.e., $\kappa = -|\kappa|$), the in-phase state is stable for $\left(2n + \frac{1}{2}\right)\pi < \Omega_{in}\tau < \left(2n + \frac{3}{2}\right)\pi$ such that $n = 0, 1, 2, 3, ...$, and when the coupling between the oscillators is attractive (i.e. $\kappa = |\kappa|$), the in-phase state is stable for $2n\pi \leq \Omega_{in}\tau < \left(2n + \frac{1}{2}\right)\pi$ and $\left(2n + \frac{3}{2}\right)\pi < \Omega_{in}\tau \leq (n+1)\,2\pi$.

For a state with a finite phase difference between the oscillators, a generalized stability analysis has been carried out by D' Huys et al. [29], who considered the phase-locked solutions of a ring of bi-directionally coupled oscillators. The phase-locked state can be characterized as,

$$\phi_m(t) = \Omega t + m\Delta\Phi, \tag{2.8}$$

where $m = 1, ..., N$ and $\Delta\Phi = 2j\pi/N,\ j \leq N/2$. The collective frequency Ω of this state is obtained from the expression

$$\Omega = \omega - \kappa \sin(\Omega\tau)\cos(\Delta\Phi). \tag{2.9}$$

To determine the stability of these phase-locked solutions, D' Huys et al. [29] performed a linear stability analysis and obtained the following equation for the eigenvalue λ:

$$\begin{aligned}\lambda = \kappa\cos\Delta\Phi\cos\Omega\tau \Bigg[-1 + e^{-\lambda\tau}\Bigg(&\cos\frac{2m\pi}{N} \\ &+ i\,\tan\Omega\tau\tan\Delta\Phi\sin\frac{2m\pi}{N}\Bigg)\Bigg].\end{aligned} \tag{2.10}$$

The above equation can be conveniently used to determine the stability of the phase-locked states for the simple systems of two coupled oscillators as well as our model of three coupled oscillators. The anti-phase synchronous state of two coupled oscillators corresponds to $\Delta\Phi = \pi$ and will only be stable when $\kappa\cos(\Omega\tau) < 0$, as discussed in

[29]. For three coupled oscillators, depending upon the choice of parameters and initial conditions, the stable equilibrium state of the system is either an in-phase synchronous state for which the phase difference is $\Delta\Phi = 0$ or an out-of phase state with $\Delta\Phi = 2\pi/3$. The collective frequency and the stability of the in-phase synchronous state are given by Eq. 2.7 and Eq. 2.6, respectively. The collective frequency Ω_{out} of the out-of-phase synchronous state is obtained by substituting $\Delta\Phi = 2\pi/3$ in Eq. 2.9, and it reads

$$\Omega_{out} = \omega + \frac{\kappa}{2}\sin(\Omega_{out}\tau), \tag{2.11}$$

and is stable when none of the eigenvalues obtained from Eq. 2.10 have a positive real part. Using these criteria, we have plotted in Fig. 2.3 the variation of the stable in-phase collective frequencies Ω_{in} (black solid lines) and stable out-of-phase collective frequencies Ω_{out} (red dashed lines) as functions of the delay parameter τ for a coupling strength $\kappa = -2$ and an intrinsic frequency $\omega = 6$. We note that for $\tau = 0$ one can only have an out-of-phase state, but beyond a certain value of τ an in-phase state can also become stable. There is also a small overlap region where both states are stable and the initial conditions would dictate the choice of the equilibrium state. The collective frequencies of both states decrease as a function of τ – the well-known phenomenon of frequency suppression that has been noted before for attractively coupled oscillators [30, 31].

2.2.2 Frustration analysis

As discussed above, the equilibrium state in the absence of time delay for the present case of three repulsively coupled Kuramoto oscillators is one in which the phase difference along each link is $2\pi/3$. Setting $\tau = 0$, $N = 3$, $\kappa = -2$, $\nu_i = 2$, and the phase

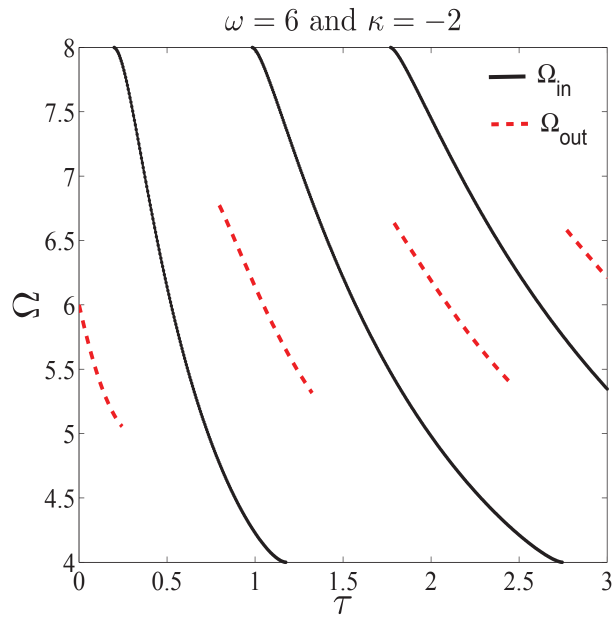

Figure 2.3: Plot of the stable collective frequencies Ω_{in} and Ω_{out} of the oscillators in the in-phase state (black solid line) and out-of-phase state (red dashed line) as functions of the delay parameter τ.

differences to be $2\pi/3$ in (2.4), the frustration value for such a state is seen to be $F = 0.5$. In the presence of time delay, (2.4) shows that frustration can vary with τ. This variation of F with τ is plotted in Fig. 2.4(a) for various values of the intrinsic frequencies ω of the individual oscillators and for a fixed value of κ. In Fig. 2.4(b), we have plotted the variation of F with τ for various values of κ and a fixed value of ω. We see that in all cases F increases at first as a function of τ, but beyond a certain value of delay, which changes for different values of ω and κ, there is a sudden drop in the value of F and thereafter it starts to decrease and eventually goes to zero such that the three oscillators become synchronized in-phase. The precipitous decrease in F beyond a critical value of τ is suggestive of a first-order phase transition phenomenon marking the evolution of the system from a finite phase-locked state to an in-phase synchronized state. Before the critical delay, the oscillators are in a phase-locked state with $\Delta\Phi = 2\pi/3$, and beyond the critical delay the oscillators are synchronized in-phase. This abrupt change in the relative phase between the oscillators at a critical delay is known as a phase-flip bifurcation [32] and is a general feature of time-delay coupled systems. This generic behavior is seen for all the values of ω plotted in Fig. 2.4(a), with the curves shifted from one another as a function of ω at a constant κ. Likewise in Fig. 2.4(b), the curves are shifted from one another as a function of κ at a fixed ω. However, the data of the shifted curves can be made to lie on a single universal curve if we plot F as a function of $\Omega\tau$ instead of τ as shown in Fig. 2.4(c). Note that data points representing the value of F for a particular set of ω and κ values that disappear beyond a value of $\Omega\tau$ on the left side of the curve continue their progress on the lower half of the right side curve, reflecting the trends seen in Figs. 2.4(a) and 2.4(b). This consolidated curve, which is common for all ω and κ values, provides a universal scaling behavior for the variation of the frustration parameter in a time delay coupled system of three Kuramoto oscillators configured in a frustrated triangular configuration. As we will shortly show, this scaling behavior continues to hold for even larger systems and different geometrical configurations and is thus of a universal nature.

The physical nature of this curve can be easily understood for the three-oscillator case from the expression for F given by (2.4). In the presence of time delay, the phase differences between the oscillators have two contributing factors: one is the phase shift of $2\pi/3$ because of the repulsive coupling, and other is the phase shift equivalent to $\Omega\tau$. It is the interplay between these two factors that governs the amount of frustration in the system and also determines the critical transition point. Analytic expressions for the universal curve can be easily obtained from the general expression for F given in (2.4) for the variation of frustration with $\Omega\tau$. As mentioned before, at $\tau = 0$, the oscillators have a phase difference of $\left(\phi_j(t) - \phi_i(t) = \pm 2\pi/3\right)$ between them and hence $F = 0.5$.

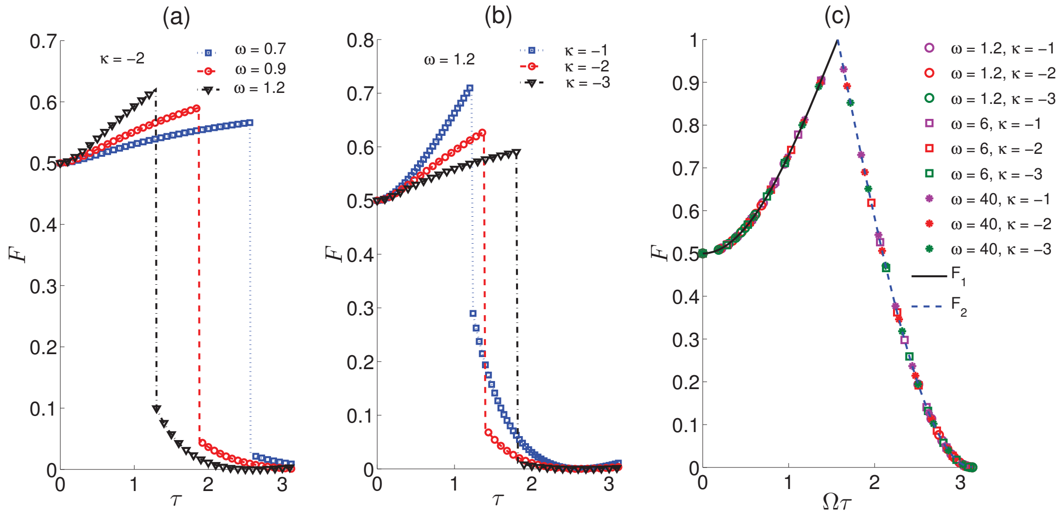

Figure 2.4: Plots showing the variation of the frustration parameter F as a function of the delay parameter. F is calculated using Eq. 2.4 from numerical solutions of Eq. 2.1 for the same set of initial phases for (a) three values of intrinsic frequency ω at fixed $\kappa = -2$, and (b) three values of coupling strength κ at fixed $\omega = 1.2$. (c) In this figure, F is plotted against the product of collective frequency Ω and delay parameter τ for various values of ω and κ and a given set of initial phases. Frustration values for different intrinsic frequencies as well as coupling strengths are seen to lie on a common curve given by F_1 and F_2, which are obtained from Eq. 2.12 and Eq. 2.13, respectively.

When we introduce delay, the time-delayed phase differences between the oscillators have another contributing factor of $\Omega\tau$, i.e., $\left(\phi_j(t-\tau) - \phi_i(t) = -\Omega\tau \pm 2\pi/3\right)$. Substituting these time-delayed phase differences in the expression of frustration (Eq. 2.4) gives one branch of the analytical curve that corresponds to the out-of-phase state (shown by the solid black line in Fig. 2.4(c)),

$$\begin{aligned} F_1 &= 1 + \frac{1}{2}\left[\cos\left(\frac{2\pi}{3} - \Omega\tau\right) + \cos\left(\frac{-2\pi}{3} - \Omega\tau\right)\right] \\ &= 1 - \frac{1}{2}\cos(\Omega\tau). \end{aligned} \tag{2.12}$$

At $\Omega\tau = \pi/2$, the frustration value reaches a maximum value of unity. Beyond $\Omega\tau = \pi/2$, the stability condition for the in-phase synchronous state, namely $\cos(\Omega\tau) < 0$, is satisfied and all the oscillators are now synchronized in-phase. The phase shift introduced by the repulsive coupling vanishes and F_1 is no longer a valid expression for determining the frustration values. Since the in-phase synchronous state corresponds to $\phi_j(t) = \Omega t$, the phase differences are $\phi_j(t-\tau) - \phi_i(t) = -\Omega\tau$, and we get the second half of the curve corresponding to the in-phase state (shown by the dashed blue line in Fig. 2.4(c)),

$$F_2 = 1 + \cos(\Omega\tau)\,. \tag{2.13}$$

F_2 decreases with an increase in $\Omega\tau$ and frustration becomes 0 at $\Omega\tau = \pi$. Therefore, the system is most frustrated at $\Omega\tau = \pi/2$ with $F = 1$ and is least frustrated at $\Omega\tau = \pi$ with $F = 0$. Beyond $\Omega\tau = \pi$, F increases monotonically till $\Omega\tau = 3\pi/2$ beyond which it starts decreasing until $\Omega\tau = 2\pi$. At $\Omega\tau = 3\pi/2$, the system transits from an in-phase state to an out-of-phase state. In other words, the behavior of F in the region $\pi < \Omega\tau < 2\pi$ is a mirror image of its behavior in the range $0 < \Omega\tau < \pi$. The behavior of frustration parameter F is 2π-periodic with respect to the product $\Omega\tau$. This is also apparent from the analytic expressions for the frustration parameter and the stability conditions for the in-phase and out-of-phase states, where $\Omega\tau$ always comes in the argument of sine or cosine, which are 2π-periodic.

To return to the analogy of a phase transition occurring at a critical value of $\tau = \tau_c$ where the precipitous drop in F is seen, it is instructive to look at the time evolution of F for various values of τ and for a fixed set of values of ω and κ. We find that as τ increases, the frustration parameter takes a longer and longer time to settle down to a constant value corresponding to the final equilibrium state. We denote the time after which the system settles down to the equilibrium state by t_{sat}. As τ approaches τ_c, this time increases in a resonant fashion and a graphical depiction of the saturation time as a function of τ is shown in Fig. 2.5. The functional behavior of t_{sat} can be closely represented by the following expression obtained from an analytical fit (solid line curve) to the numerical data points (red circles):

$$t_{sat} = t_{sat}\,|_{\tau=0} + \frac{\tau}{(\tau_c - \tau)^{\alpha}}. \tag{2.14}$$

In Fig. 2.5 we have $\omega = 40$, for which $\tau_c = 0.0389$ and α in the analytical fit curve is 1.188. The dashed line shows that $t_{sat} \to \infty$ as $\tau \to \tau_c$. As we will see, this algebraic behavior of the saturation time close to the critical value of the delay time is found in other frustrated configurations as well with a "critical index" that is greater than unity.

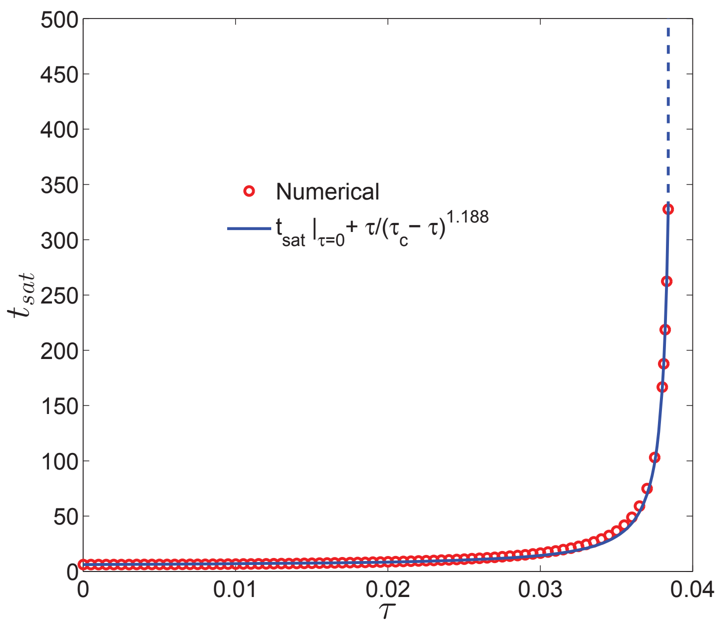

Figure 2.5: Numerical data points and analytical fit of the variation of the saturation time t_{sat} are plotted with time delay τ for a system of three repulsively oscillators for $\omega = 40$ and $\kappa = -2$, for which the critical time delay $\tau_c = 0.0389$.

2.3 Six oscillators

We next study the collective states of a network comprised of six phase-repulsive oscillators configured as shown in Fig. 2.2(b). Here oscillators are distinguishable in terms of the number of their nearest neighbors.

2.3.1 Frustration and equilibrium states

This configuration is one among a host of repulsive networks that can exhibit multiple final dynamical states characterized by different values of frustration, as discussed in [27]. The difference between the different frustration states generally lies in the competition between the constituent links in trying to minimize frustration by attempting to stretch to the maximal attainable phase difference. The final dynamical state of the system is decided by the choice of initial phases. In the absence of time delay, while the network of three oscillators studied in the previous section shows only one equilibrium state, the present configuration of six oscillators has two equilibrium states characterized by different values of the frustration parameter. In reference [27], the frustration values F for this network were computed for 10^4 different initial phases in the absence of time-delayed interactions. The author has reported that 42% of the initial phases resulted in the equilibrium state with $F = 0.5$, and for the remaining 58%, the system settled to an equilibrium state with $F = 0.5505$. In an equilibrium state, the oscillators are frequency-synchronized with phase-locked motion. The oscillators sharing the same phases are considered to form a cluster. The oscillators in different clusters have the same frequency but different instantaneous values of phases. The equilibrium state with $F = 0.5$ corresponds to the three-cluster pattern with two oscillators in each cluster. This is shown in Fig. 2.6(a), where the time evolution of the phases of all six oscillators are plotted together. The equilibrium state corresponding to $F = 0.5505$ exhibits the six-cluster pattern where the instantaneous values of individual phases of all six oscillators are different, and it is plotted in Fig. 2.6(b). The existence of multiple equilibrium states makes this system an interesting candidate to study how frustration evolves with time delay for different initial conditions for such systems.

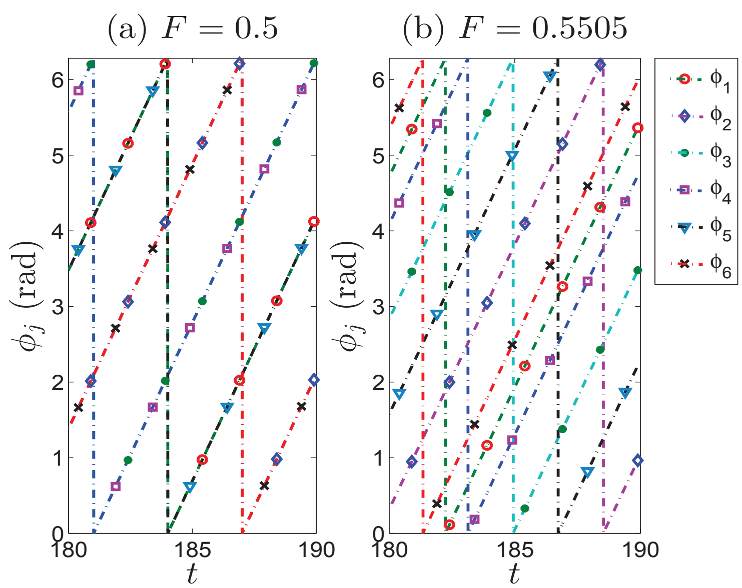

Figure 2.6: The phase patterns corresponding to the two equilibria of the six-oscillator network shown in Fig. 2.2(b) in the absence of time delay. In this figure, the phases of all six oscillators are plotted together. Part (a) is obtained from an initial condition that settles to the equilibrium state with $F = 0.5$. This equilibrium state corresponds to a three-cluster pattern such that there are two oscillators in each cluster, and the oscillators in same cluster share the same phase evolution. Part (b) is obtained from an initial condition whose equilibrium state corresponds to $F = 0.5505$. This equilibrium state has a six-cluster pattern, i.e., the instantaneous values of individual phases of all six oscillators are different. We have taken $\omega = 0.7$ and $\kappa = -2$ to get this figure.

We find that this six-oscillator network shows a similar tendency for the F vs τ and F vs $\Omega\tau$ variation as seen for the simpler three-oscillator system. In Fig. 2.7, we have plotted F against $\Omega\tau$. For some values of $\Omega\tau$, frustration F has two values. The value of F switches between these two values depending upon the choice of the initial phases. In the left half of Fig. 2.7, the lower curve corresponds to the three-cluster equilibrium state and the upper curve corresponds to the six-cluster equilibrium state. The universal scaling behavior, where the variation in frustration with $\Omega\tau$ is seen to lie on a common curve for all ω and κ values, holds for this six-oscillator configuration also. Even though the frustration for some values of $\Omega\tau$ depends on the choice of initial phases, for a given initial condition the frustration values for different intrinsic frequencies lie on the same curve. Just like the case with three coupled oscillators, the system is most frustrated at $\Omega\tau = \pi/2$ with $F = 1$ and non frustrated at $\Omega\tau = \pi$. The functional behavior of t_{sat}

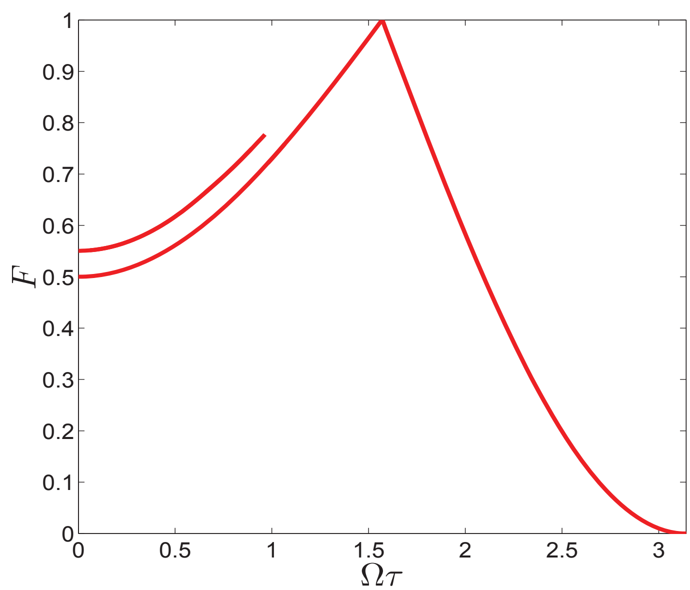

Figure 2.7: In this figure, F is plotted against the product of collective frequency Ω and delay parameter τ for the network of six oscillators. This system shows the existence of multiple equilibrium states characterized by different values of the frustration parameter for some values of delay, and therefore frustration F can have multiple values at some values of $\Omega\tau$. Depending on the choice of initial phases, the system can settle down to any of these equilibrium states.

for the lower branch of F variation with τ is similar to the three-oscillators system with

$\alpha = 1.325$ and $\tau_c = 0.0384$ in Eq. 2.14.

2.3.2 Basins of attraction

In Fig. 2.8, we have shown the variation in the sizes of the basin of attraction of different equilibrium states of the six-oscillator network with time delay parameter. The results have been obtained by evolving the system for 10^4 different initial phases. We find that in the absence of delay ($\tau = 0$), similar to the results obtained in [27], about 42% of the initial conditions settle to the equilibrium state with $F = 0.5$, and the remaining 58% settle down to the final state with $F = 0.5505$. When we introduce time delay, the value of the frustration parameter of these equilibrium states and the size of their basins, changes. For comparatively small values of time delay, the out-of-phase equilibrium state with higher value of frustration parameter has a larger basin of attraction. After a certain critical value of time delay, the in-phase state also becomes a stable state of the system, and therefore for some initial conditions, the system settles down to the in-phase state instead. Around this delay value, the basin of attraction of the equilibrium state with the lower value of F becomes larger than that of the equilibrium state with the higher value of F. With further increase in delay, the basin of attraction of the in-phase state increases, whereas the basin of attraction of the out-of-phase states decreases.

2.4 Triangular Lattice

We now investigate an extended network consisting of a triangular lattice formed by joining triangles along the edges thereby forming a multi-unit system whose basic unit cell is the system of three oscillators which we have studied in detail in section 2.2. We consider a 4×4 triangular lattice with a hexagonal coupling configuration as shown

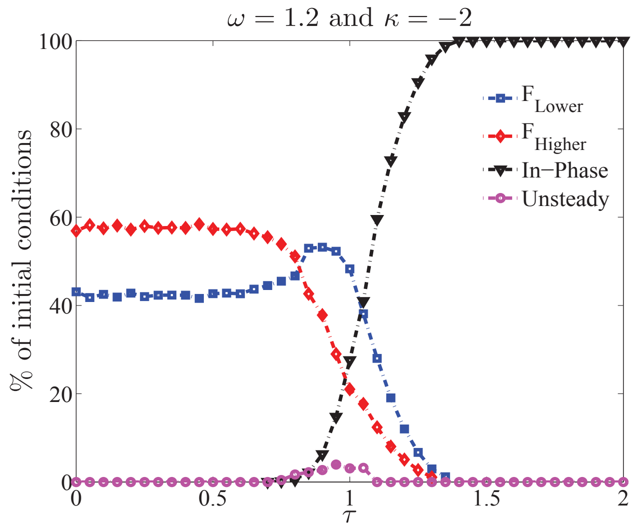

Figure 2.8: The blue dashed line with squares shows the percentage of initial phases that lead to equilibrium state with a lower value of F denoted by F_{Lower}. The red dashed line with diamonds shows the percentage of initial phases that lead to the equilibrium state with a higher value of F denoted by F_{Higher}. The black dashed line with triangles shows the percentage of initial phases that lead to the in-phase equilibrium state labeled by In-Phase, and the magenta dashed line with circles shows the percentage of initial conditions for which the system has not settled to any stable equilibrium state even for a very large time span ($t_{span} = 2000$ in simulations), and it is labeled as Unsteady.

in Fig. 2.2(c). Repulsive coupling in combination with the hexagonal coupling pattern turns all bonds into frustrated ones. Since frustration leads to the growth of the number of coexisting attractors, this system is highly multistable [16] even in the absence of time delay. Boundary conditions also play an important role in determining the final frustration states of the network.

2.4.1 Periodic boundaries

When the boundaries are periodic, then each oscillator has the same number of nearest neighbors ($\nu_i = 6$ in Eq. 2.1). When the interactions between the oscillators are instantaneous ($\tau = 0$), the system exhibits a variety of cluster patterns [16] but never goes to a single cluster state where all the oscillators are synchronized in-phase. Upon introducing time delay in the coupling between the oscillators, they are able to synchronize in-phase when time delay exceeds a critical value. Starting from the same set of initial phases if we keep on varying the value of the delay parameter τ, the cluster pattern exhibited by the system also varies as shown in Fig. 2.9. Beyond a certain value of delay, all the oscillators are synchronized in-phase into a single cluster. Since this system is highly multistable even in the absence of delay, the system can go to different cluster states at a given value of delay for different choices of initial conditions. Hence the critical value of delay at which the system first goes to the single cluster state can also be different depending upon the choice of initial conditions. The collective frequency of the in-phase state and its stability condition obey the same expressions (Eq. 2.7 and Eq. 2.6 respectively) as the system of three coupled oscillators. The phase-locked equilibrium states exhibiting different cluster patterns at a given value of $\Omega\tau$ correspond to the same value of frustration parameter F. This network seems to have a unique value of frustration at each value of time delay parameter. In the absence of time delay, the value of frustration for this system is $F = 0.6667$. The variation of F with τ and $\Omega\tau$ is similar to the systems of three repulsively coupled oscillators. The universal scaling behavior continues to hold for the sixteen-oscillator triangular lattice, too (Fig. 2.10(a)).

2.4.2 Free boundaries

If the boundaries of the triangular lattice are free, then the oscillators are distinguishable in terms of the number of their nearest neighbors, unlike the lattice with periodic boundaries where each oscillator has six neighbors. Hence this system exhibits distinct equilibrium states corresponding to different values of frustration parameter F and

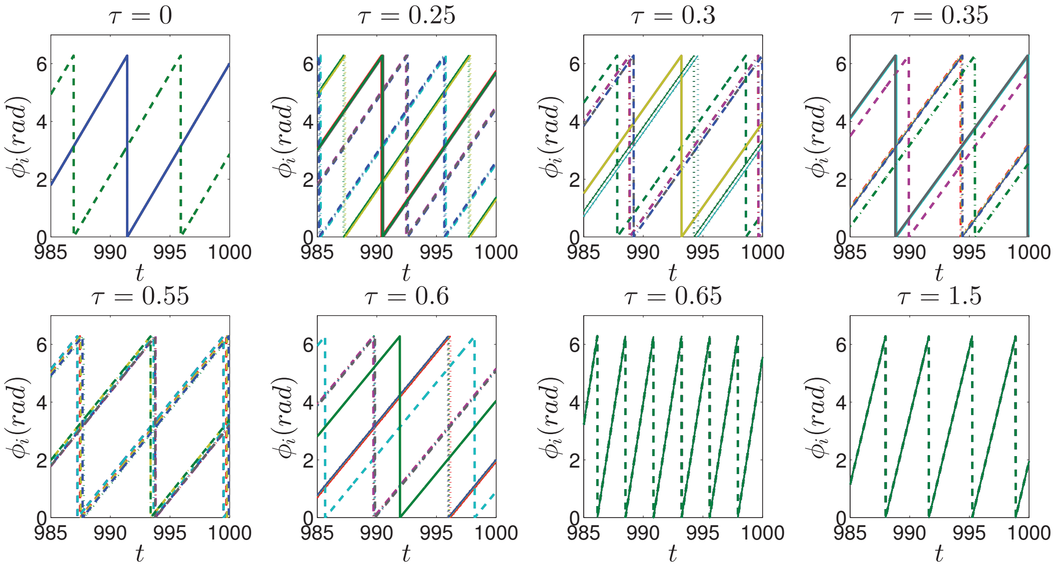

Figure 2.9: The figure shows the variation in the cluster pattern exhibited by the 4×4 lattice of repulsively coupled oscillators with change in the time delay parameter τ for a given set of initial phases. At a certain value of delay, the system starts exhibiting the single cluster in-phase state. The collective frequency of the in-phase state decreases with further increase in delay. We have taken $\omega = 0.7$ and $\kappa = -2$.

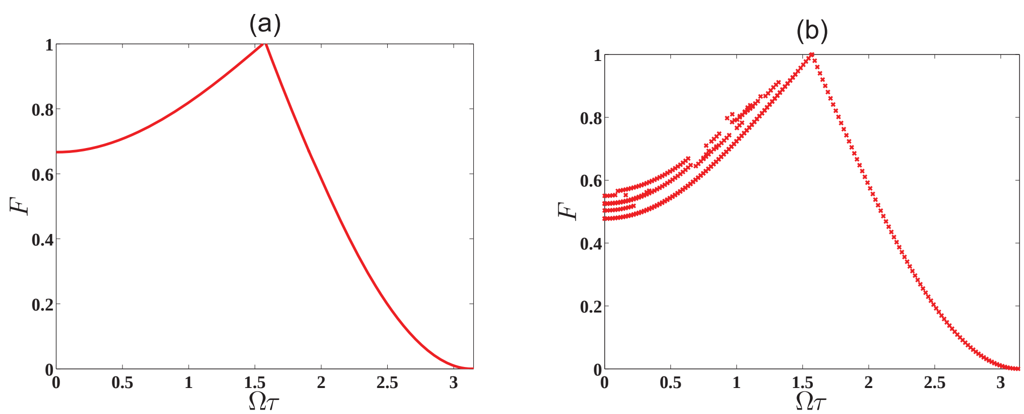

Figure 2.10: This figure shows the universal scaling behavior in the variation of F with the product of collective frequency Ω and delay parameter τ for 4×4 triangular lattice with (a) periodic boundaries, and (b) free boundaries.

cluster patterns. In the absence of delay ($\tau = 0$), the system exhibits five equilibrium states – S_1, S_2, S_3, S_4, and S_5 – with corresponding frustration values $F(S_1) = 0.4779$,

$F(S_2) = 0.5037$, $F(S_3) = 0.5249$, $F(S_4) = 0.5263$, and $F(S_5) = 0.5502$, respectively. The histogram plotted in Fig. 2.11 shows the sizes of the basin of attraction of these equilibrium states for 10^3 initial conditions. The equilibrium state S_1, with $F(S_1) = 0.4779$, has the largest basin of attraction. In the presence of time delay, similar to the six-oscillator network presented in the previous section, this system also exhibits multiple equilibrium states characterized by different values of frustration for some values of τ or $\Omega\tau$, as shown in Fig. 2.10(b). The universal scaling behavior continues to hold. The system can switch between these equilibria, corresponding to the different F values, depending upon the choice of initial phases. For each value of time delay, we have obtained the values of frustration parameter by evolving the system for 500 different initial conditions. In addition to the equilibrium states shown in Fig. 2.10(b), there might be other equilibrium states also but with the basins of attraction so small that it becomes extremely difficult to observe them numerically.

2.5 Summary and Discussion

In this chapter we have studied the effect of time-delayed coupling on the collective dynamics of various frustrated systems of repulsively coupled Kuramoto phase oscillators. For our study, we have chosen three typical frustrated configurations, namely (i) a set of three oscillators in a triangular configuration that represents the simplest possible two-dimensional frustrated geometry, (ii) a set of six oscillators configured as a triangle within a triangle that presents a slightly more complex geometry and, (iii) a set of sixteen oscillators in a hexagonal lattice geometry representing a generalization of the basic triangular configuration of three oscillators. The three configurations also have distinctly different characteristics in the absence of time delay, e.g., (i) has a single equilibrium state with a unique value of the frustration parameter, (ii) has two equilibrium states (and

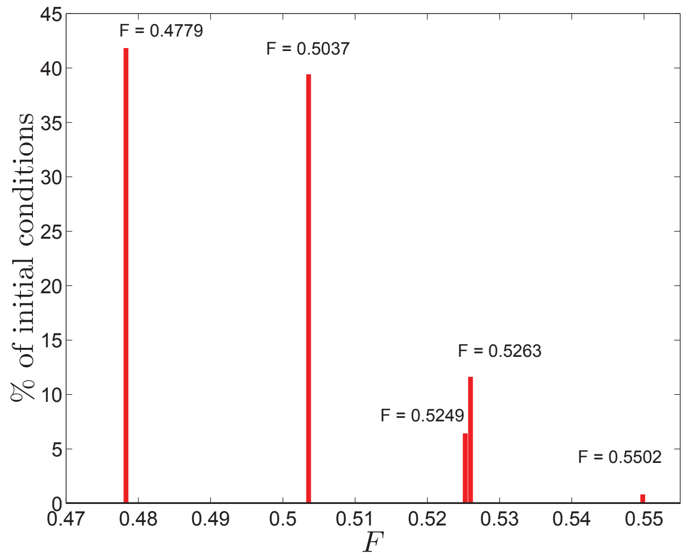

Figure 2.11: Histogram showing the sizes of the basins of attraction of the equilibrium states of 4×4 lattice with free boundaries for 10^3 initial conditions in the absence of time delay.

hence two different frustration values) that the system can go to depending upon the initial conditions, and (iii) has multiple frustration states when open-boundary conditions are applied to the lattice, and hence it displays multistable behavior that is dependent on the initial conditions. We study the dynamical behavior of these prototypical systems by a quantitative investigation of a suitably defined generalized frustration parameter that is a function of the time delay. Our numerical investigations reveal a generic behavior in all the systems where we observe that the frustration parameter initially increases with delay and then precipitously falls after a critical value to a much lower value and then decays to zero, thereby transitioning to an in-phase synchronous state. Thus the presence of a time delay in the coupling that is larger than a critical value removes a basic constraint of frustrated systems and permits them to attain a synchronous state. This happens due to the interplay between the phase-difference contributions arising from the geometry and the time delay. We also find that this behavior can be characterized by a single universal curve representing the variation of F with the product of the collective frequency Ω of the synchronous state and the time delay parameter τ. The curve is common for all values of natural frequencies ω of the individual oscillators as well as the coupling strength κ between the oscillators. An analytic description of this curve is given for three coupled oscillators. The nature of the transition is seen to have the characteristics of a first-order phase transition whose behavior near the transition point can be expressed in terms of an algebraic relation that has a "critical exponent" that is larger than (but close to) unity.

The universal scaling behavior of F with $\Omega\tau$ that holds for all three systems is the most significant finding of our investigation and underscores the important role that time delay can play in the dynamics of frustrated systems. In particular, it shows that time delay can serve as a tuning parameter to steer the system towards different values of the frustration parameter and hence to different collective multistable states. This property can be exploited in physical systems in which time delay can be varied by changing the media characteristics to change the speed of signal propagation. In biological systems, e.g., in neuronal networks where frustration and time delay are coexistent, our results may prove useful in gaining a better understanding of their underlying dynamical behavior. A possible application of our work can be in vertebrate segmentation. Vertebrate segmentation has been successfully modeled using the Delayed Coupling Theory (DCT) [33], a phase oscillator model with discrete delays. The DCT models the patterns of cyclic gene expression on the tissue level by a system of two-dimensional hexagonal lattice of phase oscillators, which is often frustrated. In the DCT, discrete delays in the coupling function account for the communication delays due to finite signal transmission time in complex biochemical signaling pathways. Since this system has hexagonal coupling configuration and communication delays, it would be really interesting to do a systematic frustration analysis by applying DCT and our definition of frustration F using the experimentally obtained parameters (such as given in [34]) to study how frustration relates to and influences the spatiotemporal dynamics of vertebrate segmentation.

Bibliography

[1] G. Toulouse, *Theory of the frustration effect in spin glasses*, Commun. Phys. **2**, 115 (1977).

[2] J. Villain, *Spin glass with non-random interactions*, J. Phys. C **10**, 1717 (1977).

[3] H. T. Diep, ed., *Frustrated Spin Systems* (World Scientific, Singapore, 2004).

[4] C. Lacroix, P. Mendels, and F. Mila, eds., *Introduction to Frustrated Magnetism: Materials, Experiments, Theory* (Springer, 2011).

[5] I. Gilbert, C. Nisoli, and P. Schiffer, *Frustration by design*, Physics Today **69**, 54–59 (2016).

[6] L. L. Gollo and M. Breakspear, *The frustrated brain: from dynamics on motifs to communities and networks*, Phil. Trans. R. Soc. B **369**, 20130532 (2014).

[7] L. L. Gollo, A. Zalesky, R. M. Hutchison, M. van den Heuvel, and M. Breakspear, *Dwelling quietly in the rich club: brain network determinants of slow cortical fluctuations*, Phil. Trans. R. Soc. B **370**, 20140165 (2015).

[8] Y. Han, Y. Shokef, A. M. Alsayed, P. Yunker, T. C. Lubensky, and A. G. Yodh, *Geometric frustration in buckled colloidal monolayers*, Nature **456**, 898–903 (2008).

[9] N. Choudhury, L. Walizer, S. Lisenkov, and L. Bellaiche, *Geometric frustration in compositionally modulated ferroelectrics*, Nature **470**, 513–517 (2011).

[10] A. Ortiz-Ambriz and P. Tierno, *Engineering of frustration in colloidal artificial ices realized on microfeatured grooved lattices*, Nat. Commun. **7**, 10575 (2016).

[11] M. H. Jensen, S. Krishna, and S. Pigolotti, *Repressor lattice: feedback, commensurability, and dynamical frustration*, Phys. Rev. Lett. **103**, 118101 (2009).

[12] S. Krishna, S. Semsey, and M. H. Jensen, *Frustrated bistability as a means to engineer oscillations in biological systems*, Phys. Biol. **6**, 036009 (2009).

[13] B. G. Wensley, S. Batey, F. A. C. Bone, Z. M. Chan, N. R. Tumelty, A. Steward, L. G. Kwa, A. Borgia, and J. Clarke, *Experimental evidence for a frustrated energy landscape in a three-helix-bundle protein family*, Nature **463**, 685–688 (2010).

[14] X. Zeng, R. Kieffer, B. Glettner, C. Nürnberger, F. Liu, et al., *Complex multicolor tilings and critical phenomena in tetraphilic liquid crystals*, Science **331**, 1302–1306 (2011).

[15] P. Wang, Y. Zheng, M. C. Fernandes, Y. Sun, K. Xu, S. Sun, S. H. Kang, V. Tournat, and K. Bertoldi, *Harnessing geometric frustration to form band gaps in acoustic channel lattices*, Phys. Rev. Lett. **118**, 084302 (2017).

[16] F. Ionita, D. Labavić, M. Zaks, and H. Meyer-Ortmanns, *Order-by-disorder in classical oscillator systems*, Eur. Phys. J. B **86**, 511 (2013).

[17] M. Nixon, E. Ronen, A. A. Friesem, and N. Davidson, *Observing geometric frustration with thousands of coupled lasers*, Phys. Rev. Lett. **110**, 184102 (2013).

[18] E. Ullner, A. Zaikin, E. I. Volkov, and J. García-Ojalvo, *Multistability and clustering in a population of synthetic genetic oscillators via phase-repulsive cell-to-cell communication*, Phys. Rev. Lett. **99**, 148103 (2007).

[19] I. Leyva, I. Sendiña-Nadal, J. A. Almendral, and M. A. F. Sanjuán, *Sparse repulsive coupling enhances synchronization in complex networks*, Phys. Rev. E **74**, 056112 (2006).

[20] T. V. Martins and R. Toral, *Synchronisation induced by repulsive interactions in a system of van der Pol oscillators*, Prog. Theor. Phys. **126**, 353–368 (2011).

[21] D. H. Zanette, *Synchronization and frustration in oscillator networks with attractive and repulsive interactions*, Europhys. Lett. **72**, 190–196 (2005).

[22] N. Kopell and B. Ermentrout, *Chemical and electrical synapses perform complementary roles in the synchronization of interneuronal networks*, Proc. Natl. Acad. Sci. U. S. A **101**, 15482–15487 (2004).

[23] M. Bartos, I. Vida, and P. Jones, *Synaptic mechanisms of synchronized gamma oscillations in inhibitory interneuron networks*, Nat. Rev. Neurosci. **8**, 45–56 (2007).

[24] R. C. Elson, A. I. Selverston, R. Huerta, N. F. Rulkov, M. I. Rabinovich, and H. D. I. Abarbanel, *Synchronous behavior of two coupled biological neurons*, Phys. Rev. Lett. **81**, 5692 (1998).

[25] H. Daido, *Quasientrainment and slow relaxation in a population of oscillators with random and frustrated interactions*, Phys. Rev. Lett. **68**, 1073 (1992).

[26] P. Kaluza and H. Meyer-Ortmanns, *On the role of frustration in excitable systems*, Chaos **20**, 043111 (2010).

[27] Z. Levnajić, *Emergent multistability and frustration in phase-repulsive networks of oscillators*, Phys. Rev. E **84**, 016231 (2011).

[28] M. G. Earl and S. H. Strogatz, *Synchronization in oscillator networks with delayed coupling: a stability criterion*, Phys. Rev. E **67**, 036204 (2003).

[29] O. D'Huys, R. Vicente, T. Erneux, J. Danckaert, and I. Fischer, *Synchronization*

properties of network motifs: Influence of coupling delay and symmetry, Chaos **18**, 037116 (2008).

[30] S. Kim, S. H. Park, and C. S. Ryu, *Multistability in coupled oscillator systems with time delay*, Phys. Rev. Lett. **79**, 2911 (1997).

[31] E. Niebur, H. G. Schuster, and D. M. Kammen, *Collective frequencies and metastability in networks of limit-cycle oscillators with time delay*, Phys. Rev. Lett. **67**, 2753 (1991).

[32] A. Prasad, J. Kurths, S. K. Dana, and R. Ramaswamy, *Phase-flip bifurcation induced by time delay*, Phys. Rev. E **74**, 035204(R) (2006).

[33] L. G. Morelli, S. Ares, L. Herrgen, C. Schröter, F. Jülicher, and A. C. Oates, *Delayed coupling theory of vertebrate segmentation*, HFSP J. **3**, 55–66 (2009).

[34] L. Herrgen, S. Ares, L. G. Morelli, C. Schröter, F. Jülicher, and A. C. Oates, *Intercellular coupling regulates the period of the segmentation clock*, Current Biology **20**, 1244–1253 (2010).

3

A dynamical framework to relate perceptual variability with multisensory information processing

Multisensory signals seamlessly enrich our knowledge of the world [1]. For example, while driving a car or attending to a vocalizer in a noisy background we cannot rely on only one sensory modality, be it visual or auditory, rather a harmonious interaction of visual and somatosensory or visual and auditory systems is required. In recent years, multisensory nature of perception has been the focus of much behavioral and neuroscientific research [2]. Merging information from different senses confers distinct behavioral advantages, for example, identification of audio-visual (AV) objects is more rapid [3] than with unimodal stimuli [4–9], especially when the signals are ambiguous [10–14]. To realize these advantages, the brain continually coordinates sensory inputs across the audiovisual [15–18], visual-tactile [19–22], and audio-somatic [23] domains and combines them into coherent perceptual objects. However, operational principles of how environmental and neural variables modulate multisensory processing underlying perception are poorly understood [24]. In this chapter we propose a theoretical framework that explains the empirical observations from a paradigmatic framework widely acknowledged to be an entry point in studying multisensory processes.

An experimental realization of the underlying complexity involved in multisensory processing is captured by the "McGurk-effect", where incongruent auditory and visual stimuli elicit the perception of illusory speech sounds. In 1976, McGurk and MacDonald [25] demonstrated that the sound of articulating /pa when superimposed on a video of lip movement during articulation of /ka, resulted in an illusory experience of /ta for the perceiver. Similar triads were also reported, such as, auditory /ba and visual /ga resulted in the perception of /da. Several researchers have used this paradigm to study the key behavioral and neural variables that can modulate perception [26–28]. Ambiguity in one of the sensory streams, arising from noisy stimuli, affects the neuronal processing of multisensory stimuli [26]. For example, adding white noise to the auditory stimuli resulted in an enhanced functional connectivity between the visual cortex and the posterior superior temporal sulcus (pSTS), a brain area populated with multisensory neurons [26]. On the other hand, an increase in ambiguity of visual stimuli (e.g., blurry video) resulted in an enhanced functional connectivity between auditory cortex and pSTS. The relative timing of different sensory input signals is another important factor in multisensory information processing [27, 29]. Temporal proximity is a critical determinant for cross-modal integration by multisensory neurons [2, 30]. For instance, the audiovisual integration of speech breaks down if the asynchrony between the visual lip movements and the auditory speech sounds becomes too long [16, 20, 27, 29, 31]. However, a large temporal window exists over which successful integration may occur [27, 32–34]. The

McGurk illusion, for example, persists even when the visual information leads (by up-to 240 ms), or lags (by up-to 60 ms) the auditory input [27, 29]. In fact, Munhall and colleagues reported that the peak of illusory response happens when the visual stimulus leads the auditory stimulus by 180-200 ms [27]. One possible explanation proposed for this asymmetrical range of temporal synchrony refers to the natural timing relations between the audio and visual events in the real world. Since the visible byproducts of speech articulation, including posturing and breath, almost always occur before acoustic output, Grant et al. [35] suggested that the human perceptual system might have adapted its processing to anticipate and tolerate multisensory events where visual input leads auditory input while maintaining the perception that the two events are bound together.

One important component not much explored in the literature is that of an integrative framework/model that can elucidate the dynamic interactions among the environmental and neural variables underlying multisensory processing of stimuli that shapes perception. The existing computational modeling literature addresses the spatial and temporal integration of incoming multisensory stimuli either at the behavioral level or at the neural level [36–42]. Typically most models have three components, two unisensory and one multisensory. They attempt to address the integration mechanisms either at the level of single units or populations at the neural level (inspired by the presence of multisensory neurons) [43] for constructing a model. Nonetheless, the modeling approaches can be broadly classified into two classes. A Bayesian framework was used by some researchers to explain how unisensory streams of audition and vision can integrate to facilitate perception by solving the spatial localization problem [36, 37]. The second approach uses dynamic models of underlying neural systems that can be further subdivided into two subclasses. The first subclass is that of biologically inspired models of neural dynamics, proposed to understand the role of predictive coding [38] as well as spatial and temporal aspects of multisensory processing [39, 42]. For a review on neurocomputational approaches to modeling multisensory integration in the brain, see [44]. The second subclass uses minimal models with least amount of parameters and variables to identify the key variables affecting the dynamic changes in behavior. For non-speech sounds and multisensory processing, a dynamic model was introduced by Dhamala and colleagues [34] that explained the phenomenon of drift for slightly asynchronous audio-visual stimuli. The study presented in this chapter incorporates the key environmental variables affecting the McGurk paradigm in a minimal model to understand their relationships with neurally relevant parameters such as the connectivity between the unisensory and multisensory systems and their potential role in oscillatory brain dynamics.

Electrophysiological signals can be conceptualized into patterned oscillations and decomposed into five frequency bands that are physiologically meaningful, delta ($0.5-3.5$ Hz), theta ($4-7$ Hz), alpha ($8-12$ Hz), beta ($13-30$ Hz), and gamma (> 30 Hz) [45]. Beta band power is enhanced in fronto-parietal areas in trials where subjects perceive McGurk illusion accompanied by a reduction in theta power [28]. In general, beta band synchronization has been associated with audio-visual stimulus perception [46]. Phase synchrony and phase modulation of oscillations across the different frequency bands have been suggested to play a key role in the organization of cortical networks engaged in complex cognitive functions such as speech processing [47] and constitute a critical component of auditory-articulatory alignment [48]. There is a mounting evidence that the coherence of oscillatory neural signals across cortical areas might be a crucial mechanism involved in multisensory processing [45, 49–51]. Theta rhythms have been particularly associated with the auditory perception of syllabic speech [52]. A recent article emphasizes the role of coherence between lip movement and brain oscillations at low frequency for the intelligibility of speech stimuli [53]. Nonetheless, how perceptual categorization parametrically varies with the window of temporal integration and how oscillatory cortical activity observed by EEG/ MEG studies using the McGurk-paradigm [3, 28, 54] relates to perception, is unclear.

The Kuramoto model [55] of coupled phase oscillators is commonly used for constructing the theoretical models of neurobiological networks with oscillatory dynamics [56, 57]. In this model, the phase of an oscillation exhibited by any node of a network becomes the key variable of interest, affected by free parameters such as coupling/connectivity terms. Thus, each Kuramoto oscillator can depict the oscillatory state of a sub-network (e.g., sections of cortical columns), captured by its circular phase alone and the overall synchronization states can capture the collective dynamics of the network. A network of Kuramoto phase oscillators provides a dynamic framework to explain the functional connectivity changes in the brain electromagnetic data [58]. The original Kuramoto model and its extensions have been used to explore mechanisms underlying oscillations in the human cortex [56]. In this chapter we propose a dynamical model comprising of three coupled Kuramoto oscillators, coupled via electric coupling and time delay. Electric coupling captures the physiological constraints of the audio-visual system and time delay captures the environmental factor of temporal asynchrony [59]. Empirically such networks can be imaged non-invasively from EEG/ MEG studies [60]. As discussed in Chapter 1, the presence of time-delays enriches the attractor space of a dynamical system [61]. Our proposed model predicts the behavior of McGurk perceivers reported under ambiguous stimuli scenarios as well as during variation of AV onset lags. The rest of the chapter is organized as follows. In Sec. 3.1, we first present the behavioral experimental paradigm using McGurk-like stimuli where one can study the relationship between perceptual experience and psychophysical parameters such as audio-visual onset lags. Then we propose a theoretical model of multisensory perception using symmetry arguments. In Sec. 3.2, we present the results of the statistical analysis on the behavioral data and the analytical and numerical results of the dynamical model under various parameter set-ups. Finally in Sec. 3.3, we discuss the theoretical results in the context of the experimental paradigm and argue how this modeling framework captures the key features of complex multisensory integration processes and can potentially be helpful for explaining other experimental paradigms as well.

3.1 Methods

In the McGurk illusion, a unitary percept emerges as a result of the integration of clearly incongruent auditory and visual information. Hence, the formation of an illusory percept corresponds to successful integration and a construction of auditory, visual or other stimuli as percept corresponds to the breakdown of audio-visual integration. Therefore, the McGurk illusion permits one to quantify the degree of integration that has taken place by evaluating the percentage of illusory responses. The behavioral experimental study presented in 3.1.1 allows us to take advantage of the McGurk illusion to explore the temporal boundaries of AV integration in speech.

3.1.1 Experimental paradigm

The experiments were conducted in the National Brain Research Centre (NBRC), Haryana, India by our collaborators Arpan Banerjee and Abhishek Mukherjee.

3.1.1.1 Subjects and stimuli

Fifty-two healthy right-handed adult participants (25 female, 27 male) of age range 20-35 years (mean age = 24.5 years, SD = 3.12) participated in a behavioral study of duration of about 45 minutes. The undertaken study design was approved by Institutional Human Ethics Committee (IHEC), National Brain Research Centre (NBRC) and the study was carried out in accordance with the guidelines set by IHEC, NBRC and in strict adherence to the declaration of Helsinki. All participants provided written informed consent in a format approved by IHEC, NBRC and reported normal vision and hearing and no history of neurological disorders. 7 video stimuli, each of 2 seconds(s) duration were prepared, of which 6 were incongruent audio-visual objects where audio recordings of a human speaker vocalizing /pa were dubbed on the lip movements of vocalization /ka (/pa-/ka) and 1 was a congruent audio-visual object /ta (/ta-/ta). The gap in the onset of auditory and visual streams was varied from -300 to 450 ms in steps of 150 ms in the 6 incongruent videos. Negative sign implies that the auditory stimulus onset preceded the lip movement onset and positive implies that lip movement starts before the sound. An asymmetric range of AV lags was chosen for incongruent trials, because a previous study by Munhall and colleagues [27] reported that the dominance of illusory perception was skewed towards positive lags where the start of lip movement precedes sound onset. The congruent /ta-/ta video had a synchronous onset of AV stimuli. The male speaker's lips were in a neutral closed position when not engaged in utterance of the syllables /ka or /ta and the articulation always started from a neutral position. Videos were created/ edited using VideoPad video-editing software (NCH Software, CO) at a frame rate of 25 frames/second and a resolution of 1280×720 pixels. The auditory /pa and /ta syllables were of 0.549 s and 0.531 s duration and were edited in Audacity software (Sourceforge.net) to minimize the background noise. The audio sampling rate was 44 kHz and had a bit rate of 128 kbps. The study was done inside a 3T MRI scanner as part of a brain imaging investigation.

3.1.1.2 Task

The task design is illustrated in Fig 3.1. Inside the MR scanner, the stimuli were presented in a block design with 20 s activation blocks consisting of 10 videos of one kind of AV lag. In total there were 28 activation blocks in the whole experiment inclusive of 4 activation blocks for each stimuli category (AV lag). There were alternating 28 resting blocks, each of 20 s duration. The order of presentation of activation blocks was randomized and the same kind of block never appeared consecutively. Within a block, the trial videos comprised of one kind of lag, and this is a limitation of the fMRI block design. AV stimuli were presented through an INVIVO MR - compatible CRT screen attached to the head-coil and MRI-compatible headphones (Philips, The Netherlands). Presentation software (Neurobehavioral Systems, CA) was used to display the stimuli. Participants were presented with the stimuli (Fig. 3.1) and asked to indicate their response based on their perception via three buttons designated for /ta, /pa, and for "any other" perceptual categories. They were instructed to attend to the audio-visual stimuli and watch the speaker at all times. A fibre-optic button-pad by Curdes (Current Designs, PA, USA) was used to record the responses of the participants.

3.1.2 Theoretical framework

Multisensory systems research has been built on analogies drawn from constituent unisensory processing modules. For example, multisensory processing of audio-visual inputs was studied in comparison to standalone auditory and visual processing [3, 43, 62]. However, increasing evidence suggests that a network of unisensory and multisensory

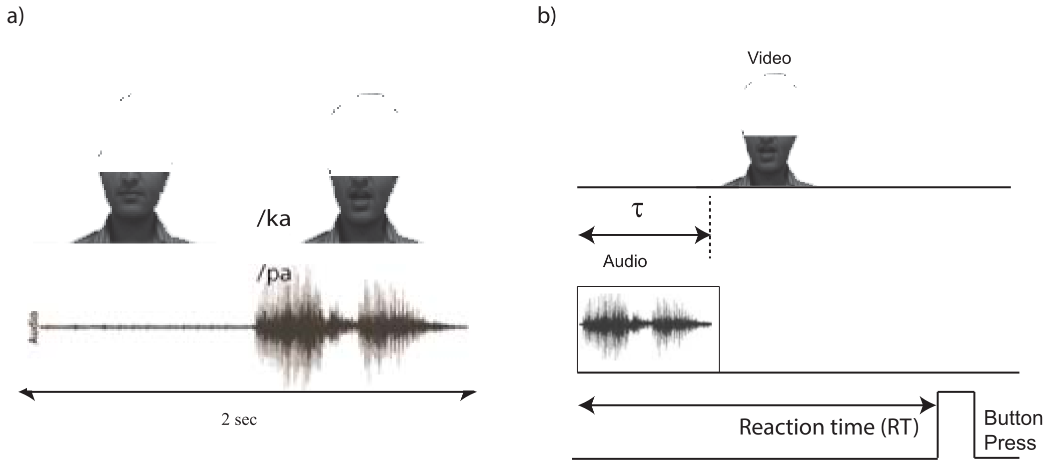

Figure 3.1: (a) Stimuli videos are created using visual lip movement of /ka superimposed on auditory /pa. Participants reported the auditory object they heard while watching the video using a button press response box. (b) Stimuli videos were created at different audio-visual lags τ, the timing difference between the onset of sound and lip movement, with values ranging from $[-300, 450]$ ms.

systems may be involved in multisensory task processing [26, 28, 34]. Thus, it is reasonable to assume that the most elemental model of multisensory perception will involve at least two unisensory systems and one multisensory system [22, 36, 38, 39] even though a recent hypothesis suggests two unisensory streams can in principle give rise to multisensory effects [24]. Furthermore, the changes in oscillatory brain rhythms such as pre-stimulus enhancement of beta power and post-stimulus depreciation of theta band power have been identified as the hallmarks of illusory perception in pre-stimuli or post-stimuli regimes [28, 63], respectively.

As discussed before, the Kuramoto model [55, 64] is increasingly becoming a handy tool to model oscillatory brain dynamics. In our model, we exploit the mathematical tractability and dynamical complexity of Kuramoto model by considering a system of three coupled Kuramoto phase oscillators configured in the manner shown in Fig. 3.2. The phase of the oscillator A representing the auditory system is θ_1, the phase of the oscillator V representing the visual system is θ_2, and the phase of the oscillator AV representing the multisensory system is θ_3. Each oscillator has a distinct natural frequency of oscillation, denoted by ω_1, ω_2, and ω_3 respectively. Our model captures the functional connectivity between unisensory systems such as auditory, visual cortices and the multisensory system, e.g., posterior superior temporal sulcus (pSTS), that has been observed in functional imaging studies [26], via the coupling parameters κ_1 and κ_2.

Furthermore, our experimental results as well as those from Munhall and colleagues [27] indicate that a crucial parameter in the creation of perceptual states is the AV lag which we capture through the time delay parameter τ. In normal hearing and visual circumstances, one can expect the coupling between individual sensory systems and multisensory system to be balanced. However, perturbations to one of the sensory streams, such as unreliable visual or auditory signals, can lead to a situation of unbalanced coupling as shown by Nath and Beauchamp [26]. There is no direct coupling between A and V oscillators in our model, though in the neural system there is evidence of connectivity between the primary auditory and visual areas A1 and V1 [65]. This is primarily because we are interested in understanding the key symmetries of the most simple multisensory dynamical model catered towards understanding oscillatory states of the brain. Nonetheless, A and V do interact functionally in our model, since they are both coupled to AV, the functional unit of multisensory system. To model the experimental situation of positive AV lags between the audio and visual stimuli, the coupling between the oscillators V and AV is time delayed by a parameter τ. When the visual stimulus precedes the auditory stimulus (positive lag), the dynamics of phase oscillators is expressed as

$$
\begin{aligned}
\dot{\theta}_1(t) &= \omega_1 + \kappa_1 \sin(\theta_3(t) - \theta_1(t)), \\
\dot{\theta}_2(t) &= \omega_2 + \kappa_2 \sin(\theta_3(t-\tau) - \theta_2(t)), \\
\dot{\theta}_3(t) &= \omega_3 + \kappa_1 \sin(\theta_1(t) - \theta_3(t)) + \kappa_2 \sin(\theta_2(t-\tau) - \theta_3(t)),
\end{aligned}
\tag{3.1}
$$

where κ_1 is the strength of interaction between the auditory (A) and the AV oscillator and κ_2 is the coupling strength between the visual (V) and the AV oscillator. When the auditory stimulus precedes the visual stimulus (negative lag), one can consider the possibility of τ being negative. However, physically it does not make sense to make the present dynamics dependent on the future. Alternatively, one can intuitively relate the situation of negative τ to a situation where oscillator A has a time delayed coupling with oscillator AV while the visual oscillator V is instantaneously coupled. Hence, when the auditory stimulus precedes the visual stimulus, the dynamics of phase oscillators can be represented as

$$\begin{aligned}
\dot{\theta}_1(t) &= \omega_1 + \kappa_1 \sin(\theta_3(t-\tau) - \theta_1(t)), \\
\dot{\theta}_2(t) &= \omega_2 + \kappa_2 \sin(\theta_3(t) - \theta_2(t)), \\
\dot{\theta}_3(t) &= \omega_3 + \kappa_1 \sin(\theta_1(t-\tau) - \theta_3(t)) + \kappa_2 \sin(\theta_2(t) - \theta_3(t)),
\end{aligned} \tag{3.2}$$

Equations 3.1 and 3.2 are similar in form but are not mirror images due to the differences in the individual frequencies of the oscillators that give rise to asymmetry. When the oscillators are allowed to interact, the frequencies of oscillations of all three units synchronize with various phase relationships (analytically derived in section 3.2 for a simple case) for sufficiently strong strengths of interactions.

States of synchronized oscillations across a chain of phase oscillators can be mathematically identified by defining a complex order parameter Z, which gives a quantitative measure of the synchronization among the oscillators and can be expressed as

$$Z = Re^{i\Phi} = \frac{1}{3}[e^{i\theta_1} + e^{i\theta_2} + e^{i\theta_3}]. \tag{3.3}$$

Here the amplitude $R(t)$ is a measure of both, the synchronization of the frequencies of

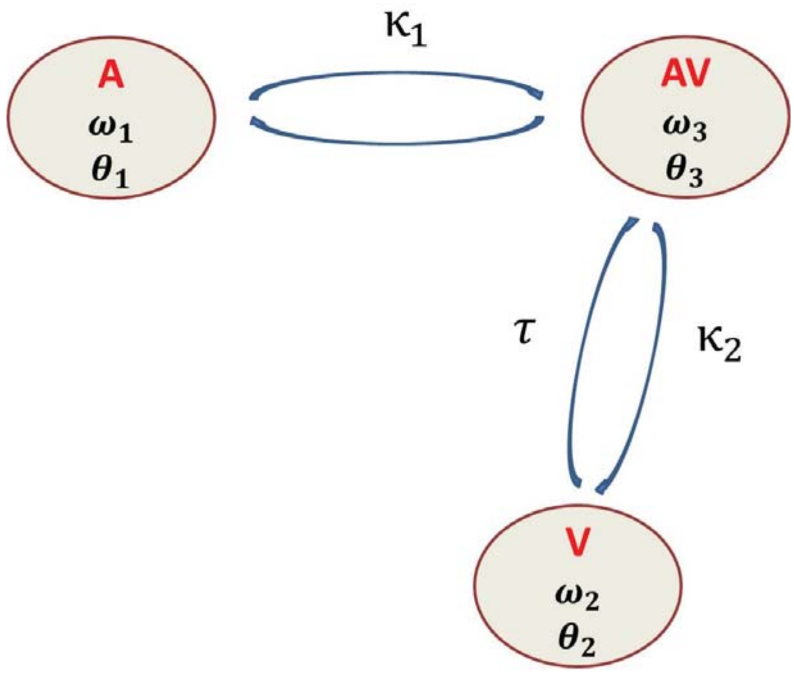

Figure 3.2: The dynamical model of multisensory speech perception for positive AV lags (i.e., when visual stimulus leads auditory stimulus). Oscillators A, V, and, AV represent the auditory, visual, and multisensory systems, respectively. Their corresponding intrinsic frequencies are ω_1, ω_2, and ω_3, and the respective phases are θ_1, θ_2, and θ_3. The coupling between A and AV is instantaneous and its strength is κ_1, whereas the coupling between V and AV is time delayed by the parameter τ and its strength is κ_2. There is no direct coupling between oscillators A and V.

the three oscillators as well as the phase coherence of the oscillators, and $\Phi(t)$ measures the average phase of the system. The system can get synchronized in frequency as the coupling strengths κ_1 and κ_2 are increased but the oscillators can still be separated in their mutual phases while oscillating at the same frequency. For such a frequency synchronized state, a value of $R = 1$ represents maximum synchronization (0 phase difference) among the oscillators and $R = 0$ means maximally separated phases among individual oscillators.

Earlier studies have proposed that the perceptual experience can be qualitatively conceptualized as attractor states of a dynamical system [34, 66]. Stable synchronization patterns at certain relative phase relationships are attractors in a dynamical system, and instabilities signify switches in the perceptual state. In this framework, the state of the order parameter or the collective variable R can be representative of the overall perceptual categorization and can be studied as a function of the interactions among constituent psychophysical variables, coupling strengths, the spread in the frequencies of the oscillators as well as the time delay parameter τ. Time delay τ can be interpreted as the temporal window over which the integration of AV information takes place.

3.2 Results

3.2.1 Behavior

The button press responses to perceptual experience collected from each participant during the experiment were analyzed offline using customized MATLAB codes. A maximum of 40 responses were expected for each AV lag condition. Tasks with less than 35 responses were rejected since estimates of perceptual categorization may be biased during the computation of percentage responses. No subject had to be rejected based on this criteria. Behavioral responses of attempted trials of each participant were converted into percentage measures for each perceptual category, /pa, /ta or "other" corresponding to AV lags over a range $[-300, 450]$ ms. Subsequently, 34 participants who reported perceiving /ta for at least 60% of the total responses at any AV Lag are defined as the "McGurk-perceivers" and simply referred to as perceivers.

We observed that perceivers report /ta maximally at an AV lag of 0 ms when the lip movement of the speaker is synchronous with the onset of the auditory stimulus (Fig. 3.3). Conversely, /pa perception was reported the least number of times at AV lag of 0 ms. Analysis of Variance (ANOVA) was performed over the percentage responses (without repetitions) in each category, /pa, /ta and "other", with lags and subjects treated as factors. For threshold of statistical significance set at $p = 0.001$, there was a significant change in /ta responses across lags ($F(5, 165) = 24.46, p < 0.001$), but not across subjects ($F(33, 165) = 1.72, p = 0.0141$). /pa responses significantly varied across lags ($F(5, 165) = 12.57, p < 0.001$) as well as across subjects ($F(33, 165) = 5.43, p < 0.001$). The "other" responses also significantly varied across lags ($F(5, 165) = 7.11, p < 0.001$) and subjects ($F(33, 165) = 4.25, p < 0.001$).

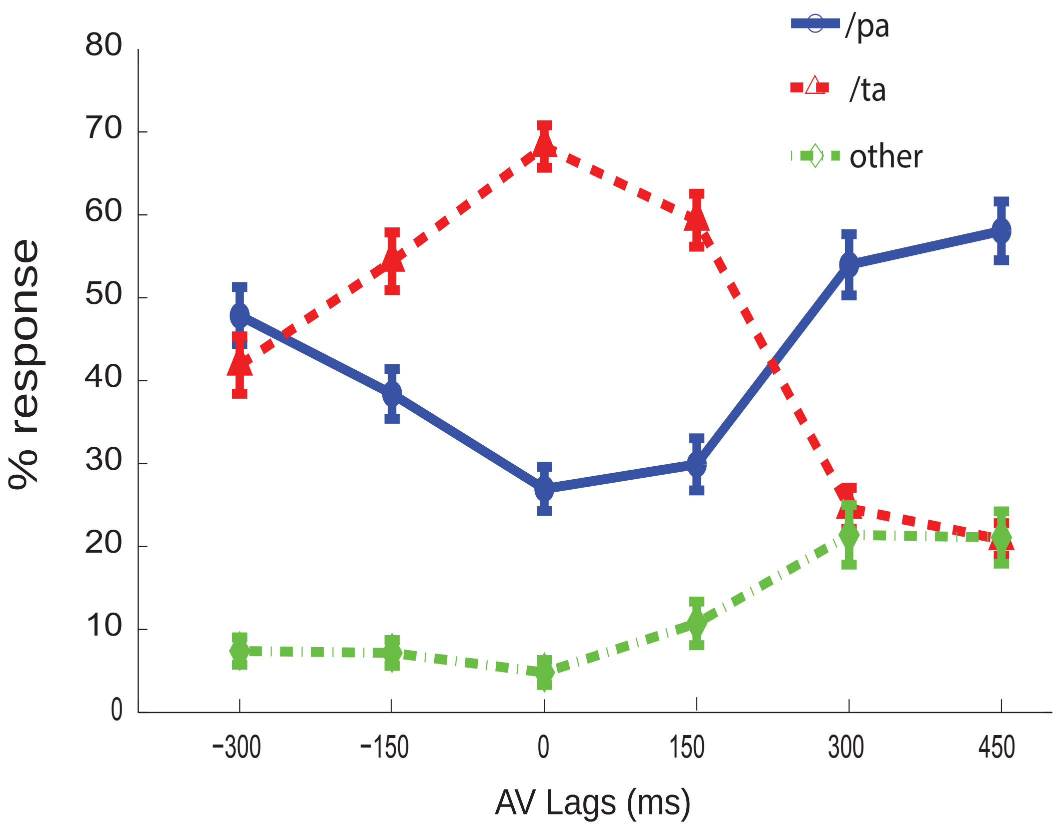

Figure 3.3: Normalized behavioral responses from 34 subjects. Mean response for each perceptual category is presented as a function of AV lag τ. The error bars reflect 95% significance thresholds.

3.2.2 Dynamical model of multisensory processing

We have investigated the system of equations 3.1 and 3.2 numerically and analytically to gain insight on how time-delays may influence the stability of perceptual states. We have studied the model under two scenarios, one with balanced coupling ($\kappa_1 = \kappa_2$) and the other with unbalanced coupling ($\kappa_1 \neq \kappa_2$). For the sake of simplicity, the analytical derivations are done for the balanced coupling conditions only, but we do investigate the unbalanced coupling scenario numerically. All numerical simulations have been performed using the customized MATLAB (www.mathworks.com) codes and delay-differential equation solver dde23. We are interested in the collective behavior of the system of oscillators (Fig. 3.2, equation 3.1), in particular the dynamics of the order parameter that quantifies the synchronized states as a function of time-delay and coupling parameters.

3.2.2.1 Balanced coupling

We have solved the system of equations 3.1 and 3.2 for a range of $\kappa = \kappa_1 = \kappa_2$ values from $3 - 20$ and for various values of the time delay (τ). In Fig. 3.4, we have plotted the time series of the phases θ_1, θ_2, and θ_3 at two delay values when the coupling strength is $\kappa = 5$. At delay $\tau = 0.07$, all three oscillators are almost synchronized in-phase and hence the order parameter $R = 0.9995$. However, at delay $\tau = 0.95$, auditory A and multisensory AV oscillators are oscillating almost in-phase whereas the visual oscillator V is out-of-phase and the order parameter $R = 0.3326$. Hence, the transition from almost complete synchronization to a lower degree of synchronization occurs at a critical value of τ. To explore the parameter space further, we have computed the order parameter for various time delays (τ) and coupling strengths (κ) (Fig. 3.5). The right halves of the curves correspond to the "positive" audio-visual lags (where the visual stimulus precedes the auditory stimulus) and are obtained from the numerical integration of equation 3.1. The left halves of the curves correspond to "negative" audio-visual lags (where the auditory stimulus precedes the visual stimulus) and are obtained numerically from equation 3.2. In Fig. 3.5(a), the intrinsic frequencies are set at $\omega_1 = 3$, $\omega_2 = 4$, and $\omega_3 = 5$. This is roughly in the θ frequency range ($3-5$ Hz) which was earlier shown to be relevant for the existence of perceptual states [28]. The initial phases for simulations are randomized to span all possible relative phase states. For weak coupling $\kappa < 1$, the existence of synchronization states is not possible consistently and R oscillates with time. For $\kappa \geq 1$, a clear synchronization state appears at least for a range of τ values. Two stable states of the order parameter emerge, one synchronization state around $R \approx 1$, and the other around $R \approx 0.33$. Furthermore, we have also observed that the critical value of τ increases with an increase in κ. In other words, the island of synchronization expands with increasing κ. For example, for $\kappa = 10$, a transition happens for a high value of τ (not shown in Fig. 3.5(a)), that is not behaviorally relevant. On the other hand, we have also observed that higher intrinsic frequencies of the oscillators can recede the island of synchronization. For example, if the intrinsic frequencies are set to $\omega_1 = 15$, $\omega_2 = 16$, and $\omega_3 = 17$ (beta band frequency), we see that the transition from the synchronization state occurs at a lower values of τ, and the extent of synchronization regime decreases (Fig. 3.5(b)). An important point to note here is that the critical transition value of τ may not be the same for "positive" and "negative" audio-visual lags. This stems from the disparity in the intrinsic frequencies of the oscillators.

Multistability and analytical solutions Multistable states of a dynamical system can be relevant for describing the perception and the action, in particular, the inter-trial and inter-subject variability. We have investigated the existence of such states in our dynamical model. The presence of a time-delayed coupling provides for a rich collective

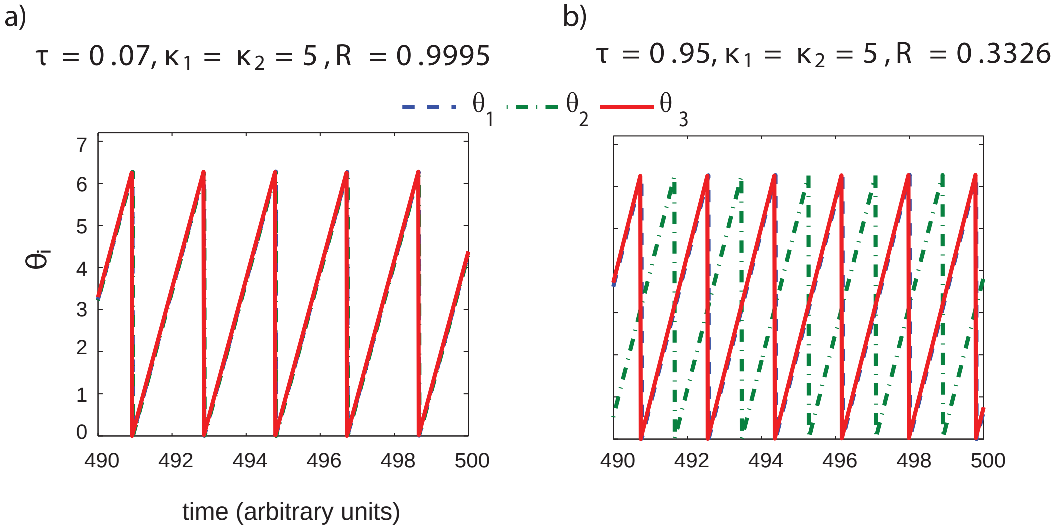

Figure 3.4: The time series of phases $\theta_1(t)$, $\theta_2(t)$, and $\theta_3(t)$ of the three Kuramoto oscillators having intrinsic frequencies $\omega_1 = 3$, $\omega_2 = 4$, and $\omega_3 = 5$ respectively, (a) at delay $\tau = 0.07$, and coupling strength $\kappa_1 = \kappa_2 = 5$. At this value of delay, all three oscillators are almost synchronized in-phase and hence the order parameter $R = 0.9995$. (b) Delay $\tau = 0.95$, and coupling strength $\kappa_1 = \kappa_2 = 5$. At this value of delay, auditory A, and multisensory AV oscillators are oscillating almost in-phase, whereas the visual oscillator V is out-of phase with the other two. Hence the order parameter $R = 0.3326$.

dynamics, including the existence of multiple collective states and the possibility of coexistence of some of these states. We have looked at this possibility by theoretical and numerical investigation of the model equations over a wide range of parameter values and randomized initial conditions in Figs. 3.5 and 3.6. The figures show that our system is multistable, i.e., the order parameter can have multiple values at a given value of τ and it can take any of these values depending on the choice of initial phases (Fig. 3.6). The multistability seen in this model system may be related to the multistability seen in the speech perception in terms of different responses registered as /pa and "others" (Fig. 3.3). The synchronized state (where all the oscillators oscillate with the same frequency Ω) is given by $\theta_i(t) = \Omega t + \psi_i$, where ψ_i's are constants. Let the phase shift between the auditory and AV oscillator be $\theta_3 - \theta_1 = \psi_3 - \psi_1 = \phi_1$ and the

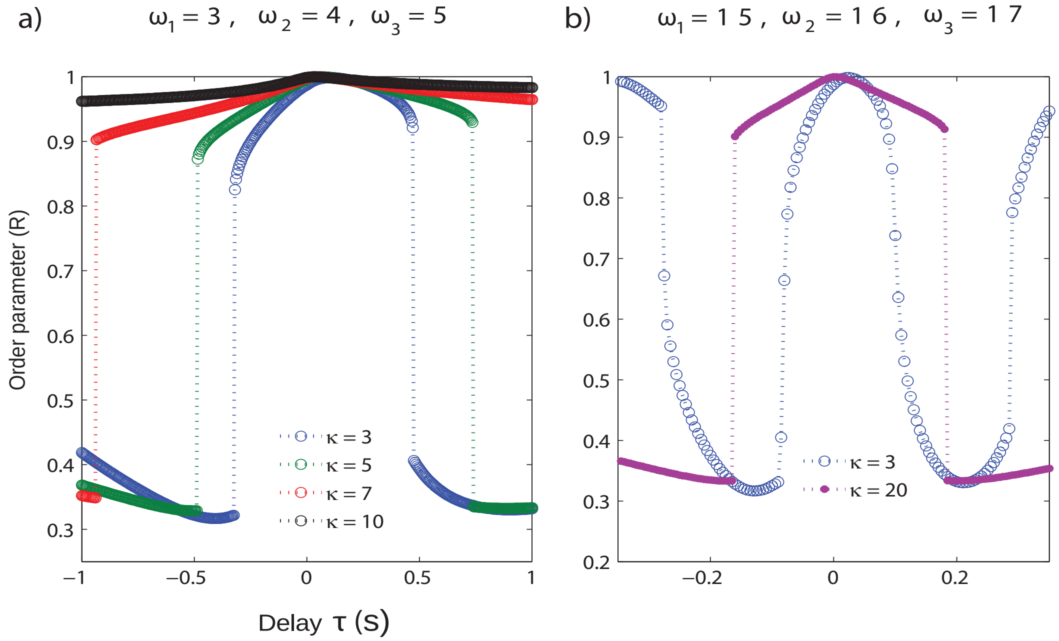

Figure 3.5: The variation of the order parameter (R) of the system of oscillators with delay (τ) for the case of balanced coupling ($\kappa_1 = \kappa_2 = \kappa$), when the intrinsic frequencies are (a) $\omega_1 = 3$, $\omega_2 = 4$, and $\omega_3 = 5$, and (b) $\omega_1 = 15$, $\omega_2 = 16$, and $\omega_3 = 17$. We have obtained the above curves for various κ values for the same set of initial phases.

phase shift between the visual and AV oscillator be $\theta_3 - \theta_2 = \psi_3 - \psi_2 = \phi_2$. This gives $\theta_2(t-\tau) - \theta_3(t) = -\phi_2 - \Omega\tau$ and $\theta_3(t-\tau) - \theta_2(t) = \phi_2 - \Omega\tau$. Using these expressions, system of equations 3.1 can be written as

$$\Omega = \omega_1 + \kappa \sin\phi_1, \tag{3.4a}$$

$$\Omega = \omega_2 + \kappa \sin(\phi_2 - \Omega\tau), \tag{3.4b}$$

$$\Omega = \omega_3 - \kappa \sin\phi_1 - \kappa \sin(\phi_2 + \Omega\tau). \tag{3.4c}$$

On summing the equations 3.4a, 3.4b, and 3.4c, we obtain

$$\Omega = \bar{\omega} - \frac{2\kappa}{3} \cos\phi_2 \sin(\Omega\tau), \tag{3.5}$$

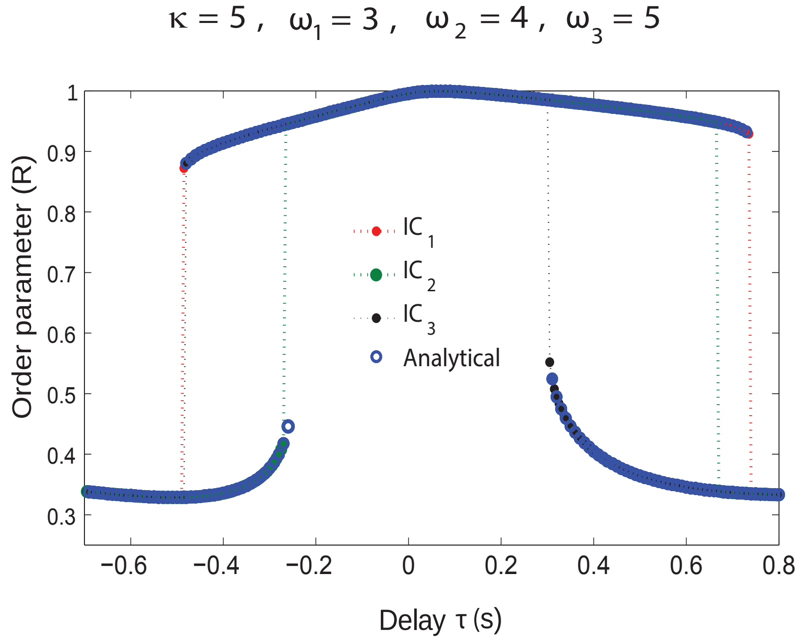

Figure 3.6: The blue circles show the order parameter (R) as a function of time delay (τ) for $\omega_1 = 3$, $\omega_2 = 4$, $\omega_3 = 5$ and coupling strengths $\kappa_1 = \kappa_2 = \kappa = 5$, computed using the analytical expression Eq. 3.14. Red dotted curve is obtained by numerically integrating the model equations (Eqs 3.1 and 3.2) to get the individual phases and then using Eq. 3.12 to get R, for one set of initial conditions IC_1. The green and black dotted curves are obtained numerically from different sets of initial phases, IC_2 and IC_3, respectively. We see that the system is multistable, i.e., the order parameter can have multiple values at a given value of τ. The analytical results are in great agreement with the numerical values of the order parameter.

where $\bar{\omega} = \frac{\omega_1+\omega_2+\omega_3}{3}$ is the average frequency. From Eq. 3.4a, we obtain $\phi_1 = \sin^{-1}\left(\frac{\Omega-\omega_1}{\kappa}\right)$ and from Eq. 3.4b, we have $\phi_2 = \Omega\tau + \sin^{-1}\left(\frac{\Omega-\omega_2}{\kappa}\right)$. Eq. 3.5 gives the collective frequency Ω as a function of delay τ when we have "positive" audio-visual lags. Since it is a transcendental equation, we get multiple values of collective frequency Ω as the solutions of Eq. 3.5 at a given value of delay. To determine which of these solutions correspond to a stable synchronization state, one has to do a stability analysis.

To obtain the expression of collective frequencies for the "negative" audio-visual lags, one has to do the same analysis as above using Eq. 3.2. For "negative" audio-visual lags, we have

$$\Omega = \bar{\omega} - \frac{2\kappa}{3}\cos\phi_1 \sin(\Omega\tau), \tag{3.6}$$

where $\bar{\omega}$ is the same as above but $\phi_1 = \Omega\tau + \sin^{-1}\left(\frac{\Omega-\omega_1}{\kappa}\right)$ and $\phi_2 = \sin^{-1}\left(\frac{\Omega-\omega_2}{\kappa}\right)$.

Derivation of the stability condition We perform a linear stability analysis to determine the local stability of the synchronization state by adding a small perturbation

$$\theta_i(t) = \Omega t + \psi_i + \epsilon\xi_i(t), \tag{3.7}$$

where $0 < \epsilon << 1$. Taking $\psi_3 - \psi_1 = \phi_1$, and $\psi_3 - \psi_2 = \phi_2$ gives

$$\begin{aligned}
\theta_3(t) - \theta_1(t) &= \epsilon\left[\xi_3(t) - \xi_1(t)\right] + \phi_1, \\
\theta_3(t-\tau) - \theta_2(t) &= \epsilon\left[\xi_3(t-\tau) - \xi_2(t)\right] + \phi_2 - \Omega\tau, \\
\theta_2(t-\tau) - \theta_3(t) &= \epsilon\left[\xi_2(t-\tau) - \xi_3(t)\right] - \phi_2 - \Omega\tau.
\end{aligned} \tag{3.8}$$

On substituting these phase differences in equations 3.1, we obtain

$$\begin{aligned}
\Omega + \epsilon\dot{\xi}_1(t) &= \omega_1 + \kappa\sin\left[\epsilon\left(\xi_3(t) - \xi_1(t)\right) + \phi_1\right], \\
\Omega + \epsilon\dot{\xi}_2(t) &= \omega_2 + \kappa\sin\left[\epsilon\left(\xi_3(t-\tau) - \xi_2(t)\right) + \phi_2 - \Omega\tau\right], \\
\Omega + \epsilon\dot{\xi}_3(t) &= \omega_3 - \kappa\sin\left[\epsilon\left(\xi_3(t) - \xi_1(t)\right) + \phi_1\right] \\
&\quad -\kappa\sin\left[\epsilon\left(\xi_3(t) - \xi_2(t-\tau)\right) + \phi_2 + \Omega\tau\right].
\end{aligned} \tag{3.9}$$

Linearizing the set of equations 3.9, and using equations 3.4a, 3.4b, and 3.4c, we obtain

$$\begin{aligned}
\dot{\xi}_1(t) &= \kappa\left[\xi_3(t) - \xi_1(t)\right]\cos\phi_1, \\
\dot{\xi}_2(t) &= \kappa\left[\xi_3(t-\tau) - \xi_2(t)\right]\cos\left(\phi_2 - \Omega\tau\right), \\
\dot{\xi}_3(t) &= -\kappa\left[\xi_3(t) - \xi_1(t)\right]\cos\phi_1 - \kappa[\xi_3(t) - \xi_2(t-\tau)]\cos\left(\phi_2 + \Omega\tau\right).
\end{aligned} \tag{3.10}$$

On taking $\xi_i(t) = v_i e^{\lambda t}$, where λ is the set of eigenvalues and v_i are the corresponding eigen-vectors, and substituting in the system of linear equations 3.10, we obtain the characteristic polynomial

$$\begin{vmatrix} -A-\lambda & 0 & A \\ 0 & -B-\lambda & Be^{-\lambda\tau} \\ A & Ce^{-\lambda\tau} & -A-C-\lambda \end{vmatrix} = 0, \tag{3.11}$$

where $A = \kappa \cos \phi_1$, $B = \kappa \cos(\phi_2 - \Omega\tau)$, and $C = \kappa \cos(\phi_2 + \Omega\tau)$. The stability of the synchronization state having frequency Ω, for a given value of κ and τ, can be checked using equation 3.11 by looking at the sign of the eigenvalues λ. The frequency synchronized state having frequency Ω is stable if none of the eigenvalues has a positive real part.

Analytical expression for order parameter The order parameter of our system is defined as

$$Re^{i\Phi} = \frac{1}{3}\sum_{j=1}^{3} e^{i\theta_j}. \tag{3.12}$$

After a little algebra, we can express R in the form

$$R = \frac{1}{3}\sqrt{3 + 2\cos(\theta_1 - \theta_2) + 2\cos(\theta_3 - \theta_2) + 2\cos(\theta_3 - \theta_1)}. \tag{3.13}$$

For a phase-locked synchronization state, $\theta_i(t) = \Omega t + \psi_i$, we have taken $\theta_3 - \theta_1 = \psi_3 - \psi_1 = \phi_1$ and $\theta_3 - \theta_2 = \psi_3 - \psi_2 = \phi_2$. Therefore the analytical expression of the order parameter R becomes

$$R = \frac{1}{3}\sqrt{3 + 2\left[\cos(\phi_1 - \phi_2) + \cos(\phi_2) + \cos(\phi_1)\right]}. \tag{3.14}$$

For an in-phase synchronization state: $\psi_1 = \psi_2 = \psi_3$. Therefore, $\phi_1 = \psi_3 - \psi_1 = 0$, $\phi_2 = \psi_3 - \psi_2 = 0$ and hence $R = 1$. We already have the analytical expressions for ϕ_1 and ϕ_2 for positive lags: $\phi_1 = \sin^{-1}\left(\frac{\Omega-\omega_1}{\kappa}\right)$, and $\phi_2 = \Omega\tau + \sin^{-1}\left(\frac{\Omega-\omega_2}{\kappa}\right)$. For a given set of κ, τ, and intrinsic frequencies, the collective frequency Ω is obtained from the transcendental equation Eq. 3.5 by a numerical root finding method and the stability of the corresponding state is then checked using Eq. 3.11. Ω values corresponding to the stable states are substituted in the expressions of ϕ_1 and ϕ_2 and the values of the order parameter R are then obtained from Eq. 3.14. For "negative" audio-visual lags, R follows the same Eq. 3.14 but here Ω is given by Eq. 3.6 with $\phi_1 = \Omega\tau + \sin^{-1}\left(\frac{\Omega-\omega_1}{\kappa}\right)$, and $\phi_2 = \sin^{-1}\left(\frac{\Omega-\omega_2}{\kappa}\right)$. In Fig 3.6 we have plotted the analytical as well as the numerical values of the order parameter (R) at the corresponding values of time delay (τ) for intrinsic frequencies $\omega_1 = 3$, $\omega_2 = 4$, $\omega_3 = 5$, and coupling strength ($\kappa_1 = \kappa_2 = \kappa = 5$) for three different sets of initial phases/conditions, labeled IC_1, IC_2, and IC_3. The order parameter R can have more than one value at a given value of delay, giving rise to multistability and hysteresis. Fig. 3.6 shows that the critical value of τ (for both positive as well as negative lags) can be different for different initial conditions. It means that the range of delay values for which the degree of synchronization, R, has a high value, can vary depending upon the choice of initial phases. This result can be related to the observation of individual differences in the width of the multisensory temporal binding window [67]. Fig. 3.6 shows that the analytical results are in excellent agreement with the numerical values of the order parameter. The analytical expression for R, given by Eq. 3.14, holds when all the oscillators are frequency synchronized and oscillating with the synchronization frequency Ω.

3.2.2.2 Unbalanced coupling

We have investigated the unbalanced coupling scenario following two routes. First we have kept κ_1 fixed at the value 3 and varied κ_2 between $[0.5, 5]$ (Fig. 3.7(a)). $\kappa_2 < \kappa_1$ is equivalent to the situation where ambiguity is introduced in the visual stream because of which the coupling changes, e.g. in the Nath and Beauchamp study [26]. $\kappa_2 > \kappa_1$ is the situation where the visual coupling is increased, auditory being unreliable. When κ_1 is fixed, the island of synchronization increases with increasing value of κ_2, indicating that time-delayed interactions with the visual-multimodal system are crucial for perception. For negative AV lags, i.e., when auditory precedes the visual stimulus, no drastic change in critical delay value occurs when κ_1 is unchanged.

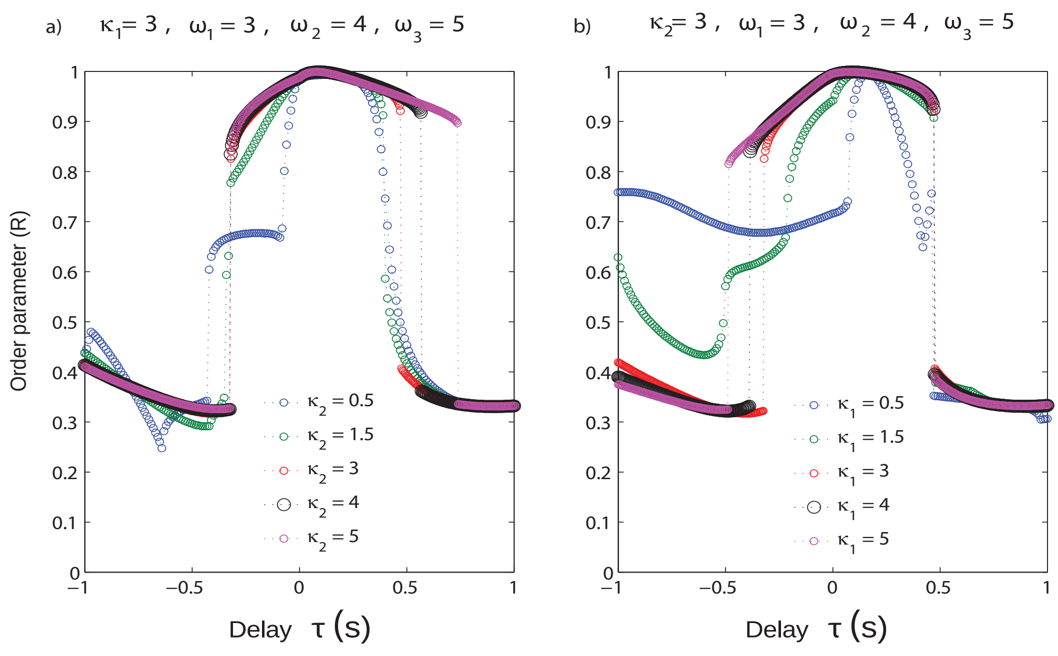

Figure 3.7: The figure shows the variation of the order parameter (R) with delay (τ) for intrinsic frequencies $\omega_1 = 3$, $\omega_2 = 4$, and $\omega_3 = 5$ when (a) the coupling strength between A and AV (κ_1) is kept constant at 3 and the coupling between V and AV (κ_2) is varied from 0.5 to 5, and (b) the coupling strength between V and AV (κ_2) is kept constant at 3 and the coupling between A and AV (κ_1) is varied from 0.5 to 5.

Second we vary κ_1 while keeping κ_2 constant. Here we see that the critical delay value, for the transition from phase-synchronous to non-phase-synchronous state, shifts such that the regime of synchronization increases for negative AV lags corresponding to the scenario where auditory stimulus precedes the visual stimulus (Fig. 3.7(b)). Multi-stable states are possible and the possibility of existence of two states, one synchronous and one non-synchronous, is critically dependent on κ_1 (Fig. 3.7(b)).

Overall we find that the time delay and coupling strength facilitate the existence of synchronous states and the intrinsic frequency of oscillations reduces the temporal window over which AV signals can integrate. Thus, the synchronization window can extend over an entire range of AV lags. This is in a qualitative agreement with the trend seen for the McGurk stimuli (Fig. 3.3). The existence of multistability is demonstrated in Fig. 3.6 explicitly, but it is also observed for the coupling scenarios discussed in Fig. 3.5 and Fig. 3.7. Small amount of perturbation from numerical instabilities was sufficient to generate transitions between the stable states of the order parameter.

3.3 Discussion

The main purpose of this work is to conceptualize the observations from an experimental paradigm, that has been over the years a bedrock to study multisensory information processing, with a simple dynamical model to illustrate the role of environmental variables and connectivity topologies between neural subsystems in the shaping of perceptual states. The Kuramoto framework provides the added advantage of linking the perceptual states to simultaneously observed neuronal oscillations from EEG/ MEG data. The perceptual dynamics observed for /ta response by Munhall and colleagues [27] and our behavioral recordings (Fig. 3.3) are in complete agreement with the order parameter dynamics observed in our model (Figs. 3.5, 3.6, and 3.7). We see that the illusory perception is reported maximally within a range of lags $[-150, 300]$ ms. Beyond this range, the auditory /pa response dominates for both positive and negative AV lags. We have considered a system of three coupled phase oscillators for representing the dynamics of auditory, visual, and multisensory systems. Superior colliculus (SC) and posterior superior temporal sulcus (pSTS) are two structures at the sub-cortical and cortical level respectively that can get representation in the multisensory system. SC is known to have bimodal neurons that can receive inputs from both the auditory and visual systems [68]. Similarly, pSTS has been established by several researchers as the locus of cortical processing of multisensory integration [26, 69–72]. Thus a network comprising of auditory, visual, and pSTS (with contributions from SC) areas can form the most elemental network for multisensory processing. Experimental validation of the presence of such networks has been provided by earlier studies such as Nath and Beauchamp [26] using a fMRI paradigm. An important parameter in our model is the coupling between AV - A and AV - V oscillators. Careful design of such coupling parameters, motivated from the experimental studies, can capture how the biophysically realistic symmetry that exists in the underlying neural system can influence behavior [59]. Broadly, the multisensory functional unit can represent qualitatively the composite contributions of all structures such as superior colliculus, pSTS, and other areas. In our model, the signals from A and V are conveyed to the multisensory oscillator (AV) where information from the two modalities is integrated. The feedback connections from the pSTS to the unimodal areas are directly considered in the form of a bidirectional coupling between pSTS and auditory and visual areas. Nevertheless, the weighted contributions of direct coupling between A1-V1 [65, 73, 74], and their interplay with the coupling between multisensory to unisensory areas can be studied in the dynamical framework. In future, a corresponding behavioral paradigm needs to be developed to test the predictions of such a model.

The coupling parameter in our model helps in two ways, first in the explanation of the existence and destabilization of perceptual states upon the variation of time delay and second to provide a link between observed perceptual dynamics and neuronal oscillations. It is well-known that environmental demands modulate the effective connectivity dynamics among individual sensory systems and multisensory system [26]. The information from the more reliable modality is given a stronger weight [75]. For the McGurk paradigm, Nath and colleagues [26] found that the STS was connected more strongly to a sensory cortex when the corresponding sensory modality was reliable (less noisy). In our model, $\kappa_1 > \kappa_2$ may correspond to a scenario of increased functional connectivity between the STS and the auditory cortex when the auditory modality is more reliable, and $\kappa_2 > \kappa_1$ can be realized as increased functional connectivity between the STS and visual cortex when the visual modality is more reliable. Since there are both top-down and bottom-up connections throughout the cortical processing hierarchy [76, 77], we have incorporated bidirectional connections into our dynamical model. Importantly, for unbalanced coupling scenarios also, the synchronized states exist indicating that the illusory experience is possible in presence of noisy stimuli. Electrophysiological studies indicate that a pre-stimulus theta band activity primes the network for multisensory information processing towards illusory perceptual categorization [28]. Our results indicate how the intrinsic frequencies of oscillators, set at theta regime, can support the perceptual dynamics as observed by varying the AV lag in the multisensory stimulus (compare Fig. 3.5 to Fig. 3.3). We predict that the tuning of oscillators at higher frequency band may shorten the window of temporal integration. In other words, a narrower window of temporal integration will require phase synchrony at a higher frequency such as beta and gamma. Interestingly, our results suggest that the coupling strength has to be relatively high if temporal integration is facilitated by beta band synchrony to produce the cross-modal percepts for a wider value of AV lags (Fig. 3.5(b)). This is in-line with the proposition of Luo and Poeppel [52], who proposed a low and high frequency segregation of auditory processing. From our study, we can predict that low frequency processing (e.g. syllabic speech) may be carried out by relatively weakly coupled unisensory and multisensory systems whereas high frequency processing e.g., diphonic speech/ tones require more stronger connectivity strengths among sensory systems. In summary, the minimal model of multisensory integration is geared towards linking the symmetries in neuronal connectivity and dynamics with environmental demands and behavior.

The existing models of multisensory integration are mostly based on the Bayesian framework and neural networks. These studies consider different kinds of interactions among multisensory and unisensory areas. One category of models considers that the unisensory stimuli are processed separately in the primary cortices, without a significant cross-modal interaction, and multisensory integration takes place in higher associative cortical areas, such as SC, via feedforward convergence from multiple unimodal areas [78]. The second category of models assumes only direct lateral connections between the two unimodal areas [41, 42] and excludes the involvement of multisensory regions. They argue that the direct connections among early processing areas (modality-specific areas such as visual and auditory cortices) play a pivotal role in multisensory integration. These models are based on recent anatomical tracing studies in monkeys (macaque) and human subjects that have shown direct connections between auditory and visual areas including primary cortices (V1 and A1) [65, 73]. Similar studies have also reported projections to/from somatosensory cortex from/to auditory and visual areas [79]. The heteromodal connections between the primary somatosensory cortex and the primary auditory cortex were also reported in the gerbils [80]. In marmosets, projections from the retroinsular area of the somatosensory cortex to the caudomedial belt of the auditory area were also observed [76] in line with a similar observation in the Old World monkeys [81]. The third category of models excludes direct connections between the unimodal areas but considers both a feedforward connection to a multisensory area, and a feedback from the multisensory area to the unisensory ones [40]. Finally, the fourth category of models incorporates all the connections together, i.e., the feedback and feedforward connections between unimodal and multimodal systems along with the direct connections between the unimodal systems [22, 82]. Most of these studies do not consider the processing of temporal relationships among the unimodal stimulus components, e.g., AV lags [27] and gap duration in speech perceptual categorization [66]. Our dynamical model (which comes under the third category), comprising of three Kuramoto oscillators, attempts to do so in a minimalist manner. An earlier attempt in this direction was made by Dhamala and colleagues [34], who modeled the rhythmic multisensory paradigm in the audio-visual domain by considering the phase dynamics of two interacting periodic oscillators and investigated the behavioral effects of relative timings of different sensory signals. In their rhythmic paradigm, temporally congruent multisensory stimuli were expected to cause a percept of synchrony. On the other hand, incongruent stimuli could cause a percept of asynchrony or another possible state, the non-phase-locked state (drift or neutral percept) because it represented a failure in multisensory integration. The non-phase-locked state was qualitatively different from the percept of asynchrony. Dhamala and colleagues then used fMRI and simultaneous behavioral recordings to confirm the involvement of a distributed brain network for the multisensory processing of periodic auditory-visual stimuli. The study proposed that the solution space of a hypothetical system of two coupled oscillators corresponded to the perceptual solution space of human multisensory integration and to selected activation of brain regions. Though the authors propose that their results indicate a definite involvement of superior colliculus in the perception of synchrony, they have not captured the dynamics of the multisensory system as a functional unit directly in the theoretical model, rather emphasizing on the periodicity as the source of categorization. Nonetheless, the rhythmic paradigm is somewhat unrealistic in the context of multisensory speech stimuli. Hence, a broader dynamical framework for multisensory perception is warranted. A key difference between our model and that of Dhamala et al. [34] is that they have not incorporated the time lag or asynchrony between the audio and visual stimuli explicitly in their theoretical model. In our model, we capture the AV lag by introducing a time delay τ between the multisensory (AV) and unisensory (V/A) oscillators and study the variation in perceptual stability as a function of this parameter. Subsequently, we propose that the order parameter or the collective variable R of the oscillator system can be representative of the overall perceptual categorization.

Multistability is a key aspect of perceptual behavior and in general biological systems [83]. In the McGurk paradigm, the presence of responses registered as /ka (the visual stimulus) or fused percepts such as /pa-ka in addition to illusory /ta or auditory /pa can be conceptualized within the framework of multistability. We propose that the different responses registered as /pa, /ta, and "others" in the behavioral data can be related to the multistability in the final dynamical state of our coupled oscillator system. The advantage of a dynamical systems approach is that the presence of multistability can be very elegantly explained [84]. Detailed analysis of multistability can be extended to psychophysics of speech perception studies [66] in future as well as with other paradigms. As we have shown in Sec. 3.2, the presence of time delay makes our dynamical system highly multi-stable. For different choices of initial conditions, the system can go to different stable synchronization states. We propose that the multistability in the final state of the dynamical system can be related to the variation observed in the responses of the participants to the same stimuli.

The significant achievement of our model is that it captures the key features of complex multisensory integration processes at the level of behavior and links the structural and functional constraints in the underlying neural systems to ongoing behavioral states. Our results show that our model successfully simulates the temporal constraints on the McGurk effect and the variation in the responses to the same stimuli. Any multisensory behavior can be broken into combinations of individual unisensory and multisensory systems. One can then map the constraints posed by the environmental variables onto the parameter space of a dynamical system and study the emerging perceptual states. For example, recent studies question the idea of multisensory awareness stemming from a mere integration of unisensory systems [24, 85]. This is a challenge to the traditional way of looking at a multisensory task from the perspective of serial or parallel unisensory processes. Dynamical systems offer an attractive approach to test the environmental constraints on a hypothesized multisensory pathway using modeling, behavior, and brain mapping tools. Here, the integration is not identified as a separate process but rather an outcome of the dynamical interactions among unisensory and multisensory neuron populations. In fact, the role of factors like attention can be incorporated in the dynamical model by introducing more mathematical complexity, either by coupling parameter or introducing a separate module, and presents a scope of future work. Experimentally this will require recording and analyzing eye-tracking data to monitor and parametrize attentional factors. Nonetheless, new experimental paradigms have to be developed to eventually test the predicted outcomes from modeling approaches such as ours.

Bibliography

[1] J. J. Gibson, *The Senses Considered as Perceptual Systems.* Boston: Houghton Mifflin, (1966).

[2] G. A. Calvert, C. Spence, and B. E. Stein, *The Handbook of Multisensory Processes.* Cambridge: MA:MIT Press, (2004).

[3] V. van Wassenhove, K. W. Grant, and D. Poeppel, *Visual speech speeds up the neural processing of auditory speech*, Proc. Natl. Acad. Sci. USA **102,** 1181–1186 (2005).

[4] M. Hershenson, *Reaction time as a measure of intersensory facilitation*, J. Exp. Psychol. **63,** 289–293 (1962).

[5] L. K. Morrell, *Temporal characteristics of sensory interaction in choice reaction times*, J. Exp. Psychol. **77,** 14–18 (1968).

[6] B. E. Stein, M. A. Meredith, W. S. Huneycutt, and L. McDade, *Behavioural indices of multisensory integration: orientation to visual cues is affected by auditory stimuli*, J. Cogn. Neurosci. **1,** 12–24 (1989).

[7] D. R. Perrott, K. Saberi, K. Brown, and T. Z. Strybel, *Auditory psychomotor coordination and visual search performance*, Atten. Percept. Psychophys. **48,** 214–226 (1990).

[8] H. C. Hughes, P. A. Reuter-Lorenz, G. Nozawa, and R. Fendrich, *Visual-auditory interactions in sensorimotor processing: saccades versus manual responses*, J. Exp. Psychol. **20,** 131–153 (1994).

[9] M. A. Frens, A. J. Van Opstal, and R. F. Van Der Willigen, *Spatial and temporal factors determine auditory-visual interactions in human saccadic eye movements*, Atten. Percept. Psychophys. **57,** 802–816 (1995).

[10] W. Sumby, and I. Pollack, *Visual contribution to speech intelligibility in noise*, J. Acoust. Soc. Am. **26,** 212–215 (1954).

[11] B. Dodd, *The role of vision in the perception of speech*, Perception **6,** 31–40 (1977).

[12] A. MacLeod, and Q. Summerfield, *Quantifying the contribution of vision to speech perception in noise*, Br. J. Audiol. **21,** 131–141 (1987).

[13] D. R. Perrott, T. Sadralodabai, K. Saberi and T. Z. Strybel, *Aurally aided visual search in the central visual field: Effects of visual load and visual enhancement of the target*, Percept Psychophys. **33,** 389–400 (1991).

[14] K. S. Helfer, and K. Nakanishi, *Auditory and auditory-visual perception of clear and conversational speech*, Journal of Speech, Language, and Hearing Research **40,** 432–443 (1997).

[15] G. A. Calvert, R. Campbell, and M. J. Brammer, *Evidence from functional magnetic resonance imaging of crossmodal binding in the human heteromodal cortex*, Curr. Biol. **10,** 649–657 (2000).

[16] K. W. Grant, and S. Greenberg, *Speech intelligibility derived from asynchronous processing of auditory-visual information*, Proc. of the AVSP 2001 Int. Conf. of Auditory-Visual Speech Proc., 132–137 (2001).

[17] L. Shams, Y. Kamitani, and S. Shimojo, *Visual illusion induced by sound*, Cogn. Brain Res. **14,** 147–152 (2002).

[18] D. E. Callan, et al., *Neural processes underlying perceptual enhancement by visual speech gestures*, NeuroReport **14,** 2213–2218 (2003).

[19] R. B. Banati, G. W. Goerres, C. Tjoa, J. P. Aggleton, and P. Grasby, *The functional anatomy of visual-tactile integration in man: a study using positron emission tomography*, Neuropsychologia **38,** 115–124 (2000).

[20] E. Macaluso, C. D. Frith, and J. Driver, *Modulation of human visual cortex by crossmodal spatial attention*, Science **289,** 1206–1208 (2000).

[21] B. E. Stein, W. Jiang, M. T. Wallace, and T. R. Stanford, *Nonvisual influences on visual-information processing in the superior colliculus*, Prog. Brain Res. **134,** 143–156 (2001).

[22] O. Guipponi, J. Cléry, S. Odouard, C. Wardak, and S. B. Hamed, *Whole brain mapping of visual and tactile convergence in the macaque monkey*, Neuroimage **117,** 93–102 (2015).

[23] M. Schulz, B. Ross, and C. Pantev, *Evidence for training-induced crossmodal reorganization of cortical functions in trumpet players*, NeuroReport **14,** 157–161 (2003).

[24] O. Deroy, Y. Chen, and C. Spence, *Multisensory constraints on awareness*, Phil. Trans. R. Soc. Lond. B Biol. Sci. **369,** 20130207 (2014).

[25] H. McGurk, and J. MacDonald, *Hearing lips and seeing voices*, Nature **264,** 746–748 (1976).

[26] A. R. Nath, and M. S. Beauchamp, *Dynamic changes in superior temporal sulcus connectivity during perception of noisy audiovisual speech*, J. Neurosci. **31,** 1704–1714 (2011).

[27] K. Munhall, P. Gribble, L. Sacco, and M. Ward, *Temporal constraints on the McGurk effect*, Atten., Percept., and Psychophys. **58,** 351–362 (1996).

[28] J. Keil, N. Müller, N. Ihssen, and N. Weisz, *On the variability of the McGurk effect: audiovisual integration depends on prestimulus brain states*, Cereb. Cortex **22,** 221–231 (2012).

[29] N. F. Dixon, and L. Spitz, *The detection of auditory visual desynchrony*, Perception **9,** 719–721 (1980).

[30] B. De Gelder, and P. Bertelson, *Multisensory integration, perception and ecological validity*, Trends Cogn. Sci. **7,** 460–467 (2003).

[31] A. Kopinska, and L. R. Harris, *Simultaneity constancy*, Perception **33,** 1049–1060 (2004).

[32] D. W. Massaro, and M. M. Cohen, *Perceiving asynchronous bimodal speech in consonant-vowel and vowel syllables*, Speech Commun. **13,** 127–134 (1993).

[33] D. W. Massaro, M. M. Cohen, and P. M. Smeele, *Perception of asynchronous and conflicting visual and auditory speech*, J. Acoust. Soc. Am. **100,** 1777–1786 (1996).

[34] M. Dhamala, C. G. Assisi, V. K. Jirsa, F. L. Steinberg, and J. A. Kelso, *Multisensory integration for timing engages different brain networks*, NeuroImage **34,** 764–773 (2007).

[35] K. W. Grant, V. Van Wassenhove, and D. Poeppel, *Detection of auditory (cross-spectral) and auditory-visual (cross-modal) synchrony*, Speech Communication **44,** 43–53 (2004).

[36] K. P. Körding, et al., *Causal inference in multisensory perception*, PLoS One **2,** e943 (2007).

[37] E. Macaluso, Spatial Constraints in Multisensory Attention. In: Murray, M. M., Wallace, M. T., (Eds.), *The Neural Bases of Multisensory Processes.* Boca Raton (FL): CRC Press/Taylor *and* Francis; 2012. Chapter 25.

[38] I. Olasagasti, S. Bouton, and A. Giraud, *Prediction across sensory modalities: A neurocomputational model of the McGurk effect*, Cortex **68,** 61–75 (2015).

[39] C. Cuppini, E. Magosso, B. Rowland, B. Stein, and M. Ursino, *Hebbian mechanisms help explain development of multisensory integration in the superior colliculus: a neural network model*, Biol. Cybern. **106,** 691–713 (2012).

[40] E. Magosso, C. Cuppini, A. Serino, G. D. Pellegrino, and M. Ursino, *A theoretical study of multisensory integration in the superior colliculus by a neural network model*, Neural Networks **21,** 817–829 (2008).

[41] E. Magosso, C. Cuppini, and M. Ursino, *A neural network model of ventriloquism effect and aftereffect*, PLoS One **7,** e42503 (2012).

[42] C. Cuppini, E. Magosso, N. Bolognini, G. Vallar, and M. Ursino, *A neurocomputational analysis of the sound-induced flash illusion*, NeuroImage **92,** 248–266 (2014).

[43] M. A. Meredith, and B. E. Stein, *Interactions among converging sensory inputs in the superior colliculus*, Science **221,** 389–391 (1983).

[44] M. Ursino, C. Cuppini, and E. Magosso, *Neurocomputational approaches to modelling multisensory integration in the brain: a review*, Neural Networks **60,** 141–165 (2014).

[45] D. Senkowski, T. R. Schneider, J. J. Foxe, and A. K. Engel, *Crossmodal binding through neural coherence: implications for multisensory processing*, Trends Neurosci. **31,** 401–409 (2008).

[46] J. F. Hipp, A. K. Engel, and M. Siegel, *Oscillatory synchronization in large-scale cortical networks predicts perception*, Neuron **69,** 387–396 (2011).

[47] C. E. Schroeder, P. Lakatos, Y. Kajikawa, S. Partan, and A. Puce, *Neuronal oscillations and visual amplification of speech*, Trends Cogn. Sci. **12,** 106–113 (2008).

[48] A. Giraud, and D. Poeppel, *Cortical oscillations and speech processing: emerging computational principles and operations*, Nat. Neurosci. **15,** 511–517 (2012).

[49] A. von Stein, P. Rappelsberger, J. Sarnthein, and H. Petsche, *Synchronization between temporal and parietal cortex during multimodal object processing in man*, Cereb. Cortex **9,** 137–150 (1999).

[50] O. W. Sakowitz, R. Quian Quiroga, M. Schürmann, and E. Basar, *Spatio-temporal frequency characteristics of intersensory components in audiovisually evoked potentials*, Cogn. Brain Res. **23,** 316–326 (2005).

[51] S. M. Doesburg, L. L. Emberson, A. Rahi, D. Cameron, and L. M. Ward, *Asynchrony from synchrony: long-range gamma-band neural synchrony accompanies perception of audiovisual speech asynchrony*, Exp. Brain Res. **185,** 11–20 (2008).

[52] H. Luo, and D. Poeppel, *Cortical oscillations in auditory perception and speech: evidence for two temporal windows in human auditory cortex*, Front. Psychol. **3,** 170 (2012).

[53] H. Park, C. Kayser, G. Thut, and J. Gross, *Lip movements entrain the observers'*

low-frequency brain oscillations to facilitate speech intelligibility, eLife **5,** e14521 (2016).

[54] A. C. Ganesh, F. Berthommier, C. Vilain, M. Sato, and J. L. Schwartz, *A possible neurophysiological correlate of audiovisual binding and unbinding in speech perception*, Front. Psychol. **5,** 1340 (2014).

[55] Y. Kuramoto, *Chemical Oscillations, Waves, and Turbulence.* New York, NY: Springer-Verlag, (1984).

[56] M. Breakspear, S. Heitmann, and A. Daffertshofer, *Generative models of cortical oscillations: neurobiological implications of the Kuramoto model*, Front. Hum. Neurosci. **4,** 1–14 (2010).

[57] J. Cabral, E. Hugues, O. Sporns, and G. Deco, *Role of local network oscillations in resting-state functional connectivity*, NeuroImage **57,** 130–139 (2011).

[58] H. Schmidt, G. Petkov, M. P. Richardson, and J. R. Terry, *Dynamics on networks: the role of local dynamics and global networks on the emergence of hypersynchronous neural activity*, PLoS Comput. Biol. **10,** e1003947 (2014).

[59] A. Banerjee, and V. K. Jirsa, *How do neural connectivity and time delays influence bimanual coordination?*, Biol. Cybern. **96,** 265–278 (2007).

[60] C. Cappe, G. Thut, V. Romei, and M. M. Murray, *Auditory-visual multisensory interactions in humans: timing, topography, directionality, and sources*, J. Neurosci. **30,** 12572–12580 (2010).

[61] V. K. Jirsa, and M. Ding, *Will a large complex system with time delays be stable?*, Phys. Rev. Lett. **93,** 070602 (2004).

[62] M. A. Meredith, and B. E. Stein, *Descending efferents from the superior colliculus relay integrated multisensory information*, Science **227,** 657–660 (1985).

[63] J. Keil, N. Müller, T. Hartmann, and N. Weisz, *Prestimulus beta power and phase synchrony influence the sound-induced flash illusion*, Cereb. Cortex **24,** 1278–1288 (2014).

[64] J. A. Acebrón, L. L. Bonilla, C. J. Pérez Vicente, F. Ritort, and R. Spigler, *The Kuramoto model: A simple paradigm for synchronization phenomena*, Rev. Mod. Phys. **77,** 137–185 (2005).

[65] A. Falchier, S. Clavagnier, P. Barone, and H. Kennedy, *Anatomical evidence of multimodal integration in primate striate cortex*, J. Neurosci. **22,** 5749–5759 (2002).

[66] B. Tuller, P. Case, M. Ding, and J. A. S. Kelso, *The nonlinear dynamics of speech categorization*, J. Exp. Psychol.-Hum. Percept. Performan. **20,** 3–16 (1994).

[67] R. A. Stevenson, R. K. Zemtsov, and M. T. Wallace, *Individual differences in the multisensory temporal binding window predict susceptibility to audiovisual illusions*, J. Exp. Psychol.-Hum. Percept. Perform. **38,** 1517–1529 (2012).

[68] C. K. Peck, *Visual-auditory integration in cat superior colliculus: implications for neuronal control of the orienting response*, Prog. Brain Res. **112,** 167–177 (1996).

[69] A. R. Powers, M. A. Hevey, and M. T. Wallace, *Neural correlates of multisensory perceptual learning*, J. Neurosci. **32,** 6263–6274 (2012).

[70] T. Kassuba, M. M. Menz, B. Röder, and H. R. Siebner, *Multisensory interactions between auditory and haptic object recognition*, Cereb. Cortex. **23,** 1097–1107 (2013).

[71] K. Okada, J. H. Venezia, W. Matchin, K. Saberi, and G. Hickok, *An f*MRI *study of audiovisual speech perception reveals multisensory interactions in auditory cortex*, PLoS One **8,** e68959 (2013).

[72] R. Watson, et al., *Crossmodal adaptation in right posterior superior temporal sulcus during face-voice emotional integration*, J. Neurosci. **34,** 6813–6821 (2014).

[73] K. S. Rockland, and H. Ojima, *Multisensory convergence in calcarine visual areas in macaque monkey*, Int. J. Psychophysiol. **50,** 19–26 (2003).

[74] M. T. Wallace, R. Ramachandran, and B. E. Stein, *A revised view of sensory cortical parcellation*, PNAS **101,** 2167–2172 (2004).

[75] M. O. Ernst and M. S. Banks, *Humans integrate visual and haptic information in a statistically optimal fashion*, Nature **415,** 429–433 (2002).

[76] L. A. de la Mothe, S. Blumell, Y. Kajikawa, and T. A. Hackett, *Cortical connections of the auditory cortex in marmoset monkeys: core and medial belt regions*, J. Comp. Neurol. **496,** 27–71 (2006).

[77] N. van Atteveldt, A. Roebroeck, and R. Goebel, *Interaction of speech and script in human auditory cortex: insights from neuro-imaging and effective connectivity*, Hear. Res. **258,** 152–164 (2009).

[78] B. A. Rowland, T. R. Stanford, and B. E. Stein, *A model of the neural mechanisms underlying multisensory integration in the superior colliculus*, Perception **36,** 1431–1443 (2007).

[79] C. Cappe, and P. Barone, *Heteromodal connections supporting multisensory integration at low levels of cortical processing in the monkey*, Eur. J. Neurosci. **22,** 2886–2902 (2005).

[80] E. Budinger, P. Heil, A. Hess, and H. Scheich, *Multisensory processing via early cortical stages: connections of the primary auditory cortical field with other sensory systems*, Neuroscience **143,** 1065–1083 (2006).

[81] J. F. Smiley, et al., *Multisensory convergence in auditory cortex, I. Cortical connections of the caudal superior temporal plane in macaque monkeys*, J. Comp. Neurol. **502,** 894–923 (2007).

[82] O. Hoshino, *Neuronal responses below firing threshold for subthreshold cross-modal enhancement*, Neural Computation **23,** 958–983 (2011).

[83] A. Pastukhov, et al., *Multi-stable perception balances stability and sensitivity*, Front. Comput. Neurosci. **7,** 17 (2013).

[84] F. Freyer, J. A. Roberts, P. Ritter, and M. Breakspear, *A canonical model of multistability and scale-invariance in biological systems*, PLoS Comput. Biol. **8,** e1002634 (2012).

[85] P. Lakatos, C. Chen, M. N. O′ Connell, A. Mills, and C. E. Schroeder, *Neuronal oscillations and multisensory interaction in primary auditory cortex*, Neuron **53,** 279–292 (2007).

4

An extended model for perceptual variability and multisensory information processing

Even though the minimalistic model presented in Chapter 3 can explain various essential features of the temporal processing involved in multisensory integration, it does not accommodate the description of the spatial aspects of multisensory processing due to its simple architecture. In this chapter we propose a more detailed model as an extension of the previous model. The model again consists of two unimodal areas (auditory and visual), which communicate via feedforward and feedback connections/synapses with a third multisensory area (pSTS or SC). However, instead of a single oscillator representing the dynamics of each area (auditory, visual, and multisensory), here we consider a two-dimensional network of coupled phase oscillators for each cortical area. Each oscillator can be representative of a single neuron or a group of neurons. The extended architecture also allows the inclusion of the physiologically plausible inhibitory interactions into the model, which was not possible under the minimalistic framework of our previous model. We consider every oscillator in each layer to be connected to all the other intra-layer oscillators according to Mexican Hat disposition. The Mexican-hat connectivity architecture is widely used in cortical neural network models [1, 2]. A recent analysis of the networks of phase-coupled oscillators with Mexican hat connectivity, by Heitmann and Ermentrout [3], showed extensively that the Mexican hat connectivity supports a broad range of spatially synchronized wave solutions. In our model, the inter-layer connections are only between the oscillators at the same spatial locations in different layers. Previously, in 2008, Magosso et al. [1] studied a neural network model of similar architecture but they only addressed the spatial aspects of multisensoy integration and did not consider the temporal aspects.

The aim of this extension is to provide a common theoretical framework to understand the spatiotemporal properties and complexities of multimodal integration that can not only explain temporal audiovisual illusions like the McGurk effect but also demonstrate spatial audiovisual illusions like the Ventriloquism effect [4]. The networks of phase-coupled oscillators are ideal for modeling the cortical oscillatory activity in a simplified mathematical framework [5]. The advantage of such models is that they show a very rich dynamical behavior that can be used to model multiple aspects of brain dynamics. Such phase-oscillator based models have been employed previously to explain bistability and traveling waves in motor cortex [6] and collective oscillations in visual cortex [7]. These studies have demonstrated that the networks of phase-coupled oscillators can be very efficient models of cortical dynamics. Our proposed model is a step in this direction, where we study the interactions between different cortical areas involved in multisensory processing.

The rest of the chapter is organized as follows. In Sec. 4.1, we present our model architecture and dynamical equations in detail. The numerical results are presented and discussed in Sec. 4.2. Finally, in Sec. 4.3, we summarize our results and discuss future work.

4.1 The model

To simulate each layer, we consider a two-dimensional $N \times M$ lattice of phase oscillators connected via Mexican-hat connectivity (shown in Fig. 4.1). The inter-layer connections are only between the oscillators at the same spatial location in different layers. To capture the positive audio-visual lags, we again consider the inter-layer connections of the oscillators of AV layer (multisensory area) with the oscillators of V layer (visual area) to be time-delayed. The dynamics of the oscillators in the three layers is governed by the following set of equations

$$\begin{aligned}\frac{d\phi_{ij}^{A}(t)}{dt} = \omega_{ij}^{A} + F^{A} \sum_{hk} G_{ij,hk}^{A} \sin\left[\phi_{hk}^{A}(t) - \phi_{ij}^{A}(t)\right] \\ + K^{AV\to A} \sin\left[\phi_{ij}^{AV}(t) - \phi_{ij}^{A}(t)\right],\end{aligned} \tag{4.1}$$

$$\begin{aligned}\frac{d\phi_{ij}^{V}(t)}{dt} = \omega_{ij}^{V} + F^{V} \sum_{hk} G_{ij,hk}^{V} \sin\left[\phi_{hk}^{V}(t) - \phi_{ij}^{V}(t)\right] \\ + K^{AV\to V} \sin\left[\phi_{ij}^{AV}(t-\tau) - \phi_{ij}^{V}(t)\right],\end{aligned} \tag{4.2}$$

$$\begin{aligned}\frac{d\phi_{ij}^{AV}(t)}{dt} = \omega_{ij}^{AV} + F^{AV} \sum_{hk} G_{ij,hk}^{AV} \sin\left[\phi_{hk}^{AV}(t) - \phi_{ij}^{AV}(t)\right] + K^{A\to AV} \sin\left[\phi_{ij}^{A}(t) - \phi_{ij}^{AV}(t)\right] \\ + K^{V\to AV} \sin\left[\phi_{ij}^{V}(t-\tau) - \phi_{ij}^{AV}(t)\right],\end{aligned} \tag{4.3}$$

where $i = 1, ..., N,\ j = 1, ..., M$, and the superscripts A, V, and AV represent auditory, visual, and audiovisual/multisensory respectively. The variable ϕ_{ij}^m is the phase and the parameter ω_{ij}^m is the intrinsic frequency of the ij^{th} oscillator in the layer $m : \{A, V, AV\}$.

The second term on the right-hand side of Eqs. 4.1-4.3 corresponds to the contribution a neuron/oscillator receives from the intra-area neurons/oscillators. $G_{ij,hk}^m$ is the strength of the synaptic connection from the neuron belonging to the area m at the position hk to the neuron at the position ij of the same area. The spatial coupling kernel for the intra-layer connections, G, is defined by the Mexican hat function

$$G = D_{ex}\, e^{-\frac{\left(dx^2+dy^2\right)}{2\sigma_{ex}^2}} - D_{in}\, e^{-\frac{\left(dx^2+dy^2\right)}{2\sigma_{in}^2}}, \tag{4.4}$$

where σ_{ex} and σ_{in} represent the spread of the excitatory and inhibitory connection densities, respectively. Parameter D_{in} controls the contribution of the inhibitory coupling, while the contribution of the excitatory coupling is controlled by manipulating D_{ex}. We have,

$$dx = \begin{cases} |i-h|\frac{L_x}{N} & \text{if } |i-h| \leq N/2 \\ (N - |i-h|)\frac{L_x}{N} & \text{if } |i-h| > N/2 \end{cases}$$

and

$$dy = \begin{cases} |j-k|\frac{L_y}{M} & \text{if } |j-k| \leq M/2 \\ (M - |j-k|)\frac{L_y}{M} & \text{if } |j-k| > M/2, \end{cases}$$

where d_x and d_y represent the distance between the pre-synaptic and post-synaptic neurons/oscillators in the horizontal and vertical coordinates respectively and L_x and L_y represent the spatial length of the cortical area in the corresponding coordinate. The boundaries of each area are considered to be periodic in order to avoid undesirable boundary effects. F^m is the normalization factor for the modality m and can be different for the

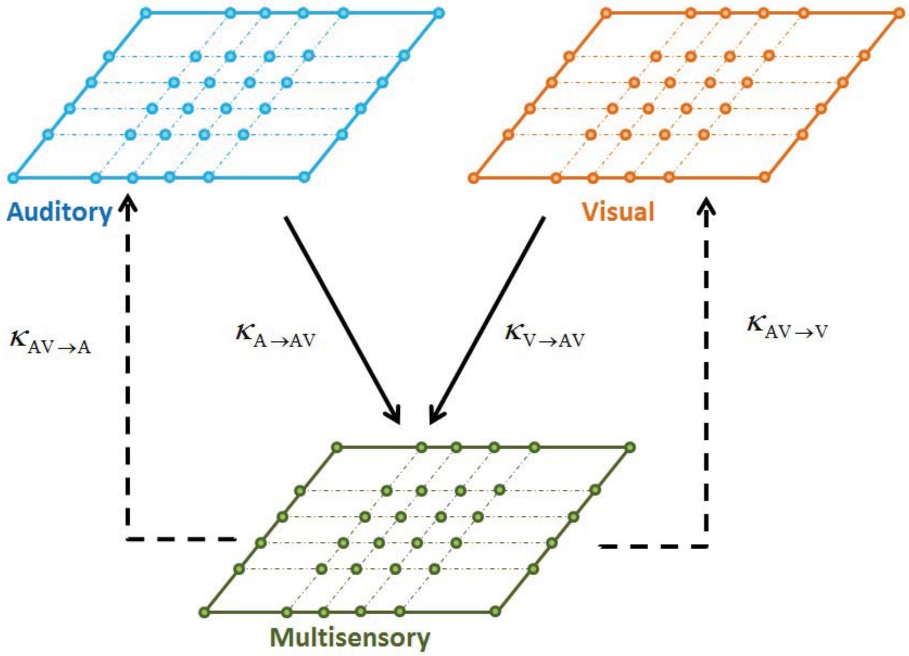

Figure 4.1: The extended model of multisensory integration consisting of three layers of 40×40 oscillators/neurons, representing the two unimodal areas (auditory and visual) and the multimodal area (pSTS or SC) involved in audio-visual integration.

excitatory and the inhibitory part of the interactions. The normalization factor for the excitatory part is given by the expression: $\frac{L_x L_y}{NM2\pi\sigma_{ex}^2 \mathrm{Erf}\left[\frac{L_x}{\sqrt{2}\sigma_{ex}}\right]\mathrm{Erf}\left[\frac{L_y}{\sqrt{2}\sigma_{ex}}\right]}$ and for the inhibitory part is given by: $\frac{L_x L_y}{NM2\pi\sigma_{in}^2 \mathrm{Erf}\left[\frac{L_x}{\sqrt{2}\sigma_{in}}\right]\mathrm{Erf}\left[\frac{L_y}{\sqrt{2}\sigma_{in}}\right]}$. The normalization factors are chosen such that the contribution from each of the excitatory and inhibitory part of the total intra-layer contribution is 1. Erf is the error function that comes because of the Gaussian nature of the excitatory and inhibitory connectivity.

The last term on the right-hand side of Eq. 4.1 and Eq. 4.2 is the feedback of strength $K^{AV \to A/V}$ that the unisensory areas (A and V) receive from the multisensory area (AV). The last two terms on the right-hand side of Eq. 4.3 give the contribution of the feed-forward connections from auditory and visual area respectively to the multisensory area and $K^{A/V \to AV}$ is the corresponding strength of the connections.

We define the global order parameter of the total system consisting of the three layers as

$$R_{total} = \left| \frac{1}{N_{total}} \sum_{j=1}^{N_{total}} e^{i\phi_j} \right|, \tag{4.5}$$

where N_{total} is the combined total of the number of oscillators in the three layers. The order parameter of each layer is defined as

$$R_m = \left| \frac{1}{N_m} \sum_{j=1}^{N_m} e^{i\phi_j} \right|, \tag{4.6}$$

where N_m is the number of oscillators of the modality $m : \{A, V, AV\}$.

4.2 Results

The set of the delay differential equations 4.1-4.3 has been numerically solved using the Fortran 90 solver DDE_SOLVER_M.F90 written by S. Thompson and L.F. Shampine [8]. We have taken a $N \times M = 40 \times 40$ lattice of phase oscillators for each cortical layer. Hence, there are $N_m = 1600$ oscillators in each layer and $N_{total} = 4800$ oscillators overall. We consider $L_x = L_y = 20$ in the simulations. To compare the numerical simulation results of the extended model with the results of the model presented in Chapter 3, we have taken oscillators within each layer to be identical. The intrinsic frequency of all the oscillators in the auditory layer is $\omega_{ij}^A = \omega^A$, in the visual layer is $\omega_{ij}^V = \omega^V$, and in the multisensory layer is $\omega_{ij}^{AV} = \omega^{AV}$.

4.2.1 Excitatory coupling only ($D_{in}^m = 0$; $m = \{A, V\&AV\}$)

We first consider the intra-layer coupling to be only excitatory so as to compare the numerical results with the results of the previous model. We study the effect of the audio and visual stimuli on the system under two scenarios. The first scenario does not consider the stimuli to be explicitly present in the dynamical equations but considers the final dynamical state of the unisensory systems to be the implicit result of the presence of stimuli. This scenario was considered in the model presented in the previous chapter. The second scenario considers the stimuli to be explicitly present in the dynamical equations of the unisensory oscillators. In the first scenario, because of the excitatory intra-layer coupling, all the oscillators within a layer/cortical area synchronize in-phase, i.e., a spatially uniform pattern is the stable state of each layer. Therefore, each layer becomes equivalent to a single oscillator and the extended model becomes equivalent to the minimalistic model and can reproduce its results. The results obtained by considering the first scenario in the model are shown in Fig. 4.2. The global order parameter variation of the total system matches the variation seen in the previous model for the case of balanced coupling with $K = 5$. The order parameter maintains a high value for a certain range of delay, implying successful multisensory integration within the temporal binding window. This integration breaks down as the delay or lag exceeds a certain critical value as shown by the transition of the dynamical system to a state with a small value of order parameter. In the second scenario, we consider the stimuli to be explicitly present in the dynamical equations of the model. In this case, the dynamical equations of the oscillators in the unisensory areas become

$$\begin{aligned}\frac{d\phi_{ij}^{A}(t)}{dt} &= \omega_{ij}^{A} + F^{A}\sum_{hk} G_{ij,hk}^{A} \sin\left[\phi_{hk}^{A}(t) - \phi_{ij}^{A}(t)\right] \\ &\quad + K^{AV\to A} \sin\left[\phi_{ij}^{AV}(t) - \phi_{ij}^{A}(t)\right] + S^{A} \qquad (4.7)\end{aligned}$$

$$\frac{d\phi^V_{ij}(t)}{dt} = \omega^V_{ij} + F^V \sum_{hk} G^V_{ij,hk} \sin\left[\phi^V_{hk}(t) - \phi^V_{ij}(t)\right]$$
$$+K^{AV\to V} \sin\left[\phi^{AV}_{ij}(t-\tau) - \phi^V_{ij}(t)\right] + S^V, \tag{4.8}$$

where S_A and S_V respectively are the auditory and visual stimulus. In our simulations, they have the form of uniformly distributed random numbers chosen from the interval $[0, 2]$ and are given in a 5×5 patch at a central location. The order parameter variation of this system, as a function of delay, is plotted in Fig. 4.3. Here again, the order parameter maintains a high value for a range of time delay parameter signifying the successful audio-visual integration and beyond a critical value, the audio-visual integration breaks down, shown by the low value of the order parameter R_{total}. In Fig. 4.4(a)-(c), we have plotted the spatial phase distribution in the auditory, visual, and multisensory layer for $\tau = 0$. For this case, the system has a high degree of synchronization shown by the high value of R_{total} and signifying successful AV integration for 0 lags. We find the phase incoherence patch to be present only at the location of presentation of stimuli in the plots, with other locations maintaining phase coherence. In Fig. 4.4(d)-(f), we have plotted the spatial phase distribution for $\tau = 0.6$. Here system shows a low degree of synchronization shown by the low value of R_{total} and signifying the breakdown of AV integration for large AV lags. In these plots, we see patches of different phase values in locations other than the location of the stimuli which can be interpreted as confusion in the perception leading to the breakdown of multisensory integration.

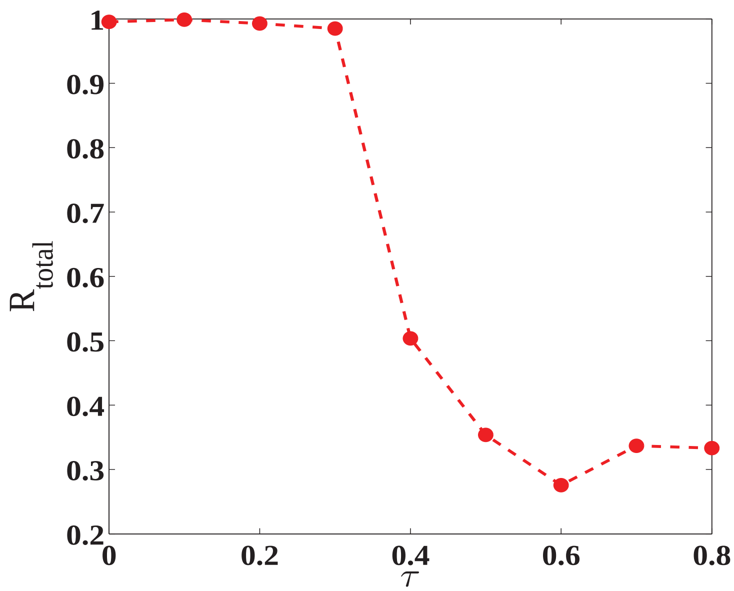

Figure 4.2: The variation of the global order parameter R_{total} as a function of the time delay parameter τ for the case of excitatory-only intra-layer coupling. The value of the parameters are : $K^{AV \to A/V} = K^{A/V \to AV} = 5$, $D^m_{ex} = 1$, $D^m_{in} = 0$, $\sigma^m_{ex} = 1$, $\sigma^m_{in} = 2$, $\omega^A = 3$, $\omega^V = 4$, and $\omega^{AV} = 5$; $m : \{A, V, AV\}$. These results mimic the results of the previous model under balanced-coupling scenario with $K = 5$.

4.2.2 Finite inhibitory coupling

Spatial wave patterns and perceptual variability

The main advantage of the dynamical oscillator-based models is that the multistability is a common occurrence in such systems. Previous studies [3, 6] have shown that, for a certain range of inhibition, a two-dimensional layer of phase-coupled oscillators shows self-organized patterns of waves. In their study on motor cortex, Heitmann et al. [6] have posited that the morphology of wave patterns may be used to encode distinct movement states in motor cortex. In this subsection, we consider a finite inhibitory coupling in the intra-layer connections of the three layers. These layers can show spatiotemporal

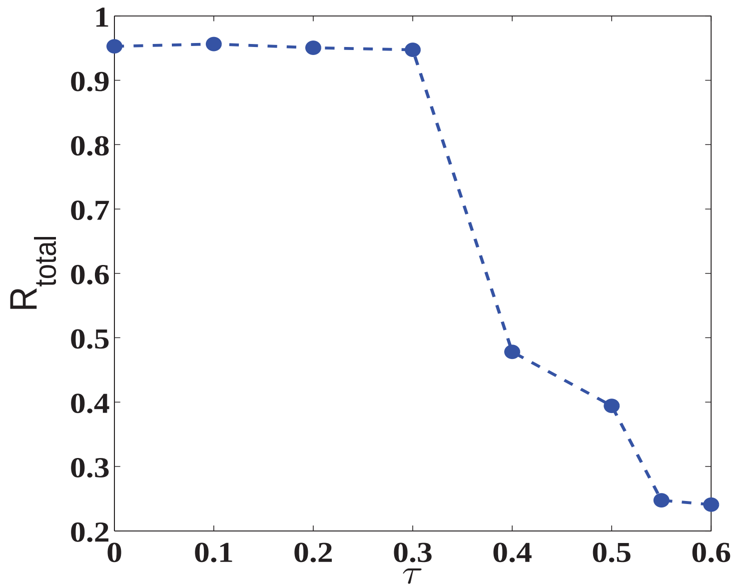

Figure 4.3: The variation of the global order parameter of the system as a function of the time delay parameter when audio and visual stimuli are included explicity in the dynamical equations. The parameters are $K^{AV\to A/V} = K^{A/V\to AV} = 5$, $D^m_{ex} = 1$, $D^m_{in} = 0$, $\sigma^m_{ex} = 1$, $\sigma^m_{in} = 2$, $\omega^A = 3$, $\omega^V = 4$, and $\omega^{AV} = 5$; $m : \{A, V, AV\}$.

wave patterns for certain range of inhibition parameter D^m_{in}. For a detailed discussion on this range, see [3]. Building on Heitmann et al.'s hypothesis, we propose here that different patterns of waves in auditory, visual, and multisensory area correspond to the different perceptual states of the brain. To support this hypothesis, we have shown in Fig. 4.5 that, for the same value of parameters but different sets of initial phases, the structure of wave patterns can vary in these layers. In Fig. 4.5(a)-(f), we have plotted the spatial phase distribution in each layer for the first set of initial conditions IC_1. In Fig. 4.5(a)-(c), we have kept the inter-layer coupling to be zero to show the different dynamical states of the uncoupled auditory, visual, and multisensory layers. We couple them in Fig. 4.5(d)-(f), and because of the feedforward and feedback connections, the three layers synchronize and show a similar pattern. This can be related to the formation

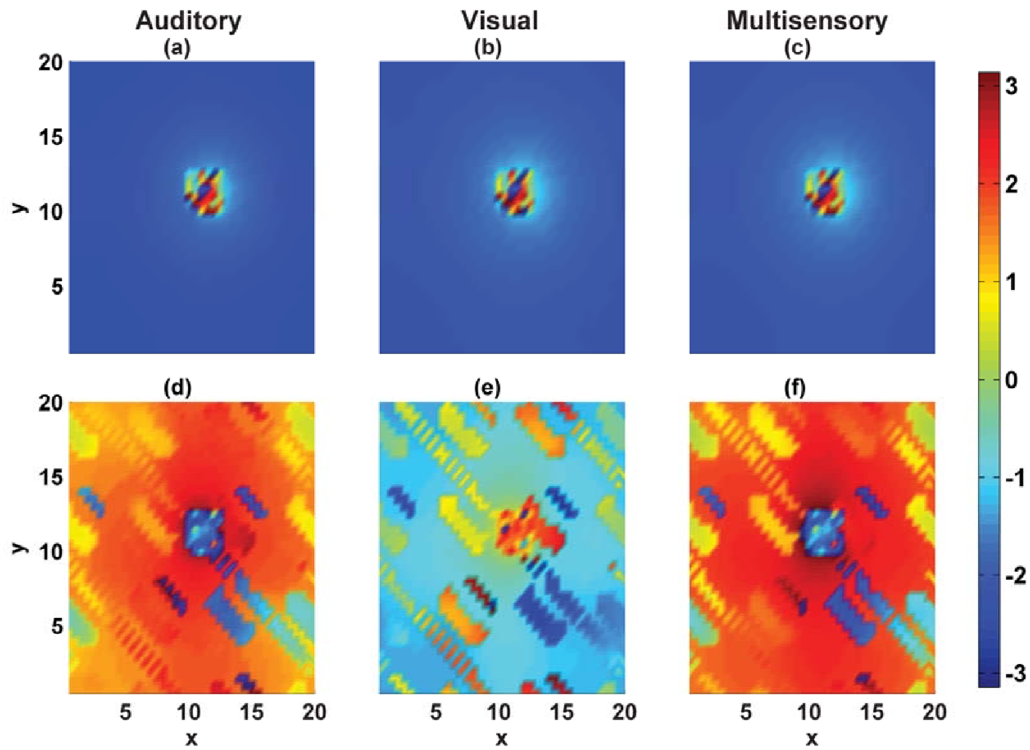

Figure 4.4: In this figure, we have plotted the spatial phase distribution in the auditory, visual, and multisensory layer at (a)-(c) $\tau = 0$ for which the system shows high degree of synchronization shown by the high value of $R_{total} = 0.9527$ and signifying successful AV integration. The phase incoherence is present only at the location of stimuli in the plots, with the other locations maintaining a phase coherence. Figures (d)-(f) show spatial phase distributions for $\tau = 0.6$. The system has a low degree of synchronization shown by the low value of $R_{total} = 0.2408$ and signifies the breakdown of AV integration for large AV lags. In these plots we see patches of different phases in locations other than the location of stimuli. This can be interpreted as confusion in perception leading to breakdown of multisensory integration. The color-bar indicates the value of the oscillator phases $\phi_{ij} \in [-\pi, \pi]$.

of a coherent percept due to multisensory integration. In Fig. 4.5(g)-(l), we have plotted the spatial phase distribution in each layer for the second set of initial conditions IC_2. The structures of the wave patterns obtained from IC_2 in Fig. 4.5(g)-(l) are different from the corresponding wave patterns obtained for IC_1 in Fig. 4.5(a)-(f), even though the parameters are the same. This multistability seen in the dynamical system can be used to explain the perceptual variability originating from the variability in the dynamical states of the brain that results in different responses to the same stimulus.

Stimuli at different locations

We next study the case where the auditory and visual stimuli are provided simultaneously at two different spatial locations. The audio and visual inputs, S_A and S_V respectively, are again given in the form of the uniformly distributed random numbers chosen from the interval $[0, 2]$ and are given in a 3×3 patch. Fig. 4.6 shows the spatial phase distribution in each layer (auditory, visual, and multisensory) for four different distances between the two stimuli. Stimuli are always presented at the same vertical coordinate but different distances, d_s, along the horizontal coordinate. We have chosen the parameters of the three layers such that each layer shows uniform synchrony in the absence of the stimuli so that we can observe the effect of the presentation of stimuli on their dynamics clearly. We observe that, in addition to generating an incoherent patch or response at the location of its presentation in the corresponding unimodal area, each stimulus results in a response/activation at the same location in the other modality and the multisensory area also. This is because of the feedback and feed-forward connections between the unimodal areas and the multisensory area. Because of the feedback connections, the two unimodal areas are indirectly connected to each other and therefore influence each other's dynamics. The variation of the global order parameter of the total system, along with the global order parameters of each layer, as a function of the distance between the stimuli, is shown in Fig. 4.7. We see that the order parameter is highest when the stimuli are at the same spatial location, representing the highest degree of multisensory integration. Though interestingly, the lowest value of order parameter is not at the largest distance between the stimuli but in-between. This may be because of the presence of inhibitory surround in the interactions as mentioned by Magosso et al. (Fig. 4 in [1]).

4.3 Discussion

This chapter gives a general idea of the study we have undertaken, where we propose an extension of the dynamical model presented in the previous chapter by simulating the auditory, visual, and multisensory area as a two-dimensional network of phase-coupled oscillators. The two unimodal areas (auditory cortex and visual cortex) are coupled to the third multimodal area via feedforward and feedback connections. We propose that the spatial and temporal aspects of multisensory integration can be explained within this framework and the synaptic strengths of the model connections and the time-delay parameter can be suitably tuned to model a variety of multisensory phenomena observed in the physiological literature. In addition, this framework can also be applied to other multisensory processes such are audio-tactile and visual-tactile multisensory interactions.

Our numerical investigation has been carried out for two main scenarios - first, when there is no inhibitory coupling in the intra-layer connections and second, when the inhibitory strength is finite in the intra-layer connections. The excitatory-only coupling is investigated for two cases - (a) when the stimuli influence the system dynamics implicitly, and (b) when the stimuli are explicitly present in the dynamical equations of the unisensory oscillators. The case (a) mimics the results of the dynamical model presented in the previous chapter. In this case, the stable state of all three layers is uniform synchrony but the global order parameter of the total system shows finite variation with the time delay parameter resulting from the inter-layer phase differences. Here each layer can be considered equivalent to a single oscillator. For a range of delay values, the order parameter maintains a high value representing successful audio-visual integration but beyond a certain value of delay, this AV integration breaks down, signified by a low value of the order parameter. When we explicitly introduce the stimuli in the dynamical equations, which is our case (b), we see a similar variation in the order parameter with time delay. Here the breakdown of audio-visual integration is signified by the appearance of patches of different phases at locations other than the location of stimuli in the spatial-phase-distribution plots. When there is a finite inhibitory coupling in the intra-layer connections of the three layers, they can show spatiotemporal wave patterns. The structure of these wave-like patterns in the three layers can depend on the initial conditions. This multistability in the wave-patterns can be related to the perceptual variability observed in the multisensory processes. We have also studied the case where the audio and visual stimuli are presented at different spatial locations. We find that, in addition to generating a response/activation at the location of its presentation in the corresponding unimodal area, each stimulus also results in a bump or response/activation at the same location in the other modality and the multisensory area. Also, the order parameter is highest when the stimuli are at the same spatial location, representing the maximum amount of multisensory integration for spatially congruent audiovisual stimuli.

Phase-coupled-oscillator based network can be a very powerful tool in understanding and modeling different aspects of cortical processing such as multisensory integration and perceptual variability, but making the model as physiologically plausible as possible can be quite challenging. The cortex has a very complex structure and the multisensory processing involving the participation of multiple such structures is even more complicated. The task of making a model more “physiologically precise” also leads to an enormous increase in the variables and parameters that one must take into account and properly tune, making a systematic study of the dynamics a daunting challenge. An important goal of the undertaken study is to one by one incorporate some of such physiological complexities into the model while keeping the overall dynamics tractable.

Some aspects that we have not yet incorporated into the model but plan to, are

1. For now we have not connected the unisensory layers directly with each other, though they do interact indirectly via the the feedback projections from the multisensory area. We do plan to add direct connections in the future since there is neurophysiological evidence of projections to/from auditory cortex from/to visual cortex, as discussed in the previous chapter.

2. We have not taken into account the individual receptive fields of auditory and visual neurons. Studies have reported that auditory processing has a higher temporal resolution, while visual processing has a higher spatial acuity [2].

3. For simplicity, we have simulated stimuli as a uniform distribution of random numbers. We would like to conduct our future studies with a more realistic space-time varying form of external stimuli.

4. The time delay parameter in our equations represents the lag between the onset of audio and visual stimuli. However, we have not yet incorporated the time delay arising from the finite axonal transmission in neuronal systems, which is dependent on the inter-areal distance. So another factor that can make the model more physiologically plausible is the inclusion of distance dependent time delays between the intra-layer neurons/oscillators.

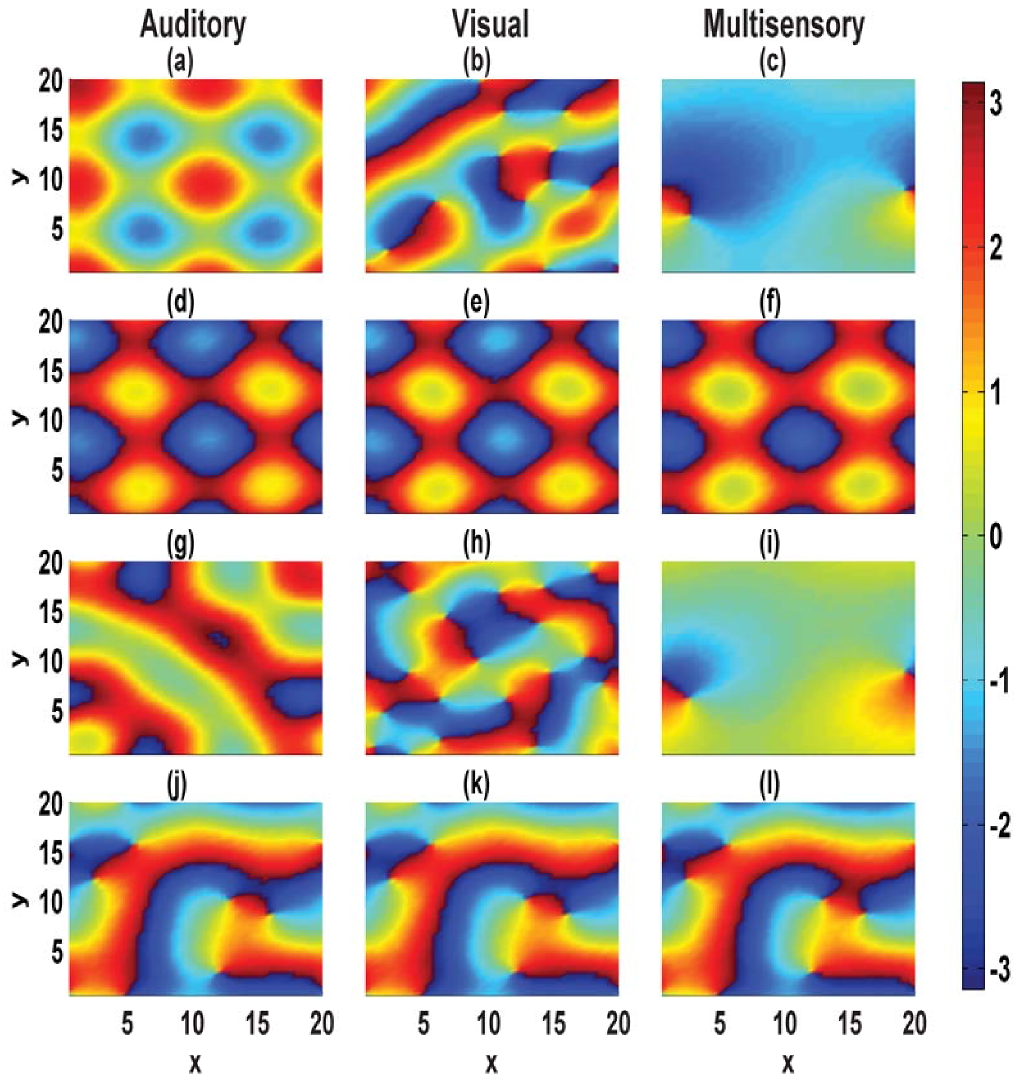

Figure 4.5: The spatial phase distribution in the three layers for the set of parameters: $\omega^A = \omega^V = 5$, $\omega^{AV} = 4$, $D^m_{ex} = 1$, $D^A_{in} = 0.5$, $D^V_{in} = 0.7$, $D^{AV}_{in} = 0.2$, $\sigma^m_{ex} = 1$, and $\sigma^m_{in} = 2$ for (a) - (c) the first set of initial phases IC_1 in the absence of inter-layer coupling, i.e., $K^{AV\to A/V} = K^{A/V\to AV} = 0$, (d) - (f) the first set of initial phases IC_1 in the presence of finite inter-layer coupling, i.e., $K^{AV\to A/V} = 0.5$, $K^{A/V\to AV} = 1$, (g)-(i) the second set of initial phases IC_2 in the absence of inter-layer coupling, i.e., $K^{AV\to A/V} = K^{A/V\to AV} = 0$, and (j) - (l) the second set of initial phases IC_2 in the presence of finite inter-layer coupling, i.e., $K^{AV\to A/V} = 0.5$, $K^{A/V\to AV} = 1$. These results show that the three layers can have different wave patterns for different sets of initial phases and this can be related to the perceptual variability observed in the multisensory processing. The color-bar indicates the value of the oscillator phases $\phi_{ij} \in [-\pi, \pi]$.

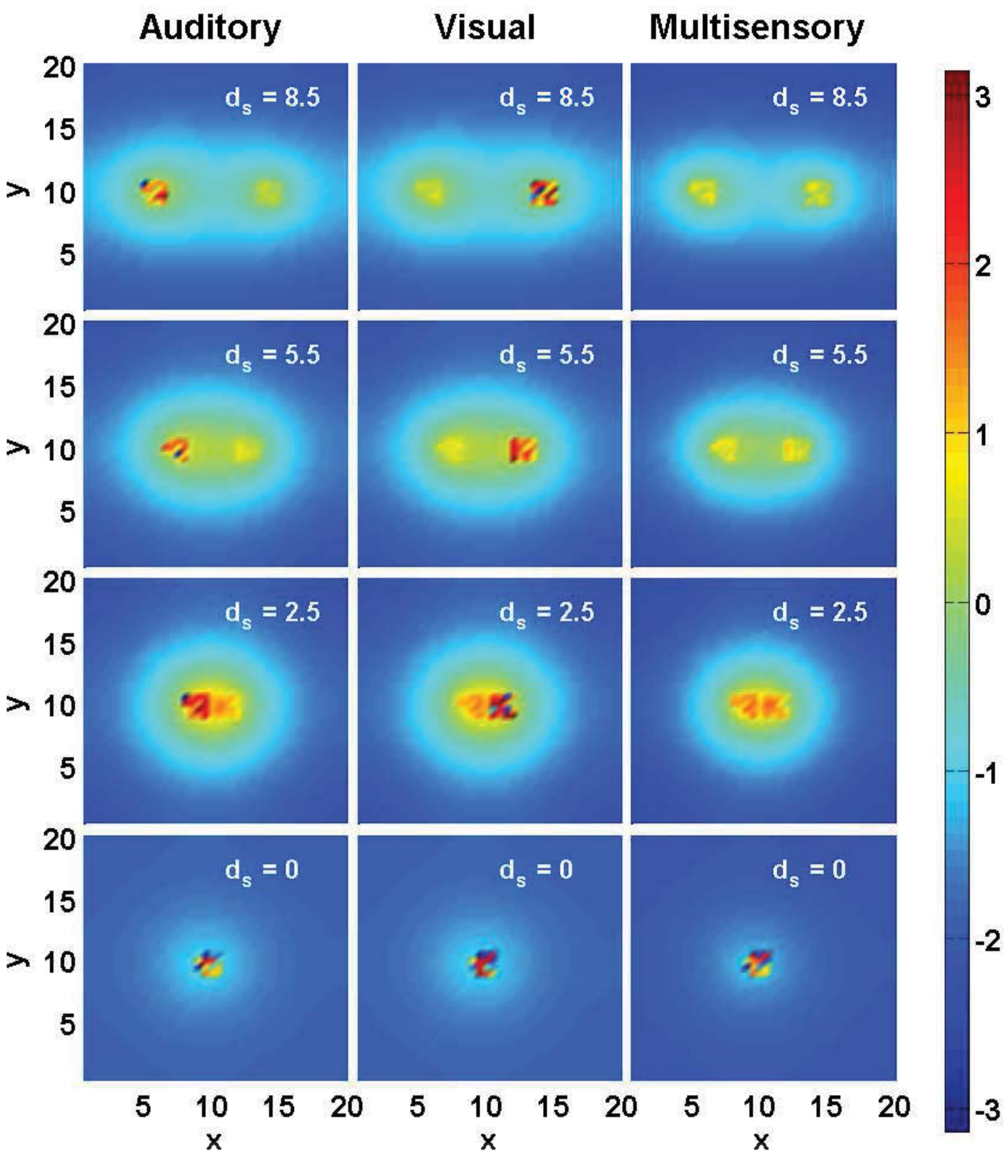

Figure 4.6: The spatial phase distribution in each layer for four different values of distance, d_s, between the two stimuli presented at different spatial locations. In addition to generating an incoherent patch or response at the location of its presentation in the corresponding unimodal area, each stimulus also results in a bump or response/activation at the same location in the other modality and the multisensory area. The parameters used to generate these results are : $\omega^A = \omega^V = 5$, $\omega^{AV} = 4$, $K^{AV \to A/V} = 1$, $K^{A/V \to AV} = 2$, $D^m_{ex} = 1$, $D^m_{in} = 0.2$, $\sigma^m_{ex} = 1$, and $\sigma^m_{in} = 2$; $m : \{A, V, AV\}$. The color-bar indicates the value of the oscillator phases $\phi_{ij} \in [-\pi, \pi]$.

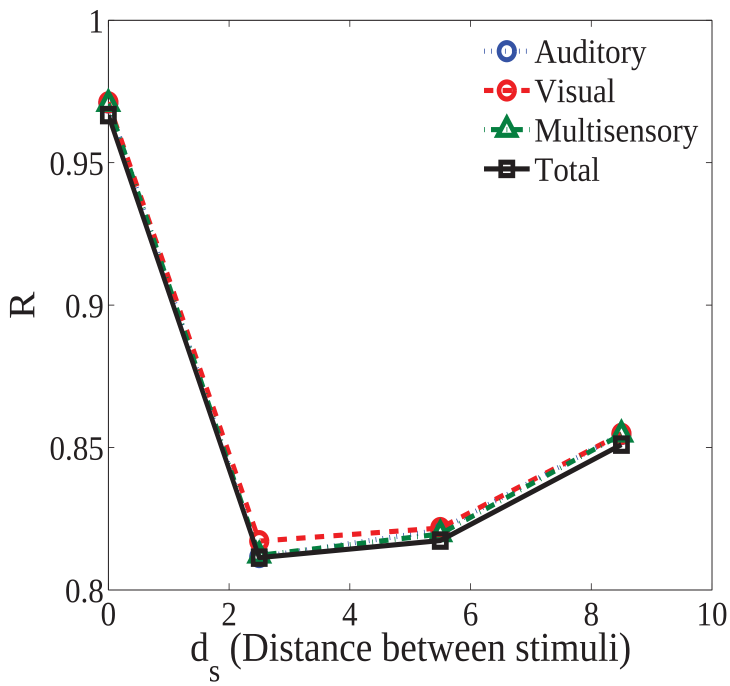

Figure 4.7: The variation of the global order parameter of the total three-layer system, along with the global order parameters of each layer as a function of the distance between the stimuli, d_s.

Bibliography

[1] E. Magosso, C. Cuppini, A. Serino, G. D. Pellegrino, and M. Ursino, *A theoretical study of multisensory integration in the superior colliculus by a neural network model*, Neural Networks **21**, 817–829 (2008).

[2] C. Cuppini, E. Magosso, N. Bolognini, G. Vallar, and M. Ursino, *A neurocomputational analysis of the sound-induced flash illusion*, NeuroImage **92**, 248–266 (2014).

[3] S. Heitmann, and G. B. Ermentrout, *Synchrony, waves and ripple in spatially coupled Kuramoto oscillators with Mexican hat connectivity*, Biol. Cybern. **109**, 333–347 (2015).

[4] D. Alais, and D. Burr, *The ventriloquist effect results from near-optimal bimodal integration*, Curr. Biol. **14**, 257–262 (2004).

[5] M. Breakspear, S. Heitmann, and A. Daffertshofer, *Generative models of cortical oscillations: neurobiological implications of the Kuramoto model*, Front. Hum. Neurosci. **4**, 1–14 (2010).

[6] S. Heitmann, P. Gong, and M. Breakspear, *A computational role for bistability and traveling waves in motor cortex*, Front. Comput. Neurosci. **6**, (2012).

[7] D. M. Kammen, C. Koch, and P. J. Holmes, *Collective oscillations in the visual cortex*, Advances in neural information processing systems, 76–83 (1990).

[8] S. Thompson, and L. F. Shampine, *A friendly Fortran DDE solver*, Appl. Num. Math. **56**, 503–516 (2006).

5

Time-delay effects on the aging transition in a population of coupled oscillators

Populations of coupled oscillators in biological and physical systems must be robust against damages and deterioration as it might happen that some elements turn non-self-oscillatory over time which has been termed as the "aging" of the system by Daido and Nakanishi [1]. The collective dynamics of such a collection of coupled oscillators in which a fraction of the oscillators are non-self-oscillatory or inactive can show very interesting behavior. In particular, for a fixed value of the coupling constant, the system may totally lose its synchronous behavior (i.e., suffer an amplitude death (AD)) as the ratio of the inactive oscillators to the active ones is progressively raised. This has been termed an aging transition and the phenomenon has been studied in the past for various model systems as a paradigm for understanding the functional robustness of diverse physical and biological systems [1, 2]. It was recently proposed [3] that a similar aging mechanism might be responsible for the deterioration of global electrical activity of micro-organs called the pancreatic inlets of Langerhans, which can result in diabetes. Among the other possible biological applications of this model system are in mammalian circadian clocks, which are known to consist of both active and inactive clock cells [4], heart pacemakers [5], and neurodegenerative diseases, such as Alzheimer's disease, since such diseases are characterized by progressive neuron fall out and also the connections between neurons are time-delayed [6]. Besides considering a mixed population of active and inactive oscillators, other forms of mixed populations such as that of passive, excitable, and oscillatory cells [7, 8] and that of two types of self-oscillatory elements with different periods [9] have also been studied. In Ref. [10] the authors presented an extension of the aging transition that takes place in a class of systems in which the oscillatory behavior is lost in a saddle-node bifurcation. Dynamical robustness has been further investigated in multilayer networks [11], weighted complex networks [12], a network of synaptically coupled quadratic integrate-and-fire neurons [13], and networks under targeted attacks [14]. The area of recovery of dynamic behavior in coupled oscillator networks is explored in Ref. [15] by providing new intact oscillators to the network. Recently, Zou et al. provided another mechanism for restoration of rhythmicity in diffusively coupled dynamical networks by introducing a feedback factor in the diffusive coupling [16].

None of the previous studies on aging transition and functional robustness considers interaction delays. Since the connections between neurons and the interactions in other real systems are often time-delayed, this chapter presents the effect of time delay on the aging transition phenomenon in a mixed population of active and inactive Stuart-Landau oscillators that are globally coupled to each other. In the simplest situation of just two coupled oscillators, one active and the other inactive, we find that time delay can significantly influence the critical coupling strength at which the system experiences amplitude death. For a population of such oscillators, the nature of the aging transition is delineated in terms of the variation of the order parameter as a function of the mean distance of the system from the Hopf bifurcation point [17]. The changes brought about by the introduction of time delay are studied both analytically and numerically. We find that time delay can hasten the process of aging by lowering the threshold coupling strength for amplitude death. These results are also found to hold for larger systems of coupled oscillators including an infinite system that is analyzed in the thermodynamic limit.

The chapter is organized as follows. We start in Sec. 5.1 by analyzing in detail the influence of time delay on the dynamics of two coupled Stuart-Landau oscillators [18] that have the same frequency but are at different distances from the Hopf bifurcation point. In Sec. 5.2, the study is extended to a large population of globally coupled oscillators where first we consider a relatively simple case of a mix of identical active and identical inactive oscillators interacting via time-delayed coupling. We then analyze a system in which an arbitrary distribution of bifurcation parameters is chosen to represent the mix of active and inactive oscillators. As a special case, the thermodynamic limit of such globally coupled oscillators is taken and analytic results are obtained for a model of a uniform distribution of the bifurcation parameter. Our results are summarized and discussed in Sec. 5.3.

5.1 Two coupled oscillators

To understand the fundamentals of a phenomenon occurring in a system of a large number of oscillators, it is often useful to analyze the dynamics of a smaller and simpler system like that of two coupled oscillators. The two oscillator model has been used in the past to explain phase transitions in human hand movements [19], circadian rhythm [20], and other collective phenomena in systems such as coupled lasers [21, 22], coupled magnetrons [23], and coupled chemical oscillators [24]. The amplitude effects in the system of two coupled limit cycle oscillators were studied in detail by Aronson et al. [25]. They found that amplitude effects introduce additional collective states in the system, most notably the amplitude death state. Later, Reddy et al. [26, 27] extensively studied the collective dynamics of such systems in the presence of time-delayed interactions. The limit cycle oscillators investigated by these previous studies are described by the Stuart-Landau equation which incorporates both phase and amplitude dynamics of individual oscillators. As discussed in Chapter 1, Stuart-Landau equation is a normal form of supercritical Hopf bifurcation given by

$$\dot{Z}(t) = (\alpha + i\omega - |Z(t)|^2)Z(t), \tag{5.1}$$

where $Z(t) = re^{i\theta}$ is the complex amplitude, ω is the intrinsic frequency, and α is the bifurcation parameter specifying the distance from a Hopf bifurcation. The oscillator exhibits periodic limit-cycle oscillations with amplitude $r = \sqrt{\alpha}$ if its bifurcation parameter $\alpha > 0$. In this case the oscillator is said to be active. It settles down to the trivial fixed point $Z = 0$ if $\alpha \leq 0$ and is considered inactive. The fixed point loses stability via supercritical Hopf bifurcation as shown in Fig. 5.1. Most of the past studies consider the bifurcation parameter α to be the same for both oscillators and usually set $\alpha = 1$. To understand the phenomenon of the aging transition we need to study the collective behavior of two oscillators that are at different distances from the Hopf bifurcation point. We investigate this by considering two coupled Stuart-Landau oscillators.

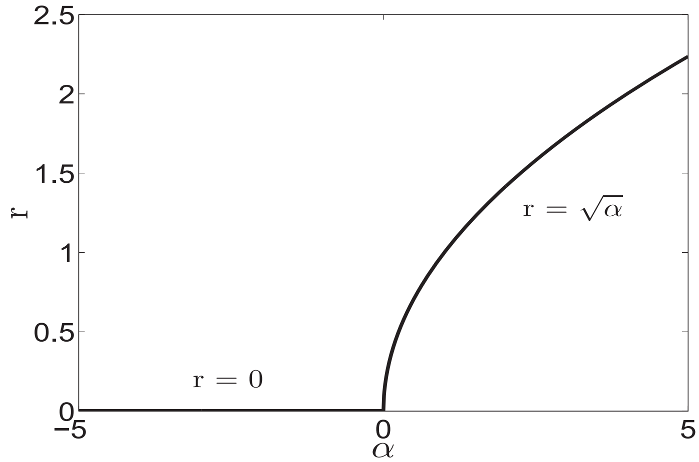

Figure 5.1: Supercritical Hopf bifurcation

5.1.1 No delay ($\tau = 0$)

The model equations for two coupled Stuart-Landau oscillators having different bifurcation parameters, represented by α_1 and α_2, respectively, in the absence of time delay are

$$\dot{Z}_1(t) = (\alpha_1 + i\omega - |Z_1(t)|^2)Z_1(t) + \kappa\,[Z_2(t) - Z_1(t)]\,, \tag{5.2}$$

$$\dot{Z}_2(t) = (\alpha_2 + i\omega - |Z_2(t)|^2)Z_2(t) + \kappa\,[Z_1(t) - Z_2(t)]\,, \tag{5.3}$$

where κ is the coupling strength, ω is the intrinsic frequency of the oscillators, and $Z_{1,2}$ are the complex amplitudes. The origin $Z_{1,2} = 0$ is always the fixed point of the system although it is not always stable. Therefore, we would like to find out the stability boundary of this non-oscillatory steady state, i.e., the amplitude death (AD) state. For that we carry out a linear perturbation analysis around the origin for the coupled system to obtain the characteristic equation

$$det(H - \lambda I) = 0, \tag{5.4}$$

where H is the linearized matrix of the Eqns. (5.2) and (5.3) and is given by

$$H = \begin{pmatrix} \alpha_1 - \kappa + i\omega & \kappa \\ \kappa & \alpha_2 - \kappa + i\omega \end{pmatrix},$$

I is the identity matrix. Assuming that the perturbations vary as $e^{\lambda t}$, the characteristic eigenvalue equation Eq. (5.4) takes the following form

$$(\alpha_1 - \kappa + i\omega - \lambda)(\alpha_2 - \kappa + i\omega - \lambda) - \kappa^2 = 0, \tag{5.5}$$

where $\lambda = \lambda_R + i\lambda_I$ is the eigenvalue, and λ_I, λ_R are real. The AD region corresponds to the region in which $\lambda_R < 0$. Separating the real and imaginary parts gives

$$(\bar{\alpha} - \kappa - \lambda_R)^2 - \frac{(\Delta\alpha)^2}{4} - (\omega - \lambda_I)^2 - \kappa^2 = 0, \tag{5.6}$$

$$(\omega - \lambda_I)(\bar{\alpha} - \kappa - \lambda_R) = 0, \tag{5.7}$$

where $\bar{\alpha} = (\alpha_1 + \alpha_2)/2$ is the average distance from the Hopf bifurcation point and $\Delta\alpha =\mid \alpha_1 - \alpha_2 \mid$. From Eq. (5.7) one gets $\lambda_I = \omega$, which upon substitution in Eq. (5.6) results in a quadratic equation in λ_R whose solutions are

$$\lambda_R = \bar{\alpha} - \kappa \mp \sqrt{\kappa^2 + \frac{(\Delta\alpha)^2}{4}}. \tag{5.8}$$

To obtain the marginal stability curves one can set $\lambda_R = 0$ and solve for $\bar{\alpha}$ as a function of κ. These curves are plotted in Fig. 5.2 for a fixed value of $\Delta\alpha = 1$. Here λ_R is positive above each of these curves and becomes negative below them. Thus the region below the lower curve (solid curve) is the only region where the real parts of both roots of the characteristic equation are negative. This is the AD region labeled II in the figure. The other regions marked I show oscillatory behavior. Thus, the lower marginal stability curve marks the aging transition from a dynamic state where both oscillators show oscillatory behavior to a non-oscillatory AD state. From the figure it is also evident that in the absence of time delay, AD can only take place if $\bar{\alpha} < 0$. This can be physically understood as follows. Suppose one of the oscillators is active and the other is inactive when the oscillators are uncoupled. When we couple them together, the inactive oscillator will try to suppress the oscillations of the active oscillator and the active oscillator will try to induce oscillations in the inactive oscillator. Whether the combined system will assume a stable phase-locked state or a stable AD state will depend on which of the two oscillators wins. The active oscillator will win when it is at a larger distance on the positive side from the Hopf bifurcation point $\alpha = 0$ and will make the inactive oscillator active. That would be the case of the average bifurcation parameter $\bar{\alpha} > 0$ and the system will be in an oscillatory state. If the inactive oscillator is at a larger distance from the Hopf bifurcation point on the other side (which means $\bar{\alpha} < 0$), then it will win and the system will go into the (non-oscillatory) AD state. We next see how time delay can influence this scenario.

5.1.2 Finite delay

In this section we examine the influence of time-delayed coupling on the collective behavior discussed previously for two coupled Stuart-Landau oscillators. We confine ourselves to finite, constant, and discrete time delay. In the presence of time delay τ, the model equations (5.2) and (5.3) take the form

$$\dot{Z}_1(t) = (\alpha_1 + i\omega - |Z_1(t)|^2)Z_1(t) + \kappa\,[Z_2(t-\tau) - Z_1(t)]\,, \tag{5.9}$$

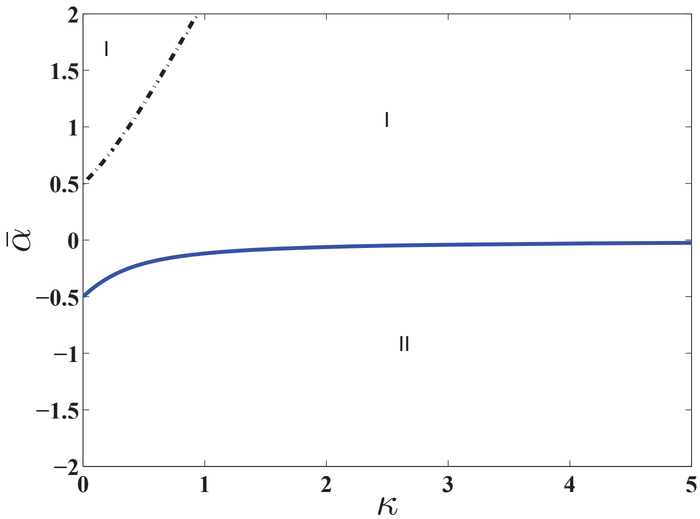

Figure 5.2: Variation of $\bar{\alpha}$ with κ at a fixed value of $\Delta\alpha = 1$ obtained from Eq. (5.8) on setting $\lambda_R = 0$. Region I corresponds to the phase-locked region and region II corresponds to the AD region.

$$\dot{Z}_2(t) = (\alpha_2 + i\omega - |Z_2(t)|^2)Z_2(t) + \kappa\,[Z_1(t-\tau) - Z_2(t)]\,. \tag{5.10}$$

The origin is still a fixed point of the system for any finite value of delay τ. A linear stability analysis of Eqs. (5.9) and (5.10) about the origin ($Z_1 = Z_2 = 0$) now gives a characteristic eigenvalue equation of the form

$$(\alpha_1 - \kappa + i\omega - \lambda)\,(\alpha_2 - \kappa + i\omega - \lambda) - \kappa^2 e^{-2\lambda\tau} = 0, \tag{5.11}$$

where the presence of time delay introduces an exponential term and makes the equation a transcendental one. The complete set of eigenvalues also includes those arising from the conjugate of Eqs. (5.9) and (5.10). Setting $\lambda_R = 0$ and separating the real and imaginary parts, we get the following marginal stability equations

$$(\bar{\alpha} - \kappa)^2 - \frac{(\Delta\alpha)^2}{4} - {\lambda_I}^2 = \kappa^2 \cos\,[2(\omega - \lambda_I)\tau]\,, \tag{5.12}$$

$$2\lambda_1(\bar{\alpha} - \kappa) = -\kappa^2 \sin[2(\omega - \lambda_1)\tau], \tag{5.13}$$

where $\lambda_1 = \omega - \lambda_I$. Defining $\gamma = 2\lambda_1$, Eq. (5.13) can be rewritten as

$$\gamma(\bar{\alpha} - \kappa) = \kappa^2 \sin(\gamma\tau - 2\omega\tau). \tag{5.14}$$

Squaring and adding Eqs. (5.12) and (5.13) we get a biquadratic equation in λ_1 that can be solved to yield

$$\lambda_1 = \pm P, \tag{5.15}$$

where

$$P = \sqrt{\sqrt{\kappa^4 + (\Delta\alpha)^2(\bar{\alpha} - \kappa)^2} - \frac{(\Delta\alpha)^2}{4} - (\bar{\alpha} - \kappa)^2}. \tag{5.16}$$

Substituting for λ_1 in (5.14), we numerically determine the phase-space diagram in the parameter space of $\bar{\alpha} - \kappa$ for various values of τ. The results are plotted in Fig. 5.3 for $\Delta\alpha = 1$ where the lowest curve is for $\tau = 0$ and corresponds to the marginal stability curve shown in Fig. 5.2. As can be seen, in the presence of time delay the domain of AD region is expanded and even extends to the region of positive-$\bar{\alpha}$ values for certain values of time delay. The result is a direct consequence of the stabilizing influence of time delay, which now aides the force exerted by the inactive component to lead the system towards the AD state. We can further mark out the death-island region in the $\kappa - \tau$ space and assess the influence of $\bar{\alpha}$ on it. Rewritting Eq. (5.12) as

$$(\bar{\alpha} - \kappa)^2 - \frac{(\Delta\alpha)^2}{4} - {\lambda_1}^2 = \kappa^2\{2\cos^2[(\omega - \lambda_1)\tau] - 1\}, \tag{5.17}$$

and rearranging the terms in the above equation, we have

$$\cos[(\omega - \lambda_1)\tau] = \pm Q, \tag{5.18}$$

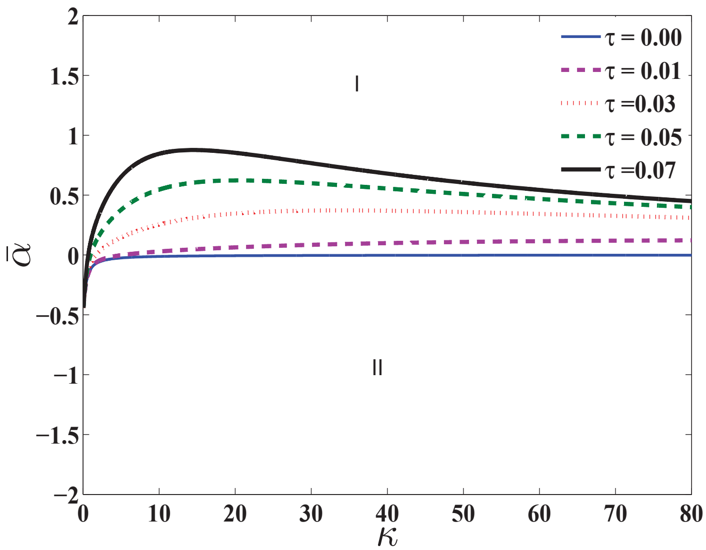

Figure 5.3: Marginal stability curves giving the AD region in $\kappa - \bar{\alpha}$ parametric space for some finite values of delay τ and $\omega = 10$. With an increase in delay τ, AD region is seen to expand and move into the space of positive $\bar{\alpha}$.

where

$$Q = \sqrt{\frac{1}{2\kappa^2}\left((\bar{\alpha} - \kappa)^2 - \frac{(\Delta\alpha)^2}{4} - \lambda_1^2 + \kappa^2\right)}. \tag{5.19}$$

From (5.18) we obtain a set of two critical curves

$$\tau_1(n,\kappa) = \frac{n\pi + cos^{-1}Q}{\omega - P}, \tag{5.20}$$

$$\text{and} \quad \tau_2(n,\kappa) = \frac{(n+1)\pi - cos^{-1}Q}{\omega + P}, \tag{5.21}$$

where $n = 0, 1, 2, ...$ These curves mark the boundary of the AD region. The death island in Fig. 5.4 (shown as a shaded region) is obtained using Eqs. (5.20) and (5.21). The further determination of the nature of the transition of pairs of eigenvalues as it crosses these curves is done by examining the sign of $d\,Re(\lambda)/d\,\tau$ at the crossing. For

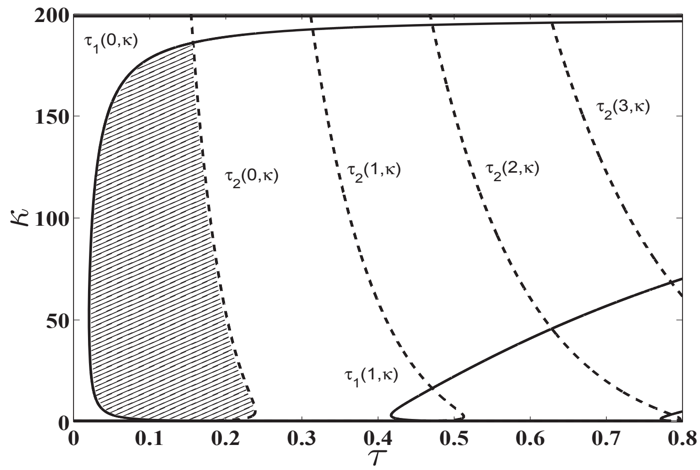

Figure 5.4: Death island obtained from Eq. (5.20) and Eq. (5.21) for two delay coupled oscillators having different bifurcation parameters $\alpha_1 = -0.5$ and $\alpha_2 = 1.0$ but identical frequencies $\omega = 10$.

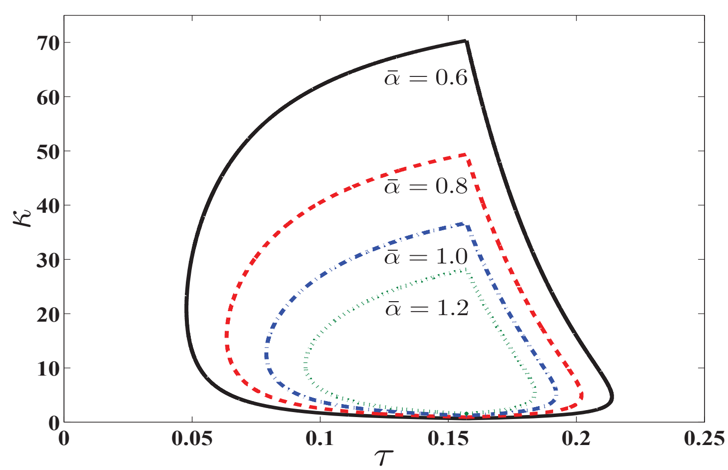

Figure 5.5: Death islands for two delay coupled oscillators at different values of the average bifurcation parameter $\bar{\alpha}$ for fixed $\Delta\alpha = 0.2$ and $\omega = 10$. It can be seen that as $\bar{\alpha}$ decreases, the area of the death-island region increases.

this we rewrite the characteristic equation (5.11) in the form

$$\begin{aligned}\lambda^2 &- 2(\bar{\alpha} - \kappa + i\omega)\lambda + i2\omega(\bar{\alpha} - \kappa) + (\bar{\alpha} - \kappa)^2 \\ &- \frac{(\Delta\alpha)^2}{4} - \omega^2 - \kappa^2 e^{-2\lambda\tau} = 0. \end{aligned} \tag{5.22}$$

Differentiating with respect to τ, we get

$$2\lambda\frac{d\lambda}{d\tau} - 2(\bar{\alpha} - \kappa + i\omega)\frac{d\lambda}{d\tau} = \kappa^2 e^{-2\lambda\tau}\left[-2\lambda - 2\tau\frac{d\lambda}{d\tau}\right] \tag{5.23}$$

and on rearranging the terms we obtain

$$\frac{d\lambda}{d\tau} = \frac{-\kappa^2\lambda e^{-2\lambda\tau}}{\lambda - (\bar{\alpha} - \kappa + i\omega) + \kappa^2\tau e^{-2\lambda\tau}}. \tag{5.24}$$

Considering the real part of the above equation, we get, at $\lambda_R = 0$,

$$\left.\frac{d\lambda_R}{d\tau}\right|_{\lambda_R=0} = \frac{\lambda_I(\lambda_I - \omega)c_1}{c_2}, \tag{5.25}$$

where

$$c_1 = (\bar{\alpha} - \kappa)^2 + \frac{(\Delta\alpha)^2}{4} + (\lambda_I - \omega)^2$$

and

$$\begin{aligned} c_2 &= [\kappa^2\tau\cos(2\lambda_I\tau) - (\bar{\alpha} - \kappa)]^2 \\ &+ [(\lambda_I - \omega) - \kappa^2\tau\sin(2\lambda_I\tau)]^2, \end{aligned} \tag{5.26}$$

which are real positive. Therefore, we have

$$\left.\frac{d\lambda_R}{d\tau}\right|_{\lambda_R=0} \begin{cases} < 0 & \text{on } \tau_1 \text{ if } \omega > P \\ > 0 & \text{on } \tau_1 \text{ if } \omega < P \\ > 0 & \text{on } \tau_2. \end{cases}$$

Thus, on a τ_1 curve, a pair of eigenvalues transits to the left half plane provided the intrinsic frequency of the oscillators is greater than P and to the right side if the frequency is smaller than P. On a τ_2 branch of the critical curves, however, a pair of eigenvalues always crosses into the right half of the complex plane. Thus, for a finite region of the AD to exist in the $\kappa - \tau$ plane it needs to be bounded by appropriate branches of the τ_1 and τ_2 curves and the condition $\omega > P$ should hold. For $\omega < P$, there would be no AD region at all. Finally, to see the impact of the average bifurcation parameter on the AD region, we have also plotted death islands for different values of $\bar{\alpha}$ in Fig. 5.5. As can be seen, when the value of the average bifurcation parameter $\bar{\alpha} > 0$ is increased, the area of AD region in $\kappa - \tau$ parametric space decreases since the active oscillator now has a higher amplitude and tends to dominate over the inactive one. A decrease in the value of $\bar{\alpha}$, i.e., moving closer to the bifurcation point, increases the size of the death island.

5.2 Globally coupled oscillators

After studying the basic effect of time delay on the aging transition in a simple model of two coupled Stuart-Landau oscillators, we now extend our investigation to a larger system of oscillators. We first consider the case where the entire population of oscillators can be divided into subpopulations of identical active and identical inactive oscillators. This study is motivated by the earlier work of Daido and Nakanishi [1] who had studied such a system in the absence of time delay. We start by discussing their results first and then we extend their study by incorporating time delay in the interaction between the oscillators. We are thus able to compare our results with theirs and identify the influence of time delay in a clear fashion.

5.2.1 No delay

Robustness of the dynamic activity of a large population of coupled oscillators was first addressed by Daido and Nakanishi [1]. They considered a population of globally coupled nonlinear oscillators with a fraction p of them being inactive, i.e., non-self-oscillatory, while the rest ($q = 1 - p$) being active, i.e., self-oscillatory. The systems dynamics is governed by the following set of coupled Stuart-Landau equations

$$\dot{Z}_j(t) = (\alpha_j + i\omega - |Z_j(t)|^2)Z_j(t) + \frac{\kappa}{N}\sum_{k=1}^{N}[Z_k(t) - Z_j(t)] \tag{5.27}$$

for $j = 1, ..., N$, and coupling strength κ. They assumed aging of the system to proceed in such a way that an active oscillator with $\alpha_j = a > 0$ turns inactive with $\alpha_j = -b < 0$. The population of oscillators is thus composed of two sub-populations: a sub-population of qN active oscillators with bifurcation parameter $\alpha = a$ and a sub-population of pN inactive oscillators with $\alpha = -b$. The system with $p = 0$ and $\kappa > 0$ attains perfect synchronization, in which each element oscillates with amplitude $\sqrt{a}$ and frequency ω. If κ is greater than a threshold value κ_c, then when the inactive oscillator ratio p exceeds a critical value, p_c, the system makes a transition from a global oscillatory state to a non-oscillatory quiescent state. This transition was termed an aging transition by Daido and Nakanishi and the parameter they used to monitor this transition was the global order parameter $\bar{Z} = \sum_{j=1}^{N} Z_j/N$. Their results are reproduced in Fig. 5.6 for $N = 500$ and $\omega = 10$. They further assumed all elements in each group to be in an identical state in order to simplify the problem and obtain the pair of critical values p_c and κ_c. Setting $Z_j = A$ for all active elements and $Z_j = I$ for all the inactive oscillators in Eq. (5.27), one gets

$$\dot{A}(t) = \left(a + i\omega - \kappa p - |A(t)|^2\right)A(t) + \kappa p I(t) \quad \text{and} \tag{5.28}$$

$$\dot{I}(t) = \left(-b + i\omega - \kappa q - |I(t)|^2\right) I(t) + \kappa q A(t). \tag{5.29}$$

The critical fraction p_c can be obtained from a linear stability analysis of the steady state $A = I = 0$ of this system:

$$p_c = \frac{a\,(\kappa + b)}{(a + b)\,\kappa}. \tag{5.30}$$

This result gives $\kappa_c = a$. The critical ratio p_c plays the role of a measure of the robustness of the system's dynamic activity against deterioration of elements. The larger the value of p_c, the more robust is the system's oscillatory activity. Fig. 5.6(a) indicates that the robustness of the system tends to weaken as the coupling strength increases since the critical value of p decreases with increasing κ. In Fig. 5.6(b), $\kappa - p$ phase diagram has been plotted that clearly shows the aging transition from dynamic oscillatory state (unshaded region) to non-oscillatory steady state (shaded region).

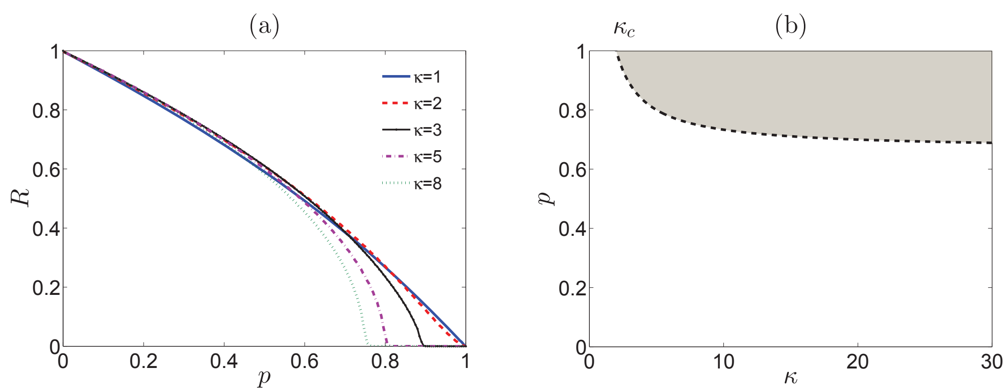

Figure 5.6: (a) Aging transition (for $\tau = 0$) in the coupled Stuart-Landau equations is represented by the variation of normalized order parameter $R = |\bar{Z}(p)|/|\bar{Z}(0)|$ as a function of the fraction of inactive oscillators p. The results are plotted for various values of coupling strength κ for $N = 500$ oscillators and parameter values $a = 2$, $b = 1$, and $\omega = 10$. The critical value of p decreases with increase in coupling strength. (b) Phase diagram in $\kappa - p$ phase space. In the shaded gray region, the oscillators show non-oscillatory behavior, i.e., suffer AD. The dashed line corresponds to the critical fraction of inactive oscillators, p_c, and marks the aging transition from global oscillatory state to non-oscillatory steady state.

5.2.2 Finite delay

Next we examine the influence of time-delayed coupling on the aging phenomenon discussed in the previous subsection. The system of N globally coupled oscillators with a linear time-delayed coupling can be described by the following set of model equations:

$$\begin{aligned}\dot{Z}_j(t) = \left[\alpha_j + i\omega - |Z_j(t)|^2\right] Z_j(t) \quad &+ \quad \frac{\kappa'}{N}\sum_{k=1}^{N}\left[Z_k(t-\tau) - Z_j(t)\right] \\ &- \quad \frac{\kappa'}{N}\left[Z_j(t-\tau) - Z_j(t)\right],\end{aligned} \tag{5.31}$$

where $\kappa' = 2\kappa$ and the last term on the right hand side has been introduced to remove the self-coupling term. Following Daido and Nakanishi [1], we set $Z_j = A$ for all active elements and $Z_j = I$ for all inactive oscillators to get

$$\begin{aligned}\dot{A}(t) = &\left[a + i\omega - \kappa'\left(1 - \frac{1}{N}\right) - |A(t)|^2\right] A(t) \\ &+\kappa' pI(t-\tau) + \kappa'\left(q - \frac{1}{N}\right)A(t-\tau),\end{aligned} \tag{5.32}$$

$$\begin{aligned}\dot{I}(t) = &\left[-b + i\omega - \kappa'\left(1 - \frac{1}{N}\right) - |I(t)|^2\right] I(t) \\ &+\kappa' qA(t-\tau) + \kappa'\left(p - \frac{1}{N}\right)I(t-\tau).\end{aligned} \tag{5.33}$$

These equations are solved numerically for a collection of 500 oscillators ($N = 500$) for various values of p. The results are shown in Fig. 5.7, where the normalized order parameter $R = |\bar{Z}(p)|/|\bar{Z}(0)|$ is plotted against p for various values of τ and for a fixed value of κ'. As can be seen, for a given value of coupling strength κ, the critical value of the fraction of inactive oscillators p at which the transition from global oscillatory to non-oscillatory quiescent state takes place decreases with an increase in delay τ. In other words, the system becomes less robust and ages faster than it would in the absence of delay.

As before, we can also carry out a linear stability analysis of Eqs. (5.32) and (5.33) around the origin to obtain a characteristic equation for the eigenvalues. Setting the real part of the eigenvalue to zero such that $\lambda = i\lambda_I$, we get the characteristic eigenvalue equation

$$\begin{aligned}
&\left[a - \kappa'\left(1 - \frac{1}{N}\right) + i(\omega - \lambda_I) + \kappa'\left(q - \frac{1}{N}\right)e^{-i\lambda_I\tau}\right] \\
\times&\left[-b - \kappa'\left(1 - \frac{1}{N}\right) + i(\omega - \lambda_I) + \kappa'\left(p - \frac{1}{N}\right)e^{-i\lambda_I\tau}\right] \\
&-{\kappa'}^2 pqe^{-i2\lambda_I\tau} = 0.
\end{aligned} \tag{5.34}$$

On separating the real and imaginary parts, we get the following set of coupled equations

$$\begin{aligned}
&[\omega - \lambda_I - B\sin(\lambda_I\tau)]\,[\omega - \lambda_I - C\sin(\lambda_I\tau)] \\
&\quad - [g_1 + B\cos(\lambda_I\tau)]\,[g_2 + C\cos(\lambda_I\tau)] \\
&\quad = -D\cos(2\lambda_I\tau),
\end{aligned} \tag{5.35}$$

$$\begin{aligned}
&[\omega - \lambda_I - C\sin(\lambda_I\tau)]\,[g_1 + B\cos(\lambda_I\tau)] \\
&\quad + [\omega - \lambda_I - B\sin(\lambda_I\tau)]\,[g_2 + C\cos(\lambda_I\tau)] \\
&\quad = -D\sin(2\lambda_I\tau),
\end{aligned} \tag{5.36}$$

where $g_1 = a - \kappa'\left(1 - \frac{1}{N}\right)$, $g_2 = -b - \kappa'\left(1 - \frac{1}{N}\right)$, $B = \kappa'(q - \frac{1}{N})$, $C = \kappa'(p - \frac{1}{N})$, and $D = {\kappa'}^2 pq$.

From this coupled set of equations, we can obtain death islands in the $\kappa - \tau$ plane (displayed in Fig. 5.8), which shows that the region of AD of the system increases as more and more oscillators turn inactive. As discussed for the simpler model calculations in the previous sections, this is a reflection of the fact that in the absence of time delay an aging transition takes place as a result of a competition between the force by inactive oscillators to suppress oscillations of active ones and the force by active oscillators to excite inactive ones. Time delay enhances the tendency to suppress the oscillations. Note that in the presence of time delay there exists a death island even for $p = 0$ (i.e., when we have no inactive element in the absence of coupling). This is a consequence of the delay-induced death in identical oscillators that has been demonstrated in the past [27]. In Fig. 5.9, $p - \tau$ phase diagram has been plotted, with the unshaded region representing the dynamic oscillatory state and the shaded region representing the non-oscillatory steady state. The dashed curved on the left-hand side of the figure corresponds to the values of p_c and represents the aging transition from the global oscillatory state to non-oscillatory steady state. The figure also shows that beyond a certain value of delay, the value of p_c again starts to increase (dashed curve on the right-hand side), indicating the increase in dynamical robustness of the network with a further increase in the delay until it again starts to decrease. But the value of p_c at a finite delay never exceeds its value at zero delay demonstrating that the presence of time delay leads to the reduction in the robustness of the dynamical activity of the network. These results highlight the point that in order to correctly determine the robustness of a network, time delay effects should be taken into account.

5.2.3 Arbitrary distribution of bifurcation parameters α_j

Considering the population of oscillators to be composed of identical active and identical inactive oscillators is a very simple realization. There can be many real systems where the population can be heterogeneous in the distribution of control parameters. Dynami-

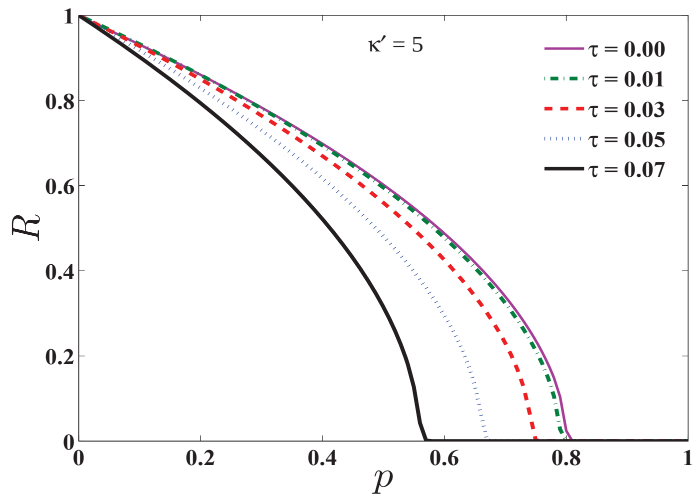

Figure 5.7: Variation of the normalized order parameter $R = |\bar{Z}(p)|/|\bar{Z}(0)|$ with the fraction of inactive oscillators p for various values of delay τ for $N = 500$ oscillators considering $a = 2$, $b = 1$, and $\omega = 10$ at $\kappa' = 5$. The critical value of p decreases with an increase in time delay.

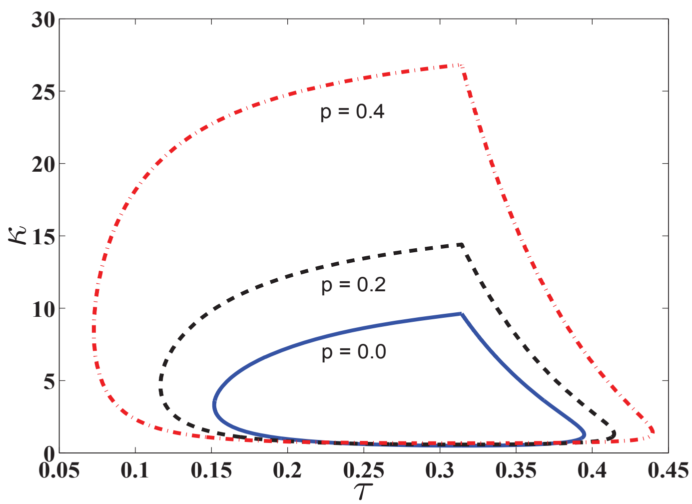

Figure 5.8: Amplitude death islands in $\kappa - \tau$ parameter space at different values of p (fraction of inactive oscillators) for $N = 500$ oscillators with $a = 2$, $b = 1$, and $\omega = 10$. We can see that the death island increases with an increase in the fraction of inactive oscillators, i.e., with decrease in the average bifurcation parameter of the coupled oscillators.

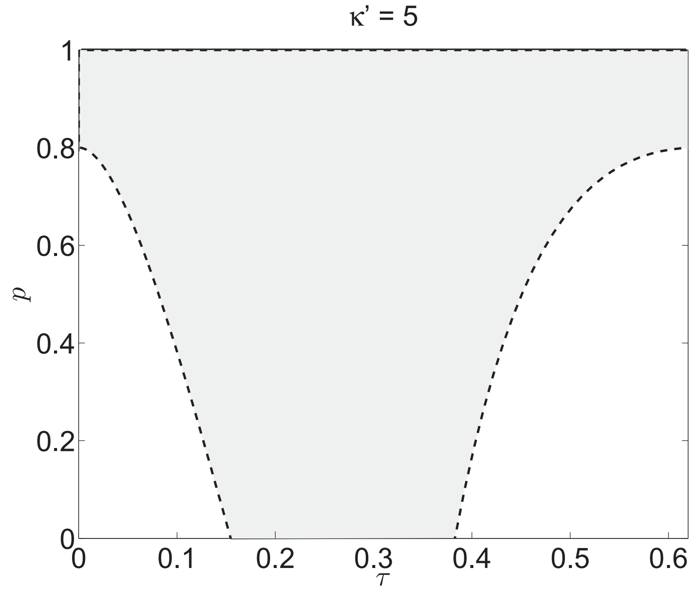

Figure 5.9: Phase diagram in the space of fraction of inactive oscillators p and delay parameter τ for $N = 500$ oscillators, $a = 2$, $b = 1$ and $\omega = 10$ at $\kappa' = 5$. The system's behavior in the unshaded region is oscillatory, while in the shaded region, the system is in a steady amplitude death state.

cal robustness of such a system of heterogeneous oscillators in the absence of time delay has been studied recently in Ref. [28]. We wish to examine the influence of time delay on such a system. The model equation for the case when we have a distribution of the bifurcation parameters α_j is

$$\begin{aligned}\dot{Z}_j(t) = (\alpha_j + i\omega - |Z_j(t)|^2)Z_j(t) + \frac{\kappa'}{N}\sum_{k=1}^{N}[Z_k(t-\tau) - Z_j(t)] \\ -\frac{\kappa'}{N}\left[Z_j(t-\tau) - Z_j(t)\right].\end{aligned} \tag{5.37}$$

In terms of the order parameter $\bar{Z} = \sum_{j=1}^{N} Z_j/N$, we have

$$\dot{Z}_j(t) = (\alpha_j - \kappa' d + i\omega - |Z_j(t)|^2)Z_j(t) + \kappa'\bar{Z}(t-\tau) - \frac{\kappa'}{N}Z_j(t-\tau), \tag{5.38}$$

where $d = 1 - 1/N$. The eigenvalue matrix from a linearized stability analysis around the origin for Eq. (5.37) is given by

$$S = \begin{pmatrix} l_1 & f & f & \cdots & f \\ f & l_2 & f & \cdots & f \\ f & f & l_3 & \cdots & f \\ \vdots & \vdots & \vdots & \ddots & \vdots \\ f & f & f & \cdots & l_N \end{pmatrix},$$

where $l_n = \alpha_n - \kappa' d + i\omega$ and $f = \kappa' e^{-\lambda\tau}/N$. Let us define another matrix M such that $M = S + (\kappa' d - i\omega)I$, where I is the identity matrix. If μ is the eigenvalue of M, then it is related to λ by the relation $\mu = \lambda + \kappa' d - i\omega$. The matrix M is given by

$$M_{mn} = \begin{cases} \alpha_m & \text{if} \quad m = n \\ f & \text{if} \quad m \neq n. \end{cases}$$

The eigenvalues are obtained by solving the eigenvalue equation $\det(M - \mu I) = 0$. This eigenvalue equation can be compactly expressed as a product of two factors

$$\left[\prod_{k=1}^{N} (\alpha_k - \mu - f)\right]\left[1 + f \sum_{j=1}^{N} \frac{1}{\alpha_j - \mu - f}\right] = 0, \tag{5.39}$$

where the first factor in the Eq. (5.39) represents the continuous spectrum of the system and the second factor corresponds to the discrete part of the spectrum [27, 29, 30]. It is difficult to solve the characteristic equation analytically (or even numerically) and therefore we simplify the analysis by taking the thermodynamic limit of this system. As pointed out in [31], the infinite system provides a fairly accurate description of the stability scenario for a large finite system. This argument is further backed by a strong confirmation obtained by numerically solving Eq. (5.37) to check the analytical results.

Taking the thermodynamic limit $N \to \infty$, the discrete equation can be written as

$$h(\lambda) = \int_{-\infty}^{\infty} \frac{g(\alpha)}{\lambda + \kappa' - \alpha - i\omega} d\alpha = \frac{1}{\kappa'} e^{\lambda\tau}, \tag{5.40}$$

where $g(\alpha)$ denotes the distribution of the bifurcation parameters. The continuous spectrum is given by

$$\lambda = \alpha - \kappa' + i\omega, \tag{5.41}$$

where $\alpha \in g(\alpha)$. From the above equation we can see that one of the critical curves is $\kappa' = \alpha$. The AD region should lie to the right of it in order for the eigenvalues to have negative real parts. The critical curves from the discrete spectrum can be obtained on substituting $\lambda = \lambda_R + i\lambda_I$, rationalizing the denominator, and equating the real and imaginary parts to zero to obtain at $\lambda_R = 0$,

$$I_1 = \int_{-\infty}^{\infty} \frac{\kappa' - \alpha}{(\kappa' - \alpha)^2 + (\lambda_I - \omega)^2} g(\alpha) d\alpha = \frac{1}{\kappa'} \cos(\lambda_I \tau), \tag{5.42}$$

$$I_2 = \int_{-\infty}^{\infty} \frac{\omega - \lambda_I}{(\kappa' - \alpha)^2 + (\lambda_I - \omega)^2} g(\alpha) d\alpha = \frac{1}{\kappa'} \sin(\lambda_I \tau). \tag{5.43}$$

These two relations define the other critical curves and along with $\kappa' = \alpha$, for a given $g(\alpha)$, provide a complete analytic description. We next take a simple form of $g(\alpha)$, namely, a uniform distribution given by

$$g(\alpha) = \begin{cases} \frac{1}{\Delta} & \text{if} \quad \alpha \in [-\sigma, \Delta - \sigma] \\ 0 & \text{otherwise.} \end{cases}$$

For a constant positive Δ, $\sigma = 0$ signifies that all oscillators are active and $\sigma = \Delta$ signifies that all oscillators are inactive. The values in between provide a measure of how many oscillators are active and how many are inactive. For this distribution, the integrals I_1 and I_2 can be explicitly carried out to obtain

$$\ln\left(\frac{(\kappa' + \sigma)^2 + (\lambda_I - \omega)^2}{(\kappa' - \Delta + \sigma)^2 + (\lambda_I - \omega)^2}\right) = \frac{2\Delta}{\kappa'}\cos(\lambda_I \tau) \tag{5.44}$$

and

$$\tan^{-1}\left(\frac{\kappa' + \sigma}{\omega - \lambda_I}\right) - \tan^{-1}\left(\frac{\kappa' - \Delta + \sigma}{\omega - \lambda_I}\right) = \frac{\Delta}{K'}\sin(\lambda_I \tau). \tag{5.45}$$

The above set of coupled transcendental equations, along with the curve obtained from the continuous spectrum, provides a complete description of the critical curves for AD in the thermodynamic limit.

For $\tau = 0$, Eq. (5.44) reduces to

$$\ln\left(\frac{\kappa' + \sigma}{\kappa' - \Delta + \sigma}\right) = \frac{\Delta}{\kappa'} \tag{5.46}$$

and gives the marginal stability curve in the absence of time delay.

In Fig. 5.10, stability curves at different values of τ are plotted by a numerical solution of Eq. (5.44) and (5.45). The regions above the curves correspond to death regions and below them the system is in an active state. Note that close to the origin ($\kappa' = 0$), the curve obtained from the continuous spectrum determines the stability boundary. As we move to higher values of κ' the curve obtained from the discrete spectrum defines the marginal boundary. We thus see that, consistent with the previous simpler models, the effect of time delay is to expand the death region. Above a certain value of τ the curves touch the $\sigma = 0$ axis, implying AD for the system even when all oscillators are active. In Fig. 5.11 we have plotted the normalized order parameter against σ for various values of τ at a given value of coupling strength to examine the effect of time delay on the critical fraction of inactive oscillators at which the system collapses to the death

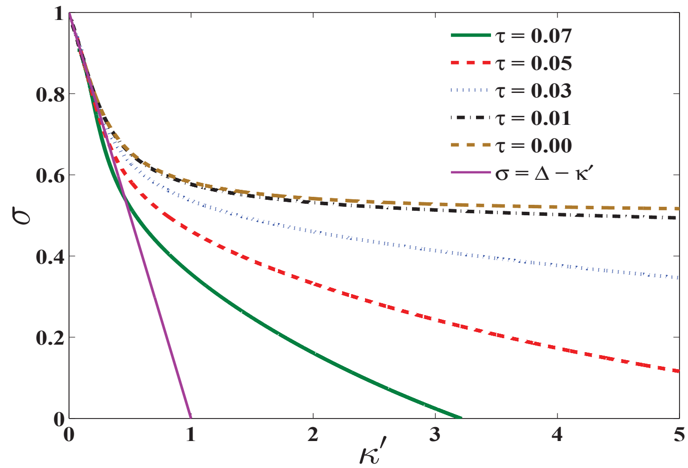

Figure 5.10: Marginal stability curves at various values of delay τ for $\Delta = 1$ and $\omega = 10$. The regions below the curves represent oscillatory states, while the death region lies above the curves. As the delay parameter τ is increased, the AD region increases and at a certain value of τ it touches the $\sigma = 0$ axis, implying the AD state for the system consisting of all active oscillators.

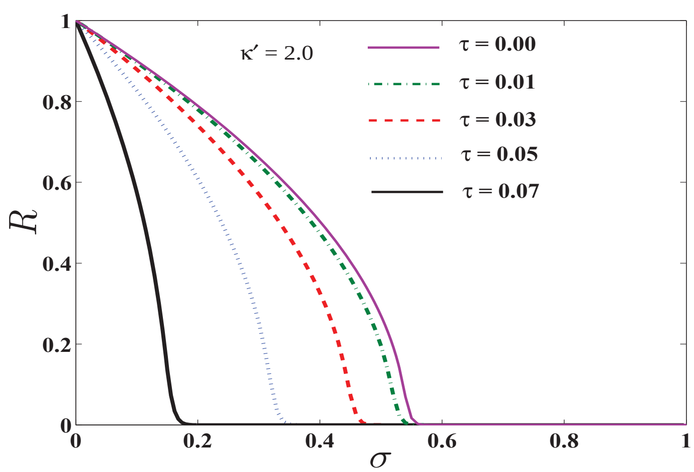

Figure 5.11: Normalized order parameter given by $R \equiv |\bar{Z}(\sigma)|/|\bar{Z}(0)|$ (for $N = 1000$ and $\omega = 10$) is plotted against σ at $\kappa' = 2$ for various values of τ. Finite τ is seen to lower the threshold for AD and thereby hasten aging.

state. The results of this figure are a generalization of those shown in Fig. (5.7), where we have moved away from a simple model to the distribution of bifurcation parameter

α and also taken the limit of $N \to \infty$. In all cases we see that time delay enlarges the AD domain and also speeds up the aging process. We have checked the analytic plots shown in Figs. 5.10 and 5.11 by carrying out numerical integration of the equations of system composed of a large number of oscillators ($N = 1000$) for some values of κ' and σ. The numerical results confirm the analytic description.

5.3 Summary and Discussion

In this chapter we have presented a detailed study of the effect of time delay on the aging of a large ensemble of globally coupled Stuart-Landau oscillators that have a mix of active ($\alpha > 0$) and inactive ($\alpha \leq 0$) oscillators where α is the bifurcation parameter. To understand the impact of the variation of the distance from the Hopf bifurcation point on the collective dynamics of the system, we considered a simple case of two coupled Stuart-Landau oscillators having different bifurcation parameters α. The parameter α controls the strength of attraction to the stable rest state. When there is no time delay in the system, the two coupled oscillators can show amplitude death only when their average bifurcation parameter $\bar{\alpha} < 0$. This is because, for $\bar{\alpha} > 0$, the active oscillator is at a larger distance from the Hopf bifurcation point ($\alpha = 0$) on the positive side compared to the distance of the inactive oscillator on the negative side. Therefore, instead of getting damped by the inactive oscillator, it induces oscillations in the inactive oscillator. On introduction of time delay, the amplitude-death region extends to positive-$\bar{\alpha}$ values and the region of amplitude death increases with an increase in delay. As the average bifurcation parameter $\bar{\alpha}$ moves towards the Hopf bifurcation point from the positive side, the domain of the amplitude-death region in $\kappa - \tau$ parametric space also increases. We then further extended our study to a large population of globally coupled oscillators with pN of them being inactive and $qN = N - pN$ being active (where N is the total number of oscillators). In this case we find that as the fraction of inactive oscillators p increases, $\bar{\alpha}$ of the system decreases, resulting in an increase in the range of $\kappa - \tau$ values (i.e., the size of the death-island region) for which the system exhibits a stable rest state. At a given value of coupling strength κ, the critical value of the fraction of inactive oscillators, p_c, at which the transition from global oscillatory to non-oscillatory quiescent state takes place decreases with an increase in delay τ. This signifies a larger domain of the amplitude-death region at higher values of time delay and also a speeding up of the aging process.

We have also analyzed the aging transition for the case of an arbitrary distribution of bifurcation parameters for the globally coupled system in the thermodynamic limit. As an example, we considered a uniform distribution of α. There again we see the expansion of the amplitude-death region with delay. All the results clearly show that the time delay enhances the domain of amplitude death and hastens aging. Thus, in a physical sense, time-delayed coupling decreases the functional robustness of the system by decreasing its tolerance to component deterioration. We find that the infinite system gives a fairly good description of the behavior of a large finite system, which we have confirmed by the numerical simulation of a large number of oscillators ($N = 1000$). This study can be further extended to various distributions of the bifurcation parameter in global, local, and nonlocal configurations for a variety of network topologies. It would also be interesting to investigate the effects of time-delayed interactions on the robustness of other forms of mixed populations such as that of excitatory and oscillatory elements.

Bibliography

[1] H. Daido and K. Nakanishi, *Aging transition and universal scaling in oscillator networks*, Phys. Rev. Lett. **93**, 104101 (2004).

[2] H. Daido, *Strong-coupling limit in heterogeneous populations of coupled oscillators*, Phys. Rev. E **84**, 016215 (2011).

[3] T. H. Hraha, et al., *Phase transitions in the multi-cellular regulatory behavior of pancreatic islet excitability*, PLoS Comput. Biol. **10**, e1003819 (2014).

[4] S. J. Aton and E. D. Herzog, *Come together, right... now: synchronization of rhythms in a mammalian circadian clock*, Neuron **48**, 531–534 (2005).

[5] J. Miake, E. Marbán, and H. B. Nuss, *Gene therapy: biological pacemaker created by gene transfer*, Nature (London) **419**, 132–133 (2002).

[6] D. E. Bredesen, R. V. Rao, and P. Mehlen, *Cell death in the nervous system*, Nature **443**, 796–802 (2006).

[7] A. K. Kryukov, V. S. Petrov, L. S. Averyanova, G. V. Osipov, W. Chen, O. Drugova, and C. K. Chan, *Synchronization phenomena in mixed media of passive, excitable, and oscillatory cells*, Chaos **18**, 037129 (2008).

[8] H. Daido, A. Kasama, and K. Nishio, *Onset of dynamic activity in globally coupled excitable and oscillatory units*, Phys. Rev. E **88**, 052907 (2013).

[9] G. Tanaka, Y. Okada, and K. Aihara, *Phase transitions in mixed populations composed of two types of self-oscillatory elements with different periods*, Phys. Rev. E **82**, 035202(R) (2010).

[10] D. Pazó and E. Montbrió, *Universal behavior in populations composed of excitable and self-oscillatory elements*, Phys. Rev. E **73**, 055202(R) (2006).

[11] K. Morino, G. Tanaka, and K. Aihara, *Robustness of multilayer oscillator networks*, Phys. Rev. E **83**, 056208 (2011).

[12] Z. He, S. Liu, and M. Zhan, *Dynamical robustness analysis of weighted complex networks*, Physica A **392**, 4181–4191 (2013).

[13] I. Ratas, and K. Pyragas, *Macroscopic self-oscillations and aging transition in a network of synaptically coupled quadratic integrate-and-fire neurons*, Phys. Rev. E **94**, 032215 (2016).

[14] T. Yuan, K. Aihara, and G. Tanaka, *Robustness and fragility in coupled oscillator networks under targeted attacks*, Phys. Rev. E **95**, 012315 (2017).

[15] K. Morino, G. Tanaka, and K. Aihara, *Efficient recovery of dynamic behavior in coupled oscillator networks*, Phys. Rev. E **88**, 032909 (2013).

[16] W. Zou, et al., *Restoration of rhythmicity in diffusively coupled dynamical networks*, Nat. Commun. **6**, 7709 (2015).

[17] S. H. Strogatz, *Nonlinear Dynamics and Chaos* (Perseus Books, Cambridge, Massachusetts, 1994).

[18] J. Guckenheimer and P. Holmes, *Nonlinear Oscillations, Dynamical Systems, and Bifurcations of Vector Fields* (Springer-Verlag, New York, 1983).

[19] H. Haken, J. A. Kelso, and H. Bunz, *A theoretical model of phase transitions in human hand movements*, Biol. Cybern. **51**, 347–356 (1985).

[20] M. Kawato and R. Suzuki, *Two coupled neural oscillators as a model of the circadian pacemaker*, J. Theor. Biol. **86**, 547–575 (1980).

[21] A. Hohl, A. Gavrielides, T. Erneux, and V. Kovanis, *Localized synchronization in two coupled nonidentical semiconductor lasers*, Phys. Rev. Lett. **78**, 4745 (1997).

[22] A. Hohl, A. Gavrielides, T. Erneux, and V. Kovanis, *Quasiperiodic synchronization for two delay-coupled semiconductor lasers*, Phys. Rev. A **59**, 3941 (1999).

[23] J. Benford, H. Sze, W. Woo, R. R. Smith, and B. Harteneck, *Phase locking of relativistic magnetrons*, Phys. Rev. Lett. **62**, 969 (1989).

[24] K. Bar-Eli, *On the stability of coupled chemical oscillators*, Physica D **14**, 242–252 (1985).

[25] D. G. Aronson, G. B. Ermentrout, and N. Kopell, *Amplitude response of coupled oscillators*, Physica D **41**, 403–449 (1990).

[26] D. V. R. Reddy, A. Sen, and G. L. Johnston, *Time delay induced death in coupled limit cycle oscillators*, Phys. Rev. Lett. **80**, 5109 (1998).

[27] D. V. R. Reddy, A. Sen, and G. L. Johnston, *Time delay effects on coupled limit cycle oscillators at Hopf bifurcation*, Physica D **129**, 15–34 (1999).

[28] G. Tanaka, K. Morino, H. Daido, and K. Aihara, *Dynamical robustness of coupled heterogeneous oscillators*, Phys. Rev. E **89**, 052906 (2014).

[29] P. C. Matthews and S. H. Strogatz, *Phase diagram for the collective behavior of limit-cycle oscillators*, Phys. Rev. Lett. **65**, 1701 (1990).

[30] P. C. Matthews, R. E. Mirollo, and S. H. Strogatz, *Dynamics of a large system of coupled nonlinear oscillators*, Physica D **52**, 293–331 (1991).

[31] R. E. Mirollo and S. H. Strogatz, *Amplitude death in an array of limit-cycle oscillators*, J. Stat. Phys. **60**, 245–262 (1990).

6

Summary and Conclusion

The focus of this thesis has been the investigation of the dynamics of networks of coupled nonlinear oscillators that interact via time-delayed coupling and some model applications of such systems. The oscillator units used in our study are limit-cycle oscillators that are coupled to each other in a variety of configurations. The main assumption followed throughout this work is that the time delay is uniform and discrete for all oscillators. In this final chapter, we summarize the problems and the results that we have presented in the thesis, draw some general conclusions based on them, and discuss some future problems emanating from the work done in this thesis.

6.1 Summary and Conclusion

The work done in this thesis can be broadly divided into two parts depending upon whether the coupling between the oscillators is "weak" or not. When the coupling between the oscillators is weak, in the sense that each individual oscillator nearly maintains its original amplitude as defined by its limit cycle, then the coupling only influences the phases of the interacting oscillators. In this “weak coupling” limit, the amplitude effects are neglected and the model simplifies to a system of coupled phase oscillators. Our first two model problems are based on such a reduced description of the coupled oscillators and are described in Chapters 2, 3, and 4. The problem addressed in Chapter 5 requires the consideration of the amplitude variations along with the phase evolution. In each of these studies, extensive analytical and numerical investigations have enabled a deep understanding of the related collective dynamics.

The first phase-oscillator based problem is presented in **Chapter 2**. Here we have examined the time-delay effects on the collective dynamics of geometrically frustrated networks of phase-repulsive oscillators. The amount or degree of frustration in such systems is quantified by a suitably defined frustration parameter. The chapter investigates in a systematic manner the variations induced in the amount of frustration in a given system as a function of time delay in interactions and the resulting system dynamics. We have thoroughly investigated three geometrical configurations - a simple three-unit triangle, a six-unit triangular network and a sixteen-unit 4×4 triangular lattice, that are representative of frustrated networks. The results show that time delay can act as a tuning parameter to significantly influence the amount of frustration in these systems and thereby control the number and nature of their equilibrium states. We find that for an amount of delay beyond a critical value, the in-phase state which is normally unstable for frustrated phase-repulsive configurations becomes a stable equilibrium state of the system. The transition to such a synchronous state is found to occur with a characteristic behavior akin to first-order phase transitions. The variation in frustration as a function of the product of time delay and the collective frequency of the system is seen to lie on a characteristic curve that is common for all values of natural frequencies of the identical oscillators and coupling strengths. This universal scaling behavior is found to hold in all networks irrespective of the coupling topology and the system size. The three-unit network and the 4×4 triangular lattice with periodic boundaries appear to have a unique value of frustration at each value of delay, whereas the six-unit network and the 4×4 triangular lattice with free/open boundaries have multiple final frustration states. The final dynamical state exhibited by such multistable networks is determined by the choice of initial conditions. Multistability seems to become more common with the increase in the network size but an extension of this work to larger systems is required to clearly understand the dependence of multistability on the system size. A generalization of this work can be in the networks with nonidentical oscillators and variable coupling. We propose that our results can be of potential importance in a host of practical applications in physical and biological systems in which frustrated configurations and time delay are known to coexist. One such possible application is related to the dynamics of the vertebrate segmentation clock which is often modeled by employing the Delayed Coupling Theory on hexagonal-coupling configuration of phase oscillators, which can often be frustrated.

We further explore the applications of the phase-oscillator based models in **Chapter 3**, where we propose a minimalistic model to capture the underlying principles of multisensory information processing in our brain. A particular focus is on explaining the principal experimental features associated with the McGurk effect and its temporal constraints that demonstrate how the audio-visual integration of speech breaks down when the lag between auditory and visual stimuli (AV lag) becomes too long. The proposed model consists of the basic ingredients of any multisensory processing - two unisensory and one multisensory subsystem, each of which is represented by a phase oscillator. The oscillators are connected such that the biophysically inspired coupling parameters and time delays become key parameters of this network. AV lag is captured by the time-delayed interaction between the oscillators and we study the variation in perceptual stability as a function of this parameter. The extent of the multisensory integration is quantified by the degree of synchronization of the dynamical system, given by its order parameter. We find that for a range of time delay values, the dynamical system remains in an almost completely synchronized state. This result corresponds to the experimental observation of a temporal binding window within which the successful AV integration can take place. We also find that at a critical value of time delay, the model system makes a transition to a state with a lower degree of synchronization represented by a low value of order parameter, demonstrating the break-down of AV integration for large AV lags. The main advantage of the dynamical systems approach presented in this chapter is that the presence of perceptual variability observed in the behavioral experiments can be very elegantly explained. The presence of time delay makes this dynamical system highly multistable and this multistability can be related to the inter-trial and inter-subject variability in the responses to the same stimuli. The model also captures the effect of an unreliable auditory or visual sensory stream on the multisensory integration by considering a lower value of the coupling parameter between the oscillator associated with the unreliable modality and the multisensory unit. In this unbalanced coupling scenario also, we observe the existence of synchronized states in the dynamical system indicating that the illusory experience is possible even in the presence of noise. By a systematic comparison of the results from the behavioral experiments with the analytic and numerical results obtained from our dynamical model, we find that despite its simplicity our model explains many basic properties of multisensory integration observed in the physiological literature such as individual differences in multisensory temporal binding window and the effect of unreliable auditory and visual stimuli on multisensory integration. Thereby, the proposed dynamical model presents a simple yet elegant quantitative framework for understanding the multisensory information processing.

Even though our minimalistic model presented in **Chapter 3** can explain various temporal aspects of multisensory integration via time-delayed dynamics, its simple design does not accommodate the description of the spatial aspects of multisensory integration. We overcome this constraint in **Chapter 4** by proposing an extension that has a more detailed architecture so as to better understand the complex spatiotemporal processes involved in the multisensory processing at various cortical levels. The model again consists of two unimodal areas (auditory and visual), which communicate via feedforward and feedback synapses with a third multisensory area. Each cortical area is represented by a two-dimensional layer of phase-coupled oscillators connected according to either (i) non-local excitatory-only coupling or (ii) Mexican-hat connectivity. Inter-layer connections are between the oscillators located at the same spatial position. For excitatory-only coupling, each layer exhibits an equilibrium state of uniform synchrony for a sufficiently strong strength of intra-layer connections. In this case, each cortical area can be considered to be equivalent to a single oscillator and the variation of the order parameter of the total system dynamics with time delay/AV lag is shown to match the results of our previous model. The inclusion of the inhibitory coupling into the intra-layer connections, in form of the Mexican hat connectivity, leads to spatiotemporal wave patterns in each layer for certain values of inhibition. The multistability observed in these wave patterns can be used to demonstrate perceptual variability in the multisensory processes. Stimuli are also explicitly included in the model and the effect of their presence is studied when the auditory and visual stimuli are presented at the (i) same spatial location, and (b) different spatial location. Our results indicate that the multisensory integration is highest when the stimuli are present at the same spatial location, represented by the higher value of the order parameter for spatially congruent audio and visual stimuli. The aim of this extension is to provide a common theoretical framework to understand the spatiotemporal properties and complexities of multimodal integration that can not only explain the temporal illusions like the McGurk effect but also demonstrate spatial audio-visual illusions like the Ventriloquism effect. The further inclusions that we would like to make in this model involve (i) direct connections between auditory and visual area, (ii) individual receptive fields of auditory and visual neurons, (iii) space-time varying and physiologically inspired form of auditory and visual stimuli, and (iv) distance dependent communication delays between intra-layer oscillators/neurons.

If the coupling between the oscillators is not weak or the attraction to the limit cycle is not large as compared to the coupling strength, the variations in amplitude cannot then be ignored. In this case, the oscillators can drive each other to the state of zero amplitude, known as the amplitude death (AD) state. AD state is an essential part of the study presented in **Chapter 5**. This chapter presents the effect of time-delayed interactions on the robustness of the dynamical systems measured by the aging transition phenomenon in a mixed population of active and inactive Stuart-Landau oscillators that are globally coupled to each other. Stuart-Landau equations are chosen because they have the information of both the phase as well as the amplitude evolution in them and they can be active or inactive depending upon their distance from the Hopf bifurcation point, characterized by their bifurcation parameter α. In the simplest situation of just two coupled oscillators, one active and other inactive, we find that in the absence of time-delay, AD can only take place when the average bifurcation parameter $\bar{\alpha}$ of the two oscillators is less than zero. This is because, for $\bar{\alpha} < 0$, the inactive oscillator is at a larger distance from the Hopf bifurcation point on the negative side than the distance of active oscillator on the positive side. Therefore, the inactive oscillator dominates and suppresses the oscillations of the active oscillator, thus stabilizing AD. For $\bar{\alpha} > 0$, the active oscillator dominates and induces oscillations in the inactive oscillator, thus destabilizing AD. We find that in the presence of time-delayed interactions, AD can become stable even for $\bar{\alpha} > 0$. This result is a direct consequence of the stabilizing influence of time delay which aides the force exerted by the inactive element to lead the system towards a non-oscillatory AD state. We also find that time delay can significantly influence the critical coupling strength at which the system experiences AD, demonstrated by the presence of "death-islands" in the coupling-delay parameter space and the size of these islands increases with a decrease in $\bar{\alpha}$. We have extended this study to a large population of globally coupled oscillators with a fraction of them being inactive. For a population of such oscillators, the nature of aging transition is delineated in terms of the variation of the order parameter as a function of time delay parameter. The results show that at a given value of coupling strength, the critical value of the fraction of inactive oscillators at which the transition from global oscillatory to non-oscillatory quiescent state takes place, decreases with an increase in time delay. This signifies a larger domain of amplitude death region at higher values of time delay and also a speeding up of the aging process. Here again, we see "death islands" in coupling-delay parameter space and their size increases with an increase in the fraction of inactive elements. We have also analyzed the aging transition for the case of an arbitrary distribution of bifurcation parameters for the globally coupled system in the thermodynamic limit. There again we see the expansion of the amplitude death region with an increase in time delay. Therefore, the main conclusion of this work is that the time delay enhances the domain of amplitude death and hastens aging transition; thereby decreasing the functional robustness of the system by decreasing its tolerance to component deterioration. Among the possible biological applications of this model system are in mammalian circadian clocks, which are known to consist of both active and inactive clock cells, heart pacemakers, and neurodegenerative diseases, such as Alzheimer's disease, since such diseases are characterized by progressive neuron fall out.

The general conclusion that can be drawn from this thesis is that the presence of time delay significantly influences the collective dynamics of all the model systems investigated in this thesis, shown explicitly by the variation of their respective order parameters with time delay parameter. In frustrated networks, delay acts as a tuning parameter to steer the system towards different frustration values and hence different dynamical states. In the model of multisensory integration, it controls the degree of synchronization of the dynamical system that represents the amount of audio-visual integration. Time delay is also shown to have a significant effect on the functional robustness of a network of oscillators characterized by its aging transition.

All the studies presented in the thesis together highlight the significance of time-delay effects on the collective dynamics of oscillator networks and the diverse model applications these studies offer in real systems.

6.2 Future scope

In the following we list some of the possible future directions emanating from the work done in the present thesis.

• In this thesis we have restricted ourselves to a single, discrete, and constant delay. While modeling real systems, such as neural dynamics, where the axonal conduction delays [1] are proportional to the distance between the pre-synaptic and post-synaptic neurons, it is more realistic to consider distance dependent delays.

• In the study of the collective dynamics of frustrated networks of delay-coupled oscillators, we have restricted ourselves to the systems of repulsively coupled oscillators. This study can be extended to the time-delayed networks with the attractive coupling between the components and to the networks having a combination of attractive as well as repulsive coupling links. An important example of such systems is the cortical dynamics, where the excitation and inhibition are coexistent [2]. Also, we have concentrated only on the topologies with triangles as the elemental units. Our study can be extended to other geometrical configurations as well.

• As mentioned in Chapter 2, in the Delayed coupling theory of vertebrate segmentation clock where time delay parameter models the signaling delays, Herrgen et al. [3] have considered the phase oscillators representing the segmentation clock's cells to be arranged in a hexagonal lattice configuration. It will be very interesting to do a systematic study of frustration in this system by taking into consideration the experimentally observed parameters. It can serve as a good experimental test for our theoretical results.

• In addition to the possible future inclusions to the dynamical model for multisensory perception discussed at the end of Chapter 4, some further interesting aspects that can be looked into are (i) role of attention in multisensory processing [4], (ii) plasticity in multisensory integration [5], and (iii) audiovisual integration in patients with visual deficit [6] and hearing loss [7]. In addition, one can also try to incorporate predictive coding mechanisms into the model.

• In the study of the time-delay effects on the robustness of oscillator networks, we have restricted ourselves only to the globally coupled oscillators. This study can be extended to systems of oscillators with local and non-local coupling and even to randomly connected networks. Daido et al. [8] have studied the robustness of the networks of chaotic oscillators in the absence of time delay. Their study can be extended to the chaotic systems with time-delayed interactions. This is something that we have not explored in our studies.

• Neurodegenerative diseases are marked by progressive neuronal death and axonal conduction delays are unavoidable. Extensive studies on the robustness of the models of populations of neurons with time-delay considerations can provide some clues regarding the onset of neurodegenerative diseases such as Parkinson's, Alzheimer's and Huntington's disease.

• One can also combine the frustration analysis presented in Chapter 2 and the robustness analysis presented in Chapter 5 with the extended model of multisensory perception presented in Chapter 4. Considering each cortical area as a two-dimensional layer of oscillators is a very simple realization. In reality, each cortical area consists of a three-dimensional complicated network of neurons. Since inhibitory interactions and time delays are part of the cortical dynamics, there is a possibility that the cortical network or parts of it are frustrated. That can also explain perceptual variability and metastability in brain states. In addition, it might happen that some of the neurons forming these cortical networks die because of some disease or accident. What happens to the robustness of the cortical dynamics and the multisensory integration is such a situation is an interesting question and would be very relevant to investigate in future. It would also be interesting to investigate how the deterioration of certain elements of a frustrated network affects its global frustration.

Bibliography

[1] S. M. Crook, G. B. Ermentrout, M. C. Vanier, and J. M. Bower, *The role of axonal delay in the synchronization of networks of coupled cortical oscillators*, J. Comput. Neurosci. **4**, 161–172 (1997).

[2] J. S. Isaacson, and M. Scanziani, *How inhibition shapes cortical activity*, Neuron **72**, 231–243 (2011).

[3] L. Herrgen, S. Ares, L. G. Morelli, C. Schröter, F. Jülicher, and A. C. Oates, *Intercellular coupling regulates the period of the segmentation clock*, Current Biology **20**, 1244–1253 (2010).

[4] D. Talsma, D. Senkowski, S. Soto-Faraco, and M. G. Woldorff, *The multifaceted interplay between attention and multisensory integration*, Trends Cogn. Sci. **14**, 400–410 (2010).

[5] B. E. Stein, and B. A. Rowland, *Organization and plasticity in multisensory integration: early and late experience affects its governing principles*, Prog. Brain Res. **191**, 145–163 (2011).

[6] F. Frassinetti, N. Bolognini, D. Bottari, A. Bonora, and E. Làdavas, *Audiovisual integration in patients with visual deficit*, J. Cogn. Neurosci. **17**, 1442–1452 (2005).

[7] T. R. Bergeson, D. M. Houston, and R. T. Miyamoto, *Effects of congenital hearing loss and cochlear implantation on audiovisual speech perception in infants and children*, Restorative neurology and neuroscience **28**, 157–165 (2010).

[8] H. Daido and K. Nakanishi, *Aging transition and universal scaling in oscillator networks*, Phys. Rev. Lett. **93**, 104101 (2004).

Contents

STATEMENT BY AUTHOR

Bhumika

Bhumika Thakur

DECLARATION

I, hereby declare that the investigation presented in the thesis has been carried out by me. The work is original and has not been submitted earlier as a whole or in part for a degree / diploma at this or any other Institution / University.

Bhumika

Bhumika Thakur

List of Publications arising from the thesis

Journal

1. **"Collective dynamics of time-delay-coupled phase oscillators in a frustrated geometry"**,
   Bhumika Thakur, Devendra Sharma, Abhijit Sen, and George L. Johnston,
   Phys. Rev. E 95, 012204, 2017.

2. **"A dynamical framework to relate perceptual variability with multisensory information processing"**,
   Bhumika Thakur, Abhishek Mukherjee, Abhijit Sen, and Arpan Banerjee,
   Scientific Reports 6, 31280, 2016.

3. **"Time-delay effects on the aging transition in a population of coupled oscillators"**,
   Bhumika Thakur, Devendra Sharma, and Abhijit Sen,
   Phys. Rev. E 90, 042904, 2014.

Conferences/Schools

International Participation

1. "A dynamical systems approach to multisensory integration"
   Crossroads in Complex Systems, June 5 - 8, 2017, Institute for Cross-Disciplinary Physics and Complex Systems, UIB-CSIC, Mallorca, Spain.

2. *Young Researchers at the Crossroads, June 2 - 4, 2017*, Institute for Cross Disciplinary Physics and Complex Systems, UIB-CSIC, Mallorca, Spain.

3. "Time delay as a possible tuning parameter for frustration in neural networks"
   Hands-on Research in Complex Systems School, July 17 - 29, 2016, International Centre for Theoretical Physics, Trieste, Italy.

4. *Santa Fe Institute's Complex Systems Winter School, December 7 - 21, 2015*, Indian Institute of Science Education and Research, Mohali, India.

5. "Time-delay effects on the aging transition in a population of coupled oscillators" 8^{th} *Dynamics Days Asia-Pacific, July 21 - 24, 2014*, Indian Institute of Technology Madras and Institute of Mathematical Sciences, Chennai, India.

National Participation

1. *Hands-on School on Nonlinear Dynamics, February 16 - 22, 2015*, Institute for Plasma Research, Gandhinagar, India.

2. *DST-SERC School on Nonlinear Dynamics, January 27 - February 18, 2014*, Panjab University, Chandigarh, India.

Bhumika

Bhumika Thakur

To my parents

and

brother

ACKNOWLEDGEMENTS

During the course of my academic career, it has been my great fortune to have received the guidance, inspiration and support of many wonderful people. Finally, here I have the opportunity to warmly acknowledge their support and express my sincere gratitude to them.

First and foremost, my deepest gratitude goes to Prof. Abhijit Sen for his excellent guidance, continued support, and indispensable suggestions throughout my PhD tenure. He has been a continued source of inspiration for me not only as a researcher and a supervisor but also as a person. He has always encouraged me to explore new avenues and motivated me to do better. His faith and patience in me has meant a lot to me. I feel deeply indebted to him and have been very fortunate to work under his guidance.

I am very grateful to my guide Dr. Devendra Sharma for his continued guidance and invaluable support at various points throughout this thesis work. I am also very thankful to him for strengthening the foundation of my computational knowledge. His positive attitude and constant encouragement have greatly helped in this journey.

I am immensely indebted to Dr. Arpan Banerjee for introducing the area of brain dynamics and neural computation to me through engaging with us in the collaborative work and continually guiding me. I am very thankful to him for inviting me to NBRC and allowing me to participate in wonderful neuroimaging and behavioral experiments there and for the many subsequent conversations sharing his knowledge with me.

I would also like to express my deep gratitude to Dr. Ramana Reddy for his valuable suggestions and comments on the “aging-transition” problem. His excellent work during his graduate studies and extremely well written thesis have always served as a great source of information and inspiration.

I am indebted to my doctoral committee members, Dr. R. Srinivasan, Dr. M. Kundu and Prof. P. K. Chattopadhyay for evaluating my work and giving helpful suggestions. I sincerely thank all the faculty members who have taught me, Prof. R. Ganesh, Prof. S. Mukherjee, Prof. S. Sengupta, Dr. M. Bandyopadhyay, Dr. A. Chattopadhyay, Dr. M. Kundu, Dr. V. P. Anitha, Dr. S. Karkari, Dr. N. Bisai, Dr. Ramasubramanian, Dr. J. Ghosh, Dr. P. Bandhopadhyay and Dr. G. Ravi.

I would like to thank Dr. Rajwinder Kaur for giving her valuable time and knowledge for teaching me the experiments on opto-electronic oscillators for demonstration in the Hands-on school on Nonlinear Dynamics organized in IPR. I would like to use this opportunity to thank Dr. R. Roy for guidance during the Hands-on school. I would also like to thank Ms. Unnati Patel and Mr. Mitesh for helping me immensely with the opto-electronic experiments in IPR's nonlinear lab.

Financial support from the HBNI, and D.A.E. (Govt. of India) are greatly acknowledged. I am also thankful to the computer center staff, library staff and administrative staff of IPR for always being cooperative and helpful.

I would like to thank my seniors Vikram Sagar, Maya, Satya, Kshitish, Deepak, Ujjwal, Sita, Gurudatt, Prabal, Rameswar, Sushil, Sanat, Pravesh, Sayak, Manjit, Aditya, Soumen, Vikram, Veda Prakash, Vidhi, Neeraj, Bibhu, Akanksha, Vara, Rupendra, Chandrasekhar, Mangilal, Meghraj, Harish, Samir and Deepa for their valuable help and support during PhD. I am especially grateful to Vidhi for taking care of me for all these years. I am also very thankful to my batchmates Debraj, Umesh, Narayan, Ramkrishna Rane, Arghya, Surabhi, Ratan, Sonu, Modhu and Amit, and juniors Sagar, Atul, Jervis, Deepak, Prabhakar, Meenakshi, Pallavi, Alamgir, Sandeep, Harshita, Arun, Rupak, Shivam, Avnish, Subroto, Niraj, Srimanto, Dipshika, Garima, Nidhi, Swapnali, Ayushi, Devshree, Pawandeep, Satadal Das, Soumen, Pradeep, Hariprasad, Sanjeev and Tanmay for making my stay at the hostel joyful and eventful. I am especially grateful to Debraj, Umesh, Narayan, Sagar, Rupak and Shivam for always looking after me and helping me on numerous occasions.

On the personal front, I am immensely grateful to Deepika didi for her constant support, love, guidance and understanding and to Disha, Arundhuti and Prasanta for always being wonderful friends to me and continually supporting me from miles away. Above all, I am infinitely grateful to my parents for their unconditional love and devotion. This thesis is dedicated to my mother for always believing in me and being a continuous source of strength to me, my father for always coming to my rescue and always trying to make me laugh with his light-hearted humor, my brother for always taking care of me and encouraging me to strive for more and my grandmother for her warm blessings and love.

Bhumika Thakur

SYNOPSIS

This thesis investigates the dynamics of coupled nonlinear oscillators that interact via time-delayed coupling and discusses some model applications of such systems. A network of coupled nonlinear oscillators [1] can display a wide spectrum of collective behavior ranging from synchronization to spatio-temporal chaos, and has therefore served as a useful paradigm to represent collective phenomena in a variety of applications in physical [2], chemical [3], biological [4] as well as social sciences [5]. When the interactions between the interacting units are not instantaneous but are time-delayed, there can be significant changes in the onset thresholds or parametric domain of collective states such as synchronized oscillations or amplitude-death state. Time delay is inevitable in real life systems due to finite interaction times between coupled units arising due to the propagation speed of signals, for instance, due to finite reaction times in chemical interactions or the finite conductance of neuronal connections. It is important therefore to include time-delayed interactions for realistic model applications. The work reported in this thesis presents the consequences of such time-delayed interactions in three model systems that can be potentially important in realistic applications.

In the first model problem, time-delay effects on the collective dynamics of a geometrically frustrated network of phase oscillators are investigated. Such frustrated networks of oscillating units are frequently used in material science (e.g. spin liquid studies) as well as biological applications (e.g. to model the dynamics of the vertebrate segmentation clock in zebrafish). A systematic quantification of the frustration of such a time-delayed network is made and it is shown that time delay significantly alters the amount of frustration in the system and thereby influences its collective dynamics. An important result is the discovery of a universal scaling relation between frustration and time delay that is found to hold in a variety of such geometrically frustrated networks.

The next study aims to provide a dynamical understanding of the multisensory information processing involved in perception through a simple coupled-phase-oscillator based model. A particular focus is on explaining the principal experimental features associated with the so-called McGurk effect and its temporal constraints that show how the audio-visual integration in speech perception starts to break down when the lag between the onset of audio and visual inputs becomes too long. Such a lag is modeled in our study by an appropriate time delay in the coupling between an oscillator representing one of the unisensory units (auditory or visual) and the multisensory oscillator (representing the audio-visual integrator such as posterior Superior Temporal Sulcus (pSTS) or Superior Colliculus (SC)). The changes in the collective behavior of our model system, as seen through the variation of the order parameter as a function of time delay, show a remarkable qualitative agreement with the experimental observations of the McGurk effect. An extension of this model is also discussed that incorporates the spatial aspects of multisensory processing into the model.

The final model study addresses the question of the effect of time delay on the robustness of the collective dynamics of a network of coupled oscillators against deterioration of some of its units, such as due to some elements turning non-self-oscillatory. Such a process can be interpreted as the aging of the system. Our results show that the presence of time-delayed interactions can lower the threshold of the aging transition of the system from a global oscillatory state to a non-oscillatory (amplitude death) state and thereby degrade its functional robustness. The coupled-oscillator model used for this investigation can serve as a simple paradigm for modeling the progress of neurodegenerative diseases due to progressive fall out of individual neurons. Our results on time-delay-induced effects (that can arise due to finite neuronal conduction) can thus have important consequences for such aging dynamics.

Thus, our studies taken together highlight the important consequences of time-delayed coupling on the collective dynamics of oscillator networks which can have potential practical implications in a variety of real life applications.
A more detailed description of the thesis in terms of chapter-wise summaries is provided below.

Chapter-1: Introduction
The introductory first chapter of the thesis outlines the motivation behind the study and defines the aim and scope of the thesis. It also provides a brief history of past synchronization studies and the background leading to the development of the Kuramoto model [6] that has been successfully applied as a paradigm to study a variety of collective phenomena ranging from synchronization to exotic states such as chimeras in physical and biological systems. Another collective phenomenon, relevant to this thesis, is the “amplitude death” state and is discussed in detail in this introductory chapter.

The chapter also highlights the importance and effects of the time-delayed interactions on the dynamics of coupled oscillator systems through real life examples and discusses the mathematical modeling of such phenomena using delay differential equations. A systematic literature survey of past studies on the amplitude death and the time-delay effects is also provided. The chapter ends with a brief outline indicating the chapter-wise organization of the contents of the thesis.

The oscillator units used in our study are based on limit-cycle oscillators that are coupled to each other in a variety of configurations. When the coupling between the oscillators is weak in the sense that each individual oscillator nearly maintains its original amplitude as defined by its limit-cycle then the coupling only influences the phases of the interacting oscillators. In this "weak coupling" limit, the amplitude effects can be neglected and the model simplifies to a system of coupled phase oscillators - the original model introduced by Kuramoto. Our first two model problems are based on such a reduced description of the coupled oscillators and are described in Chapters 2, 3, and 4.

Chapter-2: Frustrated systems of coupled oscillators
This chapter explores the effect of time-delayed interactions on the dynamics of those systems in which the combination of topology and nature of interaction manifests itself in the form of geometrical frustration. Geometrical frustration is a condition that occurs when the topological constraints prevent the simultaneous minimization of the energy of all the interacting pairs of sub-units of a system. A well-known example is that of three Ising spins that are anti-ferromagnetically coupled to each other and placed on the corners of an equilateral triangle. It is impossible to arrive at a configuration where each pair of spins is anti-parallel and as a consequence, the system continually flips between different states in trying to find a minimum energy state and thereby displays a multi-stable behavior. A large lattice model consisting of such triangular units can therefore lead to high ground state degeneracy and multiple phase transitions with increasing temperature [7]. In complex systems, frustration can arise from a combination of geometry and the nature of interactions among the sub-units and can give rise to a rich variety of collective behavior. Frustration plays an important role in the dynamics of many complex magnetic systems such as spin liquids, spin glasses and a host of magnetic alloys. More recently, geometrical frustration arising in neuronal networks has also been recognized as a pivotal factor influencing the cortical dynamics of the brain and is believed to be responsible for introducing metastability and variability

in the brain's collective states. The existence of metastability (or multiple operating regimes) is an essential and crucial feature for biological systems since it provides them with functional flexibility. The study of frustration and its dynamical consequences are therefore receiving a great deal of theoretical and experimental attention in a wide variety of physical and biological systems. Motivated by the consequences of frustration on the collective dynamics of real systems, this chapter examines in a quantitative manner, the variations induced in the amount of frustration in a given system as a function of time delay in coupling between the interacting units and the resulting system dynamics. For our study, we have considered three geometrical configurations that are representative of frustrated networks, namely, a simple triangle, a configuration enclosing a triangle within a triangle, and a triangular lattice. Each node in these configurations is populated by a Kuramoto phase oscillator and the links representing the interactions between the oscillators are repulsive in nature with an intrinsic time delay. We quantify the amount of frustration in the system by defining a frustration parameter which is a function of time-delayed phase differences between the oscillators. A quantitative study of the variation of frustration with the amount of time delay has been made and a universal scaling behavior is found. The variation in frustration as a function of the product of time delay and the collective frequency of the system is seen to lie on a characteristic curve that is common for all values of natural frequencies of the identical oscillators and coupling strengths. This universal scaling behavior holds in all networks irrespective of the coupling topology and the system size. Our principle finding is that the time delay can act as a tuning parameter to significantly influence the amount of frustration in a system and thereby control the number and nature of the equilibrium states of the system. These results can be of potential use in a host of practical applications in physical and biological systems in which frustrated configurations and time delay are known to coexist. As an illustration, one such possible application related to the dynamics of the zebrafish segmentation clock is briefly discussed at the end.

Chapter-3: Multisensory perception: A minimalistic model

This chapter proposes a minimalistic model to capture the underlying principles of multisensory information processing in our brain. Multisensory processing involves the integration of inputs from individual sensory streams, e.g., visual, auditory, and somatosensory to facilitate perception of environmental stimuli. Merging information from different senses confers distinct behavioral advantages, for example, identification of audio-visual (AV) objects is more rapid than with unimodal stimuli, especially when the signals are ambiguous. An experimental realization of the underlying complexity is captured by the "McGurk-effect" [8], where incongruent auditory and visual stimuli elicit the perception of illusory speech sounds. A key variable that modulates perception is the time lag between the onset of auditory and visual streams. For instance, the audio-visual integration breaks down if the asynchrony between the visual lip movements and the auditory speech sounds becomes too long [9]. However, a large temporal window exists over which successful integration may occur. In this chapter we present a dynamical systems model consisting of the basic ingredients of any multisensory processing, two unisensory and one multisensory subsystem (represented by phase oscillators in our model), as reported by several researchers. The oscillators are connected such that the biophysically inspired coupling parameters and time delays become key parameters of this network. The unimodal areas (auditory and visual) communicate via feedforward and feedback synapses with a third multimodal area (pSTS or Superior Colliculus). Audio-visual (AV) lag is captured by the time-delayed interactions between the oscillators. The extent of multisensory integration is quantified by the degree of synchronization of the dynamical system represented by its order parameter and its variation with time-delay parameter (representing the AV-lag) is systematically studied. The work has been done in collaboration with Dr. Arpan Banerjee and Abhishek Mukherjee from National Brain Research Centre (NBRC), Haryana, India, who provided us with the results of the behavioral study experiments conducted by them at NBRC and the expertise in this field. In the behavioral experiments, 52 healthy participants were presented with video stimuli of audio recordings of a human speaker vocalizing /pa dubbed on the lip movement of vocalization /ka. The gap in the onset of auditory and visual streams was varied from -300 to 450 ms in steps of 150 ms. The results of the behavioral study and the experimental procedure are included in the chapter. This chapter systematically compares the results obtained from the dynamical model with the experimental results and shows that despite its simplicity, our model explains many basic properties of multisensory integration observed in the physiological literature such as the temporal constraints on multisensory perception, individual differences in multisensory temporal binding window, and the effect of unreliable auditory and visual stimuli on multisensory integration. Thereby, the proposed dynamical model presents a quantitative framework for understanding multisensory information processing.

Chapter-4: Multisensory perception: An extended model

Even though our minimalistic model presented in the previous chapter can explain various temporal aspects of multisensory integration, it does not accommodate the description of the spatial aspects. To overcome this constraint, this chapter proposes an extension that has a more detailed architecture. The model again consists of two unimodal areas (auditory and visual), which communicate via feedforward and feedback synapses with a third multisensory area (pSTS or SC). However, instead of a single oscillator representing the dynamics of each area (auditory, visual, and multisensory), here we consider a two-dimensional layer of coupled phase oscillators for each cortical area. Each oscillator can be representative of a single neuron or a group of neurons. Inter-layer connections are only between the oscillators at same spatial location and intra-layer connections are arranged either according to excitatory non-local coupling or according to Mexican hat disposition. For excitatory-only coupling, the results are shown to match the results of the minimalistic model. Mexican hat coupling is shown to facilitate the presence of spatiotemporal wave-patterns and multistability that has been related to perceptual variability in multisensory processes. Stimuli are also explicitly included in the dynamical equations and effects of their presence are studied when the audio and visual stimuli are at the (i) same spatial location, and (ii) different spatial locations. This model provides a wider range of multisensory phenomena that can be studied under a common framework, for example, spatial audiovisual illusions like the Ventriloquism effect and temporal audiovisual illusions like the McGurk effect.

Chapter-5: Delay effects on Aging transition

In contrast to the models discussed in previous chapters, if the coupling between the oscillators is not weak or the attraction to the limit cycle is not large as compared to the coupling strength, variations in amplitude cannot then be ignored. An important instance where the attraction to limit cycle is not “strong” is near a Hopf bifurcation point. In this case, the attraction to the limit cycle is proportional to the distance from criticality. If we assume that such systems are coupled with a strength of the same magnitude, it is no longer possible to assume that the trajectories of the system stay in a small neighborhood of the limit cycle. In such cases, many additional phenomena can occur such as oscillators can drive one another to a state of zero amplitude - often called amplitude death (AD) which was discovered by Yamaguchi and Shimizu [10] in 1984. Amplitude death state is the main focus of the study presented in this chapter.

Populations of the coupled oscillators in biological and physical systems must be robust against damages and deterioration as it might happen that some elements can turn non-self-oscillatory over time which has been termed as the "aging" of the system by Daido and Nakanishi [11]. The collective dynamics of such an ensemble of coupled oscillators in which a fraction of the oscillators are non-self-oscillatory or inactive can show very interesting behavior. In particular, for a fixed value of coupling constant, the system may totally lose its synchronous behavior (i.e. suffer an amplitude death) as the ratio of the inactive oscillators to the active ones is progressively raised. This has been termed as an aging transition and the phenomenon has been studied in the past for various model systems as a paradigm for understanding the functional robustness of diverse physical and biological systems [11], but none of the previous studies considers interaction delays. Since the connections between neurons and interactions in other real systems are often time-delayed, this chapter presents the effect of time delay on the aging transition phenomenon in a mixed population of active and inactive Stuart-Landau oscillators that are globally coupled to each other. In the absence of coupling, whether a Stuart-Landau oscillator is active or inactive is decided by its distance from the Hopf bifurcation point, represented by the bifurcation parameter α. If the bifurcation parameter $\alpha < 0$ (i.e., it is on the left side of Hopf bifurcation point $\alpha = 0$), the oscillator is inactive, i.e., its rest state is stable. If it is on the right side of the Hopf bifurcation (i.e., $\alpha > 0$), then the oscillator exhibits stable oscillations of fixed amplitude equal to $\sqrt{\alpha}$ and is considered active. In the simplest situation of just two coupled oscillators, one active and other inactive, we find that time delay can significantly influence the critical coupling strength at which the system experiences amplitude death. We then extend our study to a large population of globally coupled oscillators with a fraction of them being inactive. Through analytical linear stability analysis of the governing equations and numerical solutions, we find that at a given value of coupling strength, the critical value of the fraction of inactive oscillators at which the transition from global oscillatory to non-oscillatory quiescent state takes place, decreases with an increase in time delay. This signifies a larger domain of amplitude death region at higher values of time delay and also a speeding up of the aging process. We have also analyzed the aging transition for the case of an arbitrary distribution of bifurcation parameters for the globally coupled system in the thermodynamic limit. There again we see the expansion of the amplitude death region with an increase in time delay. All the results clearly show that the time delay enhances the domain of amplitude death and hastens aging transition. Thus in a physical sense, time-delayed coupling decreases the functional robustness of the system by decreasing its tolerance to component deterioration. Among the possible biological applications of this model system are in mammalian circadian clocks which are known to consist of both active and inactive clock cells, heart pacemakers, and neurodegenerative diseases, such as Alzheimer's disease, since such diseases are characterized by progressive neuron fallout.

Chapter-6: Summary and Conclusion

This is the concluding chapter of the thesis and provides a chapter-wise summary and conclusions of all the research problems addressed during this thesis work. The chapter also discusses some possible future directions emanating from the work done in the thesis.

All the studies presented in the thesis together highlight the significance of time-delay effects on the collective dynamics of oscillator networks and the diverse model applications these studies offer in real systems.

Bibliography

[1] P. C. Matthews, R. E. Mirollo, and S. H. Strogatz, *Dynamics of a large system of coupled nonlinear oscillators*, Physica D **52**, 293–331 (1991).

[2] H. -J. Wünsche, et al., *Synchronization of delay-coupled oscillators: A study of semiconductor lasers*, Phys. Rev. Lett. **94**, 163901 (2005).

[3] I. R. Epstein, *Coupled chemical oscillators and emergent system properties*, Chem. Commun. **50**, 10758–10767 (2014).

[4] L. Glass, *Synchronization and rhythmic processes in physiology*, Nature **410**, 277–284 (2001).

[5] A. Pluchino, V. Latora, and A. Rapisarda, *Changing opinions in a changing world: a new perspective in sociophysics*, Int. J. Mod. Phys. C **16**, 515–531 (2005).

[6] Y. Kuramoto, H. Arakai, ed., *Self-entrainment of a population of coupled non-linear oscillators*, International Symposium on Mathematical Problems in Theoretical Physics, Lecture Notes in Physics **39**, (Springer, New York 1975).

[7] H. T. Diep, ed., *Frustrated Spin Systems* (World Scientific, Singapore, 2004).

[8] H. McGurk, & J. MacDonald, *Hearing lips and seeing voices*, Nature **264,** 746–748 (1976).

[9] K. Munhall, P. Gribble, L. Sacco, & M. Ward, Temporal constraints on the McGurk effect. *Atten., Percept., and Psychophys.* **58,** 351–362 (1996).

[10] Y. Yamaguchi, and H. Shimizu, *Theory of self-synchronization in the presence of native frequency distribution and external noises*, Physica D **11**, 212–226 (1984).

[11] H. Daido and K. Nakanishi, *Aging transition and universal scaling in oscillator networks*, Phys. Rev. Lett. **93**, 104101 (2004).

List of Figures